Molecular Simulation of Perfluorooctanoic acid (PFOA) Removal from Water

A dissertation submitted in partial fulfilment of the requirements for the Degree of

Doctor of Philosophy

of

University College London

PhD Thesis
Turan Selman Erkal
Dec 2022

Supervisors:
Dr. Ozgur Yazaydin
Dr. George Manos

UCL Research Paper Declaration Form: referencing the doctoral candidate's own published work(s)

Please use this form to declare if parts of your thesis are already available in another format, e.g. if data, text, or figures:

- have been uploaded to a preprint server;
- are in submission to a peer-reviewed publication;
- have been published in a peer-reviewed publication, e.g. journal, textbook.

This form should be completed as many times as necessary. For instance, if you have seven thesis chapters, two of which containing material that has already been published, you would complete this form twice.

1. For a research manuscript that has already been published (if not yet published, please skip to section 2)**:**		
a) Where was the work published? (e.g. journal name)	ACS Applied Materials & Interfaces	
b) Who published the work? (e.g. Elsevier/Oxford University Press):	American Chemical Society	
c) When was the work published?	27/08/2020	
d) Was the work subject to academic peer review?	Yes	
e) Have you retained the copyright for the work?	Yes	
[If no, please seek permission from the relevant publisher and check the box next to the below statement]: ☐ *I acknowledge permission of the publisher named under 1b to include in this thesis portions of the publication named as included in 1a.*		
2. For a research manuscript prepared for publication but that has not yet been published (if already published, please skip to section 3)**:**		
a) Has the manuscript been uploaded to a preprint server? (e.g. medRxiv):	Please select.	**If yes, which server?** Click or tap here to enter text.
b) Where is the work intended to be published? (e.g. names of journals that you are planning to submit to)	Click or tap here to enter text.	
c) List the manuscript's authors in the intended authorship order:	Click or tap here to enter text.	

d) Stage of publication	Please select.

3. For multi-authored work, please give a statement of contribution covering all authors (if single-author, please skip to section 4**):**

Dinesh Shetty, Ilma Jahović, Tina Skorjanc, , Liaqat Ali, Jesus Raya, Zouhair Asfari, Mark A Olson, Serdal Kirmizialtin, Ali Trabolsi: Synthesis and characterization of calixarene polymers, PFOA uptake experiments, Writing the main text and supporting information that are explaining the synthesis procedure and molecules also performing chemical and physical characterization of the molecules.; Turan Selman Erkal: Performing simulations with calixarene molecules and PFOA molecules, writing the materials methods part of simulation and analysis of the simulation data; A Ozgur Yazaydin: Supervising the simulations, review and editing simulation parts of article.

4. In which chapter(s) of your thesis can this material be found?

Chapter 4

5. e-Signatures confirming that the information above is accurate (this form should be co-signed by the supervisor/ senior author unless this is not appropriate, e.g. if the paper was a single-author work):

Candidate:	Click or tap here to enter text.	**Date:**	Click or tap to enter a date.
Supervisor/ Senior Author (where appropriate)**:**	Ozgur Yazaydin	**Date:**	14/12/2022

UCL Research Paper Declaration Form: referencing the doctoral candidate's own published work(s)

Please use this form to declare if parts of your thesis are already available in another format, e.g. if data, text, or figures:

- have been uploaded to a preprint server;
- are in submission to a peer-reviewed publication;
- have been published in a peer-reviewed publication, e.g. journal, textbook.

This form should be completed as many times as necessary. For instance, if you have seven thesis chapters, two of which containing material that has already been published, you would complete this form twice.

6. For a research manuscript that has already been published (if not yet published, please skip to section 2)**:**		
f) Where was the work published? (e.g. journal name)	The Journal of Physical Chemistry C	
g) Who published the work? (e.g. Elsevier/Oxford University Press):	American Chemical Society	
h) When was the work published?	Click or tap to enter a date.	
i) Was the work subject to academic peer review?	Please select.	
j) Have you retained the copyright for the work?	Please select.	
[If no, please seek permission from the relevant publisher and check the box next to the below statement]: ☐ *I acknowledge permission of the publisher named under 1b to include in this thesis portions of the publication named as included in 1a.*		
7. For a research manuscript prepared for publication but that has not yet been published (if already published, please skip to section 3)**:**		
e) Has the manuscript been uploaded to a preprint server? (e.g. medRxiv):	No	**If yes, which server?** Click or tap here to enter text.
f) Where is the work intended to be published? (e.g. names of journals that you are planning to submit to)	Journal of Physical Chemistry C	

g) List the manuscript's authors in the intended authorship order:	Turan Selman Erkal, Norazanita Shamsuddin, Serdal Kirmizialtin and A. Ozgur Yazaydin
h) Stage of publication	Undergoing revision after peer review

8. For multi-authored work, please give a statement of contribution covering all authors (if single-author, please skip to section 4**):**

Turan Selman Erkal: Data curation, Formal analysis, Methodology, Visualization, Writing – original draft; Norazanita Shamsuddin, Serdal Kirmizialtin and A. Ozgur Yazaydin: Conceptualization, Methodology, Writing – review & editing, Project administration

9. In which chapter(s) of your thesis can this material be found?

Chapter 5

10. e-Signatures confirming that the information above is accurate (this form should be co-signed by the supervisor/ senior author unless this is not appropriate, e.g. if the paper was a single-author work):

Candidate:	Click or tap here to enter text.	**Date:**	Click or tap to enter a date.
Supervisor/ Senior Author (where appropriate)**:**	Ozgur Yazaydin	**Date:**	14/12/2022

Declaration of Authorship

I, Turan Selman Erkal, declare that this thesis titled “Molecular Simulations of Removal Perfluorooctanoic acid (PFOA) from Water with Porous Materials” and the work presented in it are my own. Where information has been derived from other sources, I confirm that they have been properly indicated in the thesis.

Turan Selman Erkal

Abstract

Per- and polyfluoroalkyl substances (PFAS) are an emerging class of persistent polluters that do not break down in nature due to strong carbon-fluorine covalent bonds that are present in their structures. Since they are soluble in water, PFAS compounds leads to spreading widely in surface and ground water sources, and persistent nature prevent their degradation. Hence, capturing PFAS from water with adsorbent materials is one of the promising options to clean water resources. In this thesis, among numerous types of adsorbent materials for the removal of PFAS contaminants, Metal Organic Frameworks (MOFs), calixarene-based porous polymers and all-silica zeolite Beta are investigated as a viable PFAS removal agent from water. By using molecular simulations, two calixarene-based porous polymers and their fluorinated versions, which are acquired by using fluorinated linkers instead, are investigated. Perfluorooctanoic acid (PFOA), which is one of the most widely encountered PFAS in water sources, was used as the probe molecule. The simulation results of calixarene-based porous polymers agreed with experimental results. Therefore, we investigated fluorinated MOFs that are synthesized by employing different methods. Our simulations show that fluorine functionalization by incorporating fluorinated anions as bridging ligands in MOFs creates specific sites that PFOA binds strongly; however, the same sites are also preferred adsorption sites for water molecules, which casts doubt on the potential of using this approach to develop efficient PFOA removing materials as they lack sufficient hydrophobicity. On the other hand, trifluoromethyl or fluorine substitution of the MOF ligands result in much higher hydrophobicity; however, pores fluorinated with this method should have the optimum size and shape in order to obtain high PFOA affinities. Likewise, post-

synthetic fluorine functionalization of a MOF through grafting of perfluorinated alkanes can lead to a significant increase in PFOA affinity compared to the parent MOF.

Impact Statement

Water pollution is one of the biggest issues of the highly industrialized world. As air, soil and any other type of pollutions unfortunately, the effect of the water pollutions are also recognised late. There are many on-going researches to remove toxic substances from water. However, water pollution is caused by a wide range of toxic substances that can come from various industries. Some techniques and capturing materials can help eliminating a broad range of toxic substances from water but there can be specific toxic substances that are hard to capture and remove from water. Per- and polyfluoroalkyl substances (PFAS) are one of them and detected in water resources close to industrial areas. The adverse effects of this toxic substances are also presented in medical journals which explained that there is a strong correlation indicating cancerous effects of these toxic molecules [1].

The increasing concentration of PFAS in water resources created a driving force for researchers to find suitable adsorbent material to capture PFAS from water. However, the usual adsorbing materials like activated carbons (AC), clays, sediments and minerals [2] are not capable enough to remove this resilient molecule. Therefore, this research focused on modification of effective adsorbent materials like calixarene-based porous polymers and Metal Organic Frameworks (MOFs). With this research we aimed to provide an effective simulation model to find viable removal adsorbents without wasting more materials during synthesis procedures and understanding the adsorption behaviour of PFAS. The results of this study will help researchers in academia to look at this problem from a different angle and provide more insight into their research. Additionally, the improvement in this area will have a huge impact in protecting human health and preventing further pollution of water resources globally.

Acknowledgements

First of all, I would like to thank to my supervisor Dr Ozgur Yazaydin for his guidance and support throughout my PhD study. I am grateful for the opportunity he has provided me. With his insights and inspirational views, I am confident to say that I have improved myself a lot throughout this journey.

I would like to express my gratitude to my second supervisor Dr George Manos and my upgrade examiner Dr Matteo Salvalaglio for their constructive comments and invaluable suggestions.

Furthermore, I would like to thank my previous group members Dr Sada Namsani, Dr Benjamin Tam and Dr Aydin Ozcan; and my current group members Ms. Mengru Zhang and Dr Fan Li for their friendships that helped me through my research life.

My special thanks to my dear Friends, Mr Kai Bin Yu and Dr Francois Sicard for their personal friendship and constant support that helped me a lot through tough times in research and life.

Finally, I would like to thank my family, particularly my dear parents for their constant support throughout all my life.

Publications

1. Zorlu, Y., Erbahar, D., Cetinkaya, A., Bulut, A., **Erkal, T.S.**, Yazaydin, A. O., Beckmann, J., Yücesan, G.; "A Cobalt Arylphosphonate MOF - Superior Stability, Sorption and Curie Magnetism Properties", Chemical Communications, 2019, 55, 3053-3056. DOI: 10.1039/C8CC09655D
2. Yücesan, G., Tholen, P., Peeples, C.A., Schaper, R., Bayraktar, C., **Erkal, T.S.**, Ayhan, M. M., Cosut, B., Beckmann, J., Yazaydin, A. O., Mark, W., Hanna, G., Zorlu, Y.D.; "Semiconductive microporous hydrogen-bonded organophosphonic acid frameworks", Nature Communications, 2020, 11, 3180. DOI: 10.1038/s41467-020-16977-0

List of publication associated with this thesis:

3. Shetty, D., Jahovic, I., Skorjanc, T., **Erkal, T.S.**, Ali, L., Raya, J., Asfari, Z., Olson, M.A., Kirmizialtin, S., Yazaydin AO, Trabolsi, A.; "Rapid and Efficient Removal of Perfluorooctanoic Acid from Water with Fluorine-Rich Calixarene-Based Porous Polymers", ACS Applied Materials & Interfaces, 2020, 12, 43160-43166. DOI: 10.1021/acsami.0c13400
4. **Turan Selman Erkal,** Shamsuddin Norazanita, Serdal Kirmizialtin and A. Ozgur Yazaydin, “Computational Investigation of Structure-Function Relationship in Fluorine Functionalized MOFs for PFOA Capture from Water” (Manuscript under revision)

Contents

List of Figures

List of Tables

Chapter 1. Introduction

Environmental pollution has been one of the most significant topics of the world for a long time. Despite vast effort to clean environment and prevent further pollution, the effects of pollution are still affecting and endangering the health of living beings. Due to high industrialization and rapid advancement in science and technology, the adverse results of them are detected or recognised generally after the negative effects on environment become obvious and create serious problems in nature, animal health or habitat. Although the negative effects of chemicals like pesticides can show their toxicity by damaging plants [3], the effects of some chemical pollutions cannot be detected until after long term exposure, which is detected after human health starts to be influenced by pollutions. There are three major types of pollutions that are air, water and soil [4, 5].

History of air pollution can go back to early times but London fog in 1952 event is one of the important incidents that shows adverse health effects of air pollution [6] and similar event in Meuse valley, Belgium in 1930 [7]. The main reason of these pollutions is related to industrialization that has led to increase in the consumption of fossil fuels, and diesel engines have found application to be used both in industry and transportation [8]. The result of these events was observed by lung problems and mortality of people [6-8]. However, car exhausts and industrial fumes dispersed particles into air and can cause long term effects that can be detected later after accumulation within human body and this accumulation does not affect only lungs but also various systems like cardiovascular, nervous, digestive, urinary systems and DNA mechanism [9, 10].

Soil pollution has been caused by different sources: industrial activities, mining, waste and sewage disposal, agricultural activities and urbanisation [11]. These activities result in accumulation of pollutants like heavy metals, pesticides, pathogenic microorganisms and persistent organic pollutants in soil [11]. The soil pollution can influence the growth of plants, soil fertility and eventually affect human health [12]. Therefore, different types of removal methods are applied to clean soil from pollutants. These methods are categorised in to three methodologies that are physical, chemical and biological [11]. One of the pollutant removal methods is adsorption that can be physical, chemical or both physical and chemical.

This thesis focuses on water pollution and removal of pollutants from water. Like soil pollution water pollution can be caused with different sources which can be waste products of industrial activities, mining activities that lead to release of heavy metals, agricultural chemicals like fertilizers or pesticides and oil spills etc. [13] Among many water pollutants this thesis focuses on one type of resilient pollutant; which are not degraded or eliminated easily hence needed to be captured to prevent its harmful effects; and understanding its removal mechanism with porous materials.

1.1. Per- and polyfluoroalkyl substances (PFAS) pollution in water

The release of chemicals to the environment, whether accidental or as a result of their utilization, has inevitably led to the contamination of soil and ground water [14, 15]. One group of pollutants that has attracted a great deal of attention recently is per- and polyfluoroalkyl substances (PFAS) that are composed of fluorinated carbon chain and functional group like perfluorobutanoic, perfluoropentanoic, perfluorooctanoic acids (PFOA), perfluorobutane and perfluorooactane sulfonic acids (PFOS) [16]. These toxic compounds are found in various household products and

used in different industries such as textile, carpeting, leather and fire-fighting [17, 18]. PFAS are known to be highly resistant to degradation and decomposition due to the strong carbon-fluorine covalent bonds, as such they are ideal for use in harsh conditions [19]. But the chemical stability of PFAS also means that they do not break down in nature, as such they are considered as persistent polluters. PFAS easily contaminate soil and eventually get into the ground water [19-23]. The concentration of total PFAS in soil ranged from <0.001 to 237 μg/kg, among them PFOA and PFOS are the most commonly found [23]. Due to PFAS pollution of a wide range of water sources they have even been found in bottled drinking water [24]. Furthermore, toxicology tests carried out on human urine and serum samples detected concerning amounts of PFAS [25]. Human and animal studies of PFAS revealed that these substances can lead to neurological, liver and lung problems and disrupt the hormonal balance [26-29]. Additionally, the cancerous effect of PFAS was investigated and results indicate that PFAS exposure increases the risk of getting kidney and testicular cancer [1].

1.2. Removal techniques of PFAS from water

Currently, the removal of PFAS from water applications can be performed at individual home water treatment, public water system and wastewater treatment plants by filters to prevent harmful effects of this toxic substance [30, 31]. Although filtrations are applied to remove this toxic substance, the removal of PFAS from water has been investigated extensively to improve the efficiency of cleaning water supplies from PFAS due to their potential harmful effects. Biological degradation of PFAS with fungal enzymes, microorganisms or their removal with phytoremediation are simple, cost-effective and environmentally friendly methods, yet require several

months to work [32]. Degradation of PFAS in water with oxidation processes; i.e. chemical, photochemical or ultrasonic, can be an effective method but scaling up of oxidation processes for the removal of large amounts of PFAS is not trivial [32-34]. Another method to remove PFAS from water is coagulation. Several coagulants such as alum and iron salts have been employed to precipitate PFAS in water [16, 32, 35]. While coagulation is an effective method in laboratory, difficulties in controlling agglomeration and possibility of side reactions present challenges for its commercial application for PFAS removal [32]. In addition to the aforementioned methods, PFAS can also be removed from water by adsorbents. As one of the cheapest and simplest adsorbents, activated carbon (AC), which is already used for water remediation and filtering applications, both in powdered and granular form, has been tested for PFAS removal and often considered as benchmark material for all new adsorbent techniques on perfluorochemicals. [16, 32, 35]. This benchmark materials performed 20-40% efficiency for perfluorooctanoic acid (PFOA) and 40-50% efficiency for perfluorooctanesulfonic acid (PFOS) based on a study on granular activated carbon water filters in 2022 [36]. Other carbon based adsorbents, such as carbon nanotubes (CNTs) and graphene, have higher specific surface areas, porosity and adsorption capacity, hence better PFAS removal performance compared to AC, but they are also more expensive [37]. Ion exchange resins capture PFAS through electrostatic and hydrophobic interactions [16, 18, 37, 38], and some of them showed better PFAS better performance and adsorption capacity (4-5 mmol/g) compared to AC (around 1 mmol/g) [16, 37]. However, regeneration (removing the adsorbed chemical from materials) of the ion exchange resins have been a formidable issue that still needs to be addressed to be able to reuse the resins repeatedly [16, 18, 39]. Other polymeric

materials such as polyaniline nanotube (PANT), which is more porous than resin polymers, demonstrated high affinity to PFOA and PFOS when they are in their anionic forms in low pH solutions [32, 40, 41]. The affinity of polyaniline materials is investigated by adsorption studies that indicated polyaniline adsorbent removed 98% of PFOA from aqueous solution [42]. Polymer networks that contain macrocyclic hosts such as calixarene or β-cyclodextrin have shown promising performance for capturing PFAS from water [41, 43, 44]. Besides polymeric materials, Zeolites, which are crystalline and microporous materials, have been studied both experimentally and computationally for PFAS removal from water [45, 46]. In particular, zeolite Beta showed faster adsorption kinetics and larger uptake compared to AC [45]. Similar to zeolites, covalent organic frameworks (COFs) and metal organic frameworks (MOFs) are porous crystalline structures. Amine functionalized, triazine based and cationic forms of COFs have been used as PFAS removal agents from water [47-49]. Likewise, MOFs such as ZIF-7, ZIF-8, UiO-66, MIL-101(Cr) and NU-1000 have been considered for PFAS removal and their performance were studied experimentally [50-53]. These experimental studies on MOFs indicated that there are different adsorption mechanisms for PFAS removal from water. For instance, the study with UiO-66 MOFs compared the fluorinated and non-fluorinated version of UiO-66, which concluded that hydrophobic interaction between pollutant and adsorbent has significant effect on adsorption efficiency [50]. However, the study with zeolitic imidazole frameworks (ZIF) discovered how crystal structure and surface functionality determine the adsorption performance of MOFs [51].

Among all the removal methods adsorption is the effective and cost efficient one, hence AC is currently employed commercially at home scale and in water

treatment places to adsorb PFAS from water. Due to the promising PFAS removal results this thesis will focus on investigating the adsorption mechanism of PFAS molecules on calixarene based polymers and MOFs. In order to provide better understanding for the thesis, Chapter 2 will deliver literature review information on three pivotal subjects: calixarene molecules, metal organic frameworks (MOFs) and the fluorination methods applied to MOFs. Chapter 3 will explain simulation methods and their background information that are applied in this thesis. After essential understanding on materials and techniques Chapter 4 will present study on removal of one of the PFAS from water that is collaborated with experimental study. Chapter 5 will explain the adsorption mechanism of a perfluoroalkyl substance within MOFs and investigate how fluorination influence the adsorption mechanism of the molecules. Chapter 6 will cover the adsorption study of perfluorooctanoic acid within MOFs and zeolite structures. Finally, Chapter 7 will explain the conclusion of the researches performed in the thesis and provide insight about future studies that can be performed to improve what has been discovered in the thesis.

Chapter 2. Literature Review

In this chapter, an overview of the materials, chemicals and techniques employed in this thesis will be presented. This background information help providing more comprehensive understanding why these materials, chemicals and techniques employed. Firstly, calixarene compounds and their capturing ability will be explained, Secondly, metal organic frameworks and their wide range of application characteristics will be presented. Finally, functionalization methods of metal organic frameworks will be explained to give better understanding for upcoming chapters.

2.1. Calixarenes

Calixarenes are an important part of macrocyclic host family and due to their functionalization ability and widespread application of capturing characteristics they can also be employed to adsorb toxic substances. Calixarenes are phenol-derived cyclic oligomers that are discovered in 1940s by Zinke [54]. However, the importance of this discovery was not noticed until 1970s. Gutsche et al. developed the synthesis method of the cyclic oligomers and called this cyclic oligomers as calixarene (In Greek calix means chalice and arene indicate the involvement of aromatic ring in the structure) [55, 56]. This development made it possible to explore characteristics of these compounds because this new method increases yield and success of the synthesis [54]. Hence, calixarene compounds become more accessible for different research areas. During the extensive research on calixarenes scientists have found out that their chemical and physical properties can be modified based on the need of the application by changing the functional groups upper and lower rim parts in addition to introducing different conformation to calixarene compounds. Calixarene macrocyclic compound

composed of upper rim and lower rim parts that can be functionalized for different purposes (Figure 2-1) [57].

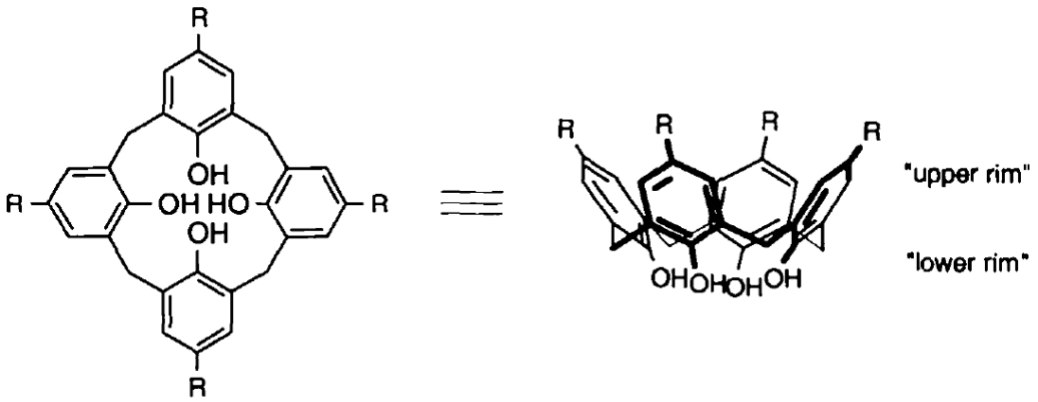

Figure 2-1. Schematic of calixarene [57]

In addition to the functionalization of the two rims of calixarene, these molecules can be also found in different conformations [57, 58]. The conformations of calixarene influence the behaviour of calixarenes because the position of hydroxyl groups are changing. This leads to hydrogen bonding capabilities of molecules with each other and in case of interaction with guest molecules the conformation determine how strongly calixarene molecule attach to guest molecules [58, 59]. Four different conformations of calixarene are determined that are named cone, partial cone, 1,3-alternate and 1,2-alternate (Figure 2-2) [54, 58-60].

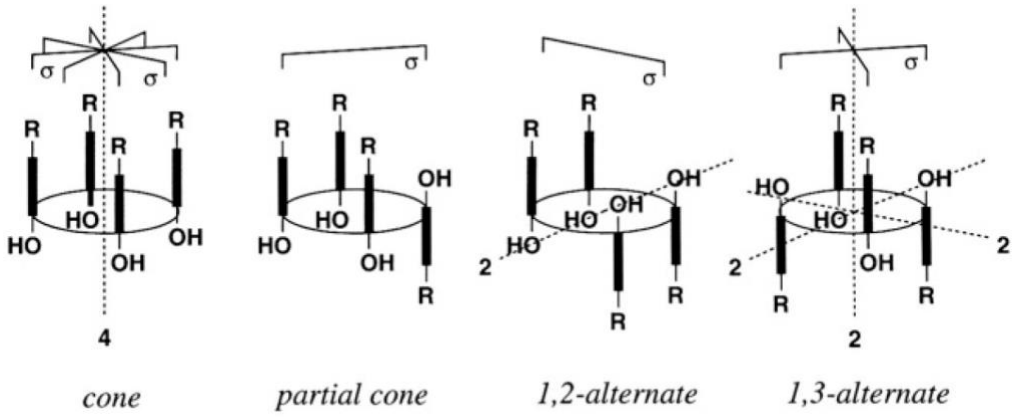

Figure 2-2. Schematic of four different conformations of calixarene [54]

Due to aforementioned characteristics of calixarenes they can be employed for different purposes in different areas by modifying the functional groups and conformation of the calixarene structure. In pharmacology calixarenes can be applied with photodynamic therapy as anti-cancer agent, their catalytic and inhibitor activity are helpful to control biological enzymatic activities, with the help of functionalization of calixarenes drugs that are insoluble in water can be delivered to body and are detected to analyse solutions and captured for purification [61]. Another function of calixarenes are recognition of metal (alkali, alkaline earth and transition metals) ions and capturing them from water and aqueous solutions through coordination between ions and phenol group in lower rim [62-64]. Calixarenes cannot only recognize specific ions but also detect chiral molecules by introducing the chirality within cavity of calixarenes [64, 65]. Hence, they can be used for enantiomer separation or asymmetric synthesis to acquire desired isomer [64-68]. Due to desired chemical capturing ability of calixarenes from aqueous solutions they are viable candidate to remove toxic molecules from water.

2.2. Metal Organic frameworks

Metal Organic Frameworks (MOFs) are coordination polymers that are comprised of metal ions and organic ligands to form one - (1D), two- (2D) or three-dimensional (3D) structures [69, 70]. These polymers are crystalline solid structures that have regular porosity from micro to nanopore scale [71]. MOFs are built through the self-assembly of organic linkers and metal ions or metal containing nodes (secondary building units-SBUs), which are like coordination centres (Figure 2-3) [71, 72]. Since these structures are the combination of two building blocks, they can contain the properties of both building blocks and even if currently over 90,000 MOFs have been synthesized and over 500,000 predicted [73], there are still numerous possibilities of creating different MOFs because every possible metal node can be combined with each possible organic linker.

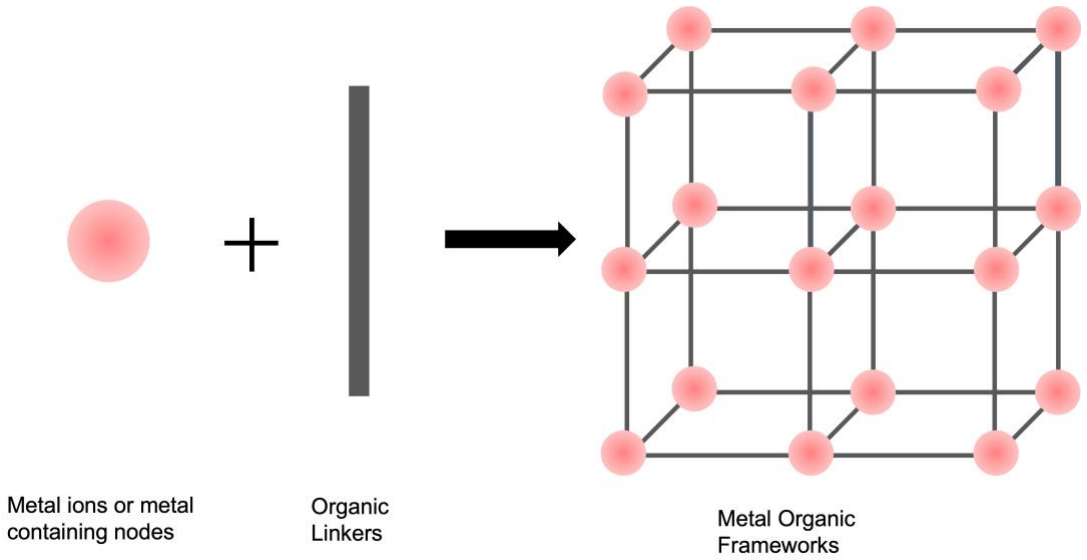

Figure 2-3. Schematic of building metal organic frameworks

The porous characteristics of these materials make the diffusion of guest molecules easier, hence these materials prone to accept guest molecules into the

structure and keep guest molecules within the pores. The porosity of these materials can be extremely high that free volume of the structure can go up to 90% and this high porosity helps acquiring high internal surface area [74]. In addition to porous characteristics, the chemical environment of pores, internal surface area and surface of MOFs can be determined and modified easily. The desired chemical properties can be introduced by either building blocks or post-synthetically modifying the structure [75].

Having high porosity and surface area makes MOFs an important material to be used as an adsorbent that can be applied for capturing and storing. In addition to capturing and storing, the adsorptive characteristics of MOFs indicate that these materials can interact with other molecules strongly, which is also significant for other applications like sensing, detecting or catalytic activities. Besides these properties, MOFs have the flexibility to adjust chemical environment, size and shape of pores and surface areas. Therefore, MOFs are versatile and excellent candidate to be employed in various areas of science and industry.

The capturing and storing ability of MOFs are exploited for different purposes and applications. One of the application areas is capturing greenhouse gases like carbon dioxide (CO_2) and other toxic gases like nitrogen oxides (NO_x) and sulphur dioxide (SO2) as a result of combustion of fossil fuels [76, 77]. Among aforementioned gases CO_2 has significant adverse effect on nature and its capturing methods are investigated extensively in cases like pre-combustion and post-combustion gas capturing, using membranes to separate CO_2 from gas mixture, and employing adsorptive materials like activated carbon, zeolites and MOFs [78]. The capturing mechanism employed by MOFs is through adsorption and the capture of

CO_2 can be applied by direct air capture (DAC) from atmosphere, or capturing it after combustion of fossil fuels in industry [76]. To increase the effectivity of DAC plants MOFs can be a viable option because water molecules in the air can be a significant obstacle to capture only CO_2 molecules, hence core-shell MOF design, which consists of a core MOF structure that is surrounded by another MOF results in a composite material, is presented to overcome this issue [76]. In addition to employing core-shell design to capture CO_2, MOFs' capturing ability can also be improved by ligand functionalization with amine, amide, carboxylate and other functional groups [79]. Although ligand functionalization decreases the porosity of MOFs, it enhances the interaction between MOFs and CO_2 molecules[79]. In another attempt of increasing the CO_2 adsorption capacity, MOF structure is modified with simple annealing procedure, which creates defects that provide more binding sites for CO_2 molecules without disrupting stability and order of the structure [80].

2.3. Fluorine functionalization methods applied on MOFs

Due to fluorine rich chemistry of PFAS, adsorptive materials with fluorine rich environment have been studied to exploit fluorine-fluorine interaction and hydrophobic interaction mechanism by scientists. The fluorine rich environment can be introduced by functionalization of existing adsorptive materials and there are materials with promising results that show positive effects on capturing PFAS through fluorine functionalization [43].

As we know MOFs' chemical environment can be modified or introduced with various methods. Desired chemical environment can be introduced either during synthesis process using modified linkers and node or post-synthetically implement desired atoms or molecules in the structure.

- The first method fluorination method is through introducing fluorinated anions into the structure. These anions are proved to be effective repel water molecules from the porous network, hence it can provide necessary environment for capturing fluorinated molecules from water solutions.

- Another method fluorination technique is using trifluromethyl or fluorine substituted ligands. These ligands are acquired before the synthesis procedure of MOFs and used during the synthesis.

- A third method is functionalizing the MOFs post-synthetically. It is proven that MOFs can be functionalized in different ways with various molecules after acquiring the structure [75] and this post-synthetic modification is very helpful for keeping the robust structure and many original characteristics of the structure. Besides, keeping the desired intrinsic capability of the structure additional characteristics can be introduced with modification of the chemical environment within the structure.

Chapter 3. Simulation Methods and Theory

In this chapter, an overview of molecular simulations, molecular interactions and force field parameters, different types of simulation methods will be explained. Molecular simulations can help us understand and examine molecular behaviour at atomic and molecular level, hence provide detailed knowledge of molecular mechanism. This leads to reducing experimental costs and environmental impact of chemicals by eliminating unnecessary experimental procedures.

3.1. Molecular Simulations

One and a half centuries ago the discovery of thermodynamics has changed the scientific understanding of the world drastically. The first law of thermodynamics on the equivalence between heat and work and the introduction of the concept of entropy were two of the greatest achievements in early thermodynamics. Although revolutionizing the study of nature in many ways, thermodynamics cannot explain the causal relationships behind the phenomena that it describes. The laws of thermodynamics can for example describe the expansion of gases when heated, yet they do not explain underlying principles of the behavior of gases.

Statistical mechanics is the tool that answers the question of why. In statistical mechanics, the motions of atoms and molecules such as translation, rotation and vibration. are described in a mathematical framework. This framework can also be used to derive thermodynamic relationships.

Partition functions are key elements of statistical mechanics' mathematical framework. To define these partition functions, we first need to define the existence probability ($1/_Z\, e^{-\frac{E_i}{k_B T}}$). Existence probability defines the likelihood that a single

state will occur and it has a Boltzmann distribution. Sum of all such Boltzmann distributions over all possible states is defined as a partition function.

$$Z = \sum_{i} e^{-\frac{E_i}{k_B T}} \qquad (1)$$

E_i is energy of the i-th state, k_B is the Boltzmann constant and T is absolute temperature

Partition function of a canonical ensemble system with discrete energy levels is shown in equation 1. If the energy levels of the system are continuous, an integral is used instead of summation. Total number of particles in the system *(N)* defines the dimension of this integral. This integral becomes intractable in the thermodynamical limit as N goes to Avogadro number.

Some believed that computers could be used in calculating those intractable heavy integration [81]. But later, thanks to advances in both computing hardware and algorithms, simulation became more important than the calculation.

Before moving in to these simulation algorithms, we will revisit equation 1. E_i is defined as the energy of **i^{th}** state in equation 1. Hamiltonian mechanics provides the mathematical framework to describe the energy of a state. In this approach, "The Hamiltonian (H)" needs to be defined that connects every state to its energy. Hamiltonian consists of a kinetic and a potential part. The potential part is related to position coordinates, whereas the kinetic part is related to the momentum coordinates of the state.

$$\mathrm{H}(r_1, r_2, \ldots . r_N, p_1 \ldots . p_N) = K(p_1, \ldots . p_N) + V(r_1, \ldots . r_N) \qquad (2)$$

Kinetic part is defined as a simple quadratic equation between momentum (p) and energy. Defining potential part of Hamiltonian is not trivial, it will be revisited in detail in the "Molecular Interactions" section.

3.2. Molecular Interactions

The interaction between atoms and molecules is an important research area and comprises an inevitable step toward modelling materials. Molecular interactions affect molecular motion, which in turn determines molecular trajectories. Inter- and intramolecular interactions are two main classes of molecular interactions. Historically, the first studies of molecular interactions were modelled for simple ideal gases and hard spheres, which means that studies of intermolecular interactions began earlier than studies of intramolecular interactions.

A simple representation of the interactions between hard spheres can be defined by the Lennard-Jones potential as follows:

$$V_{LJ}(r_{ij}) = 4\varepsilon\left[\left(\frac{\sigma}{r_{ij}}\right)^{12} - \left(\frac{\sigma}{r_{ij}}\right)^{6}\right] \quad (3)$$

In this equation, r_{ij} is the distance between the **ith** and **jth** particles. Size and interaction are defined by σ (nm) and ε (kJ/mol). The 6-term corresponds to the attractive part of the Lennard-Jones potential, while the 12-term corresponds to the repulsive part. For charged particles, the electrostatic interaction should also be considered. The Coulomb potential for the electrostatic interaction can be written as follows:

$$V_C(r_{ij}) = \frac{1}{4\pi\varepsilon_o}\frac{q_i q_i}{r_{ij}} \quad (4)$$

In this equation, ε_o is the vacuum permittivity, r_{ij} is the distance between the **ith** and **jth** particles and q_i and q_j are the electron charges around particle **i** and **j**, respectively.

Intramolecular interactions can be described as below. In this equation, the total energy of the bonded system is written as a Taylor expansion-like expression:

$$\begin{aligned} \mathrm{U} = \sum_{bonds} u_b(r) + \sum_{bends} u_\theta(\theta) + \sum_{torsion} u_\phi(\phi) + \sum_{improper} u_\chi(\chi) \\ + \sum_{bond-bond} u_{bb'}(r, r') + \sum_{bond-bend} u_{b\theta'}(r, \theta') \\ + \sum_{bend-bend} u_{\theta\theta'}(\theta, \theta') + \cdots \end{aligned} \quad (5)$$

Here, the first term corresponds to the harmonic interaction between two bonded atoms, the second term corresponds to the harmonic bending interaction between three bonded atoms, and the third term corresponds to the periodic interaction between four bonded atoms, and so on. For simplicity, we have used the first three terms to model the interactions between bonded atoms.

For Eq. 3, Eq. 4 and Eq. 5, a set of pre-defined parameters called "force fields" are needed. AMBER [82], OPLS [83], CHARMM [84], DREIDING [85] and UFF [86] are some widely known examples of generic force fields.

3.3. Molecular Simulation Methods

Two of the most common simulation methods for materials modelling at the molecular level are Monte Carlo simulations and Molecular Dynamics methods. Monte Carlo (MC) is method for determining the equilibrium properties of materials,

whereas Molecular Dynamics (MD) is a method for realistically describing the dynamics of microsystems. MC is a probabilistic method, while MD is a deterministic one.

3.4. Monte Carlo (MC) Simulations

We will revisit the partition function given in equation 1. In statistical mechanics, the mean value of an observable A can be calculated using the following equation:

$$< A \geq \frac{\sum_i A_i e^{-\frac{E_i}{kT}}}{\sum_i e^{-\frac{E_i}{kT}}} \qquad (6)$$

As stated earlier, the summations in equation 6 turn into integration when the energy spectrum system is continuous. Moreover, the energy term should be calculated as a Hamiltonian, which is a function of position and momenta. Thus, the integration is done over the coordinates r and p of the system. Thanks to the quadratic relation between the kinetic part of the Hamiltonian and the momenta, the integration over the momenta is analytically solvable. However, the complex dependence of the Potential part of the Hamiltonian on the position complicates the integration over the position coordinates. If the observable A in equation 6 depends only on the position coordination, the equation becomes:

$$< A >= \frac{\int dr_1 dr_2 \ldots . dr_n e^{\frac{U(r_1,\ldots,r_N)}{kT}} A(r_1, \ldots, r_N)}{\int dr_1 dr_2 \ldots . dr_n e^{\frac{U(r_1,\ldots,r_N)}{kT}}} \qquad (7)$$

Computation of partition functions is not feasible for large systems (N > 100) and for complex functional forms of potential energy. Monte Carlo simulations provide an alternative way to estimate this integration. In MC simulations the phase

space is sampled with random movements. Starting with an initial system configuration and then randomly jumping to a new system configuration, they calculate the energy difference between the configurations (ΔU) and the Boltzmann factor with the energy difference ($\exp(-\Delta U/kT)$. Then, they use this Boltzmann factor to decide whether or not to accept the new configuration by choosing energetically favourable position.

3.5. Grand Canonical Monte Carlo (GCMC) Simulations

The simulation conditions can be set to sample the desired characteristics of the system and MC simulations can be performed in various ensembles such as canonical, microcanonical, isothermal-isobaric, and grand-canonical ensembles [87]. In each of these ensembles, certain conditions such as temperature, pressure, energy, etc. are kept constant. In the case of the grand-canonical ensemble, the chemical potential (μ), volume (V) and temperature (T) of the system are fixed. This ensemble is very common for adsorption simulation because, unlike other ensembles, the total number of particles is not fixed and it can give the average number of particles under certain external conditions.

3.6. Molecular Dynamics (MD) Simulation

Molecular Dynamics simulation is a deterministic approach rather than a statistical one and is based on the integration of Newton's equation of motion. In a given time period, the trajectories and forces are calculated. The intermolecular force between molecules i and j can be calculated as follows:

$$f_{ij} = -\frac{\partial u_{ij}}{\partial r_{ij}} \tag{8}$$

In Eq. 8, f_{ij} stands for the intermolecular forces between particles i and j, u_{ij} for the intermolecular potential energy, and r_{ij} for the distance between particles i and j. After determining the forces between all particles in the initial configuration, Newton's equations can be integrated. According to the Leap-Frog algorithm (Hockney, Goel, and Eastwood 1974), Newton's law of motion is integrated by discretising the differential definition of acceleration and velocity:

$$v\left(t+\frac{1}{2}\Delta t\right)=v\left(t-\frac{1}{2}\Delta t\right)+\frac{\Delta t f(t)}{m} \tag{9}$$

$$r(t+\Delta t)=r(t)+\Delta t v\left(t+\frac{1}{2}\Delta t\right) \tag{10}$$

$v: velocity, t: time, r: position, f$: force, m: mass

The Leap-frog algorithm uses forces to update the velocity at the mid-time interval and the updated velocity to update the position data, as shown in Eq. 9 and Eq. 10.

3.7. Tricks of Trade

Calculation interactions between too many particles is computationally infeasible. A number of "tricks" (methods) have been applied to reduce the computational time for molecular simulations.

The number of particles is excessively limited with respect to the thermodynamic limit of the particles. To overcome this limitation, Periodic Boundary Conditions (PBC) is a commonly used trick. In PBC, a single cell of the simulation box (indicated with green box in Figure 1) is treated as the center of a periodic lattice of identical cells. When PBC is applied, the number of pairwise interactions increases

due to the periodic “images” of the particles within the simulation box. To overcome the issue of increased number of image’s interactions, the minimum image convention is applied. This implies that each particle can interact with only one single “image” of any other particle.

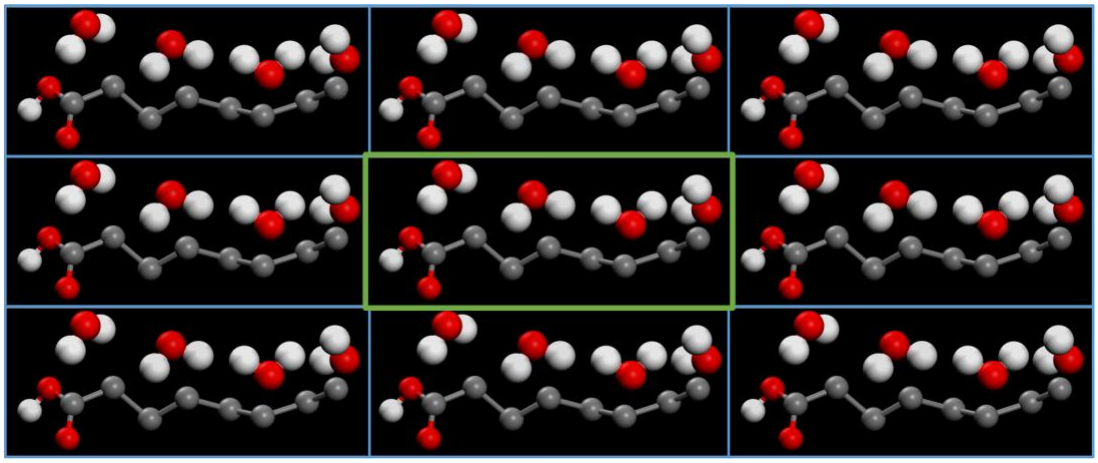

Figure 3-1. Periodic boundary condition in molecular simulations

Another short cut implementation to reduce the calculation of the amount of interactions is the *cut-off radius*. This trick implies that only interactions within the cut-off radius around a particle are taken into account and the interaction across the truncation is implicitly accounted for.

The implicit correlation to the total energy is called as the tail correction and is calculated as follows:

$$\Delta U_{tail} = \frac{\rho}{2} \int_{r_c}^{\infty} u(r) 4\pi r^2 dr \qquad (11)$$

In Eq. 11, ρ is the molecular density, $u(r)$ is the pairwise interaction between the molecules, and r_c is the cut-off radius.

An additional approximation for the calculation of Lennard-Jones sites is the *Lorentz-Berthelot mixing rule,* which suggests the calculation with the following approach:

$$\sigma_{AB} = \frac{\sigma_A + \sigma_B}{2} \tag{12}$$

$$\varepsilon_{AB} = \sqrt{\varepsilon_A \varepsilon_B} \tag{13}$$

The Lennard-Jones interaction between type A molecules and type B molecules can be calculated using the parameters defined in Eq. 12 and Eq. 13.

3.8. Density Functional Theory (DFT)

MC and MD modellings based on probabilistic and deterministic approach to molecular simulations. Hohenberg, Kohn and Sham developed a quantum mechanical modelling method approach to perform realistic calculations of properties of atoms, molecules and solids [88]. Although quantum mechanical calculations were needing too much calculation power, density functional theory (DFT) introduced effective approximations that decrease computational need and made probable to use quantum mechanical approach to perform simulations. By employing this model electronic, optical and mechanical properties of solid state materials can be calculated.

Chapter 4. Investigation of perfluorooctanoic acid removal from water in fluorine-rich calixarene-based porous polymers with molecular simulations

The study presented in this Chapter was published in 2020 in volume 12, pages 43160-43166 of ACS Applied Materials & Interfaces.

4.1. Introduction

One of the most widely used perfluoroalkyl substances (PFAS) chemical found in water resources is perfluorooctanoic acid (PFOA) [89]. The removal of perfluorooctanoic acid (PFOA) can be performed by degradation, coagulation or adsorption. Among these methods we investigated the adsorbent materials that can capture the PFOA molecules (Figure 4-1), which are dissolved in water. In this chapter

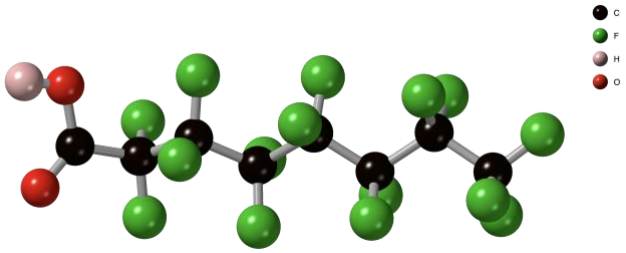

Figure 4-1. All atom PFOA molecule

among many adsorbent materials calixarene-based polymers are examined due to selective and effective capturing ability of calixarene compounds. The macrocyclic structure of calixarene molecules and fluorinated linkers of calixarene-based porous polymer can improve the interactions between PFOA molecules and polymer network. The non-fluorinated and fluorinated calixarene based polymers in this study are CX4-

P, CX4-BP, FCX4-P and FCX4-BP because of their adsorption capacity and efficiency [43]. The monomers of these polymers are indicated in Figure 4-2.

4.2. Materials and Methods

Monte Carlo (MC) simulations were carried out to understand the physical mechanism of PFOA binding and how binding properties change as the chemistry of the polymer is varied. Given the size of the PFAO molecules and amorphous nature of the polymers, probing the binding energy landscape of the calixarenes with a guest molecule is deemed to be a more efficient approach than undertaking PFOA+water mixture adsorption simulations. In this approach a PFOA molecule (Figure 4-1) was used to exhaustively probe the accessible surface of the calixarene polymer sheets to identify preferred binding sites. Same procedure was employed with a water molecule for comparison.

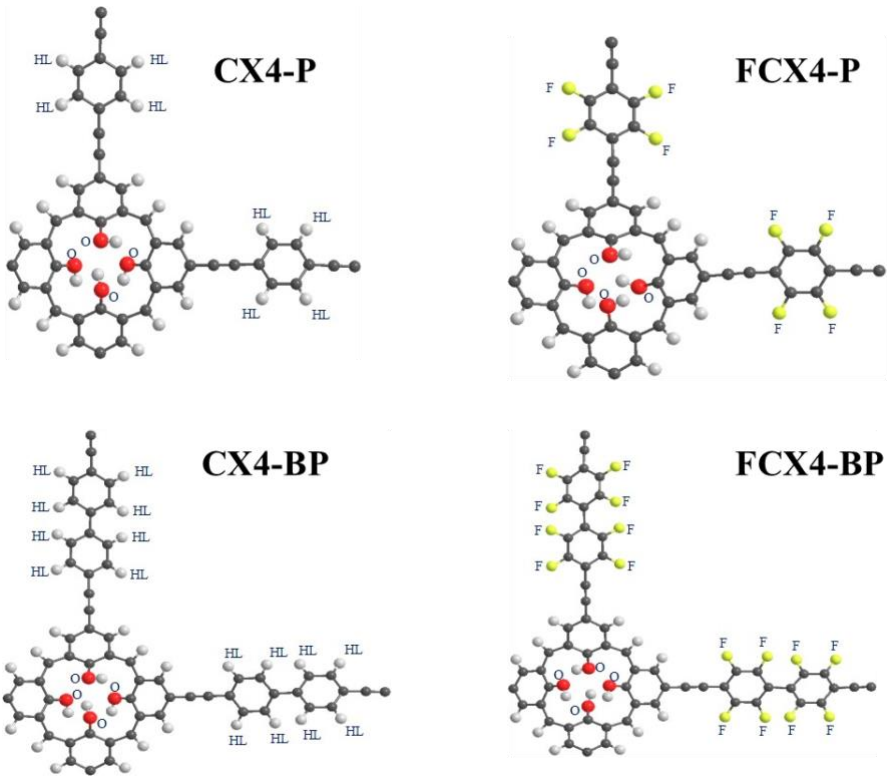

Figure 4-2. The monomers that are used to construct the polymeric sheets

4.2.1. DFT calculations

Given the highly mesoporous nature of the polymers it would have been impossible to construct atomistic models that would reproduce the surface area and pore size distribution of the polymers. Therefore, polymer sheets of CX4-P, CX4-BP, FCX4-P and FCX4-BP were constructed. For this, unit cells, which contain periodic monomers of CX4-P, CX4-BP, FCX4-P and FCX4-BP, were first geometrically optimized with plane wave density functional theory (DFT) calculations. The dimension and angles of the unit cells were allowed to vary independently to allow complete relaxing of the polymer sheets. The periodic dispersion-corrected DFT calculations were carried out using the CASTEP 17.21 software [90] and employing the PBE functional and ultrasoft pseudopotentials with a 550 eV energy cutoff. Once optimized the unit cells were replicated 2 times in the x and y directions. To create simulation boxes for the MC simulations void space was added above and below the polymer sheets.

4.2.2. Monte Carlo Simulations

Single molecule probing of the optimized calixarene polymer structures (Figure 4-3) with PFOA and water were carried out by MC simulations using the RASPA molecular simulation package [91]. Translation, rotation and reinsertion moves of the PFOA molecule and the water were sampled in the calixarene polymer sheet structures with equal probability in the NVT ensemble at room temperature with periodic boundary conditions (PBC) and 2x2x5 unit cell setup. For each system, we ran for 2,200,000 cycles of MC simulations. RDFs were computed from the last 2,000,000 cycles. Since it is a large molecule, 10 independent MC simulations for PFOA were carried out in each polymer to improve sampling and results were

averaged. In the MC simulations Lennard-Jones (LJ) potential was used to account for the short-range van der Waals interactions and the electrostatic interactions were computed using a Ewald sum.

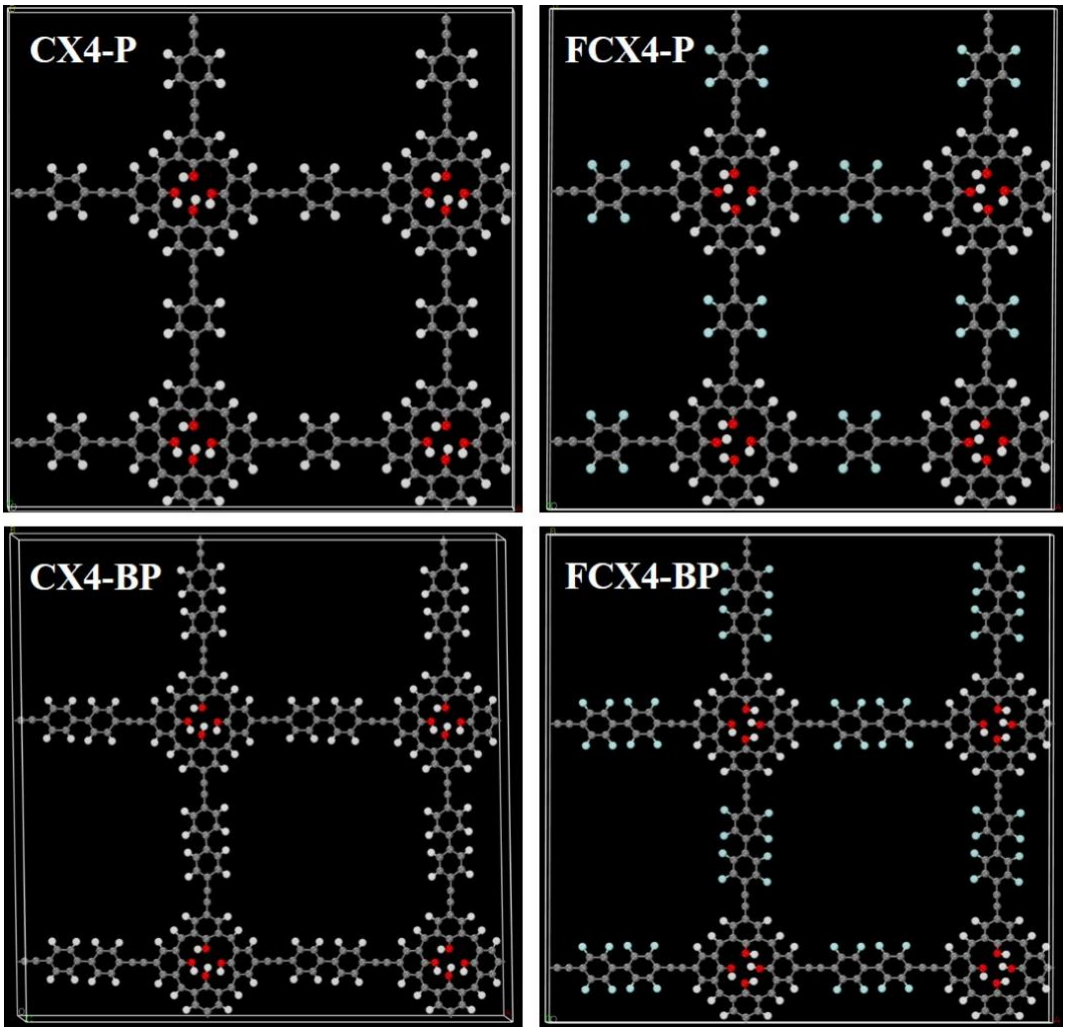

Figure 4-3. Simulation boxes that contain polymeric sheets of **CX4-P** (a=41.45, b=40.967, c=25.0; α=89.15°, β=90.32°, γ=89.99°), **FCX4-P** (a=41.442, b=41.165, c=25.0; α=89.85°, β=90.55°, γ=89.67°), **CX4-BP** (a=49.634, b=49.336, c=25.0; α=91.55°, β=87.89°, γ=90.89°) and **FCX4-BP** (a=49.135, b=49.635, c=25.0; α=89.74°, β=90.88°, γ=89.89°) used in the MC simulations

The cut-off distance for the LJ potential and the real part of the Ewald sum was set to 12 Å. The water molecule was represented by the TIP4P-Ew model [92] while for PFOA we used the CVFF force field [93] with partial charges derived from quantum

chemical calculations obtained using the Gaussian09 software [94]. For the polymer sheets, LJ parameters were taken from the DREIDING force field [85]. Partial atomic charges of the polymer atoms were calculated using the REPEAT method [95], which essentially fits point charges against the periodic electrostatic potential of the polymers derived from DFT calculations using the CASTEP 17.21 software and by employing the PBE functional and ultrasoft pseudopotentials with a 550 eV energy cutoff.

4.3. Results and Discussion

Given the findings of Omorodion et al., who studied the nature of noncovalent interactions in calixarene-PFOA host−guest complexes [95, 96], we speculated that the primary interaction responsible for the successful adsorption of PFOA by the polymers is the hydrogen bond between the carboxylic group of PFOA and a hydroxyl oxygen of the calixarene. We also surmise that additional stabilization may be achieved by C−F···F−C interactions between PFOA and the fluorinated linkers in FCX4-P and FCX4-BP. To test these hypotheses, we resorted to atomistic Monte Carlo (MC) simulations of PFOA and water.

4.3.1. Radial distribution function analysis

Polymer sheet representatives of CX4-P, CX4-BP, FCX4-P, and FCX4-BP (Figure 4-3) were sampled for binding sites using a PFOA and a water molecule. Radial distribution functions (RDF) obtained from MC simulations allowed for comparisons to be made between the interactions of the polymers with PFOA/water (Figure 4-4). The hydroxyl groups of the calixarenes are the preferential binding sites for both PFOA and water. For PFOA, this is evidenced by peaks near 1.8 Å between the oxygen of the calixarenes and the carboxyl hydrogen of PFOA, denoted as O-Ho (Figure 4-4a and Figure 4-6). Similarly, water hydrogen bonds with the oxygen atoms

of the calixarene ring, denoted as O-Hw (Figure 4-4b). It is clear that both PFOA and water are expected to compete for the calixarene ring during adsorption for all polymers, whether fluorinated or not.

For all polymers, we found that hydrogen bonding is the main interaction between the polymer and its environment and that the effect of C-F···F-C interaction is rather marginal (Figure 4-5).

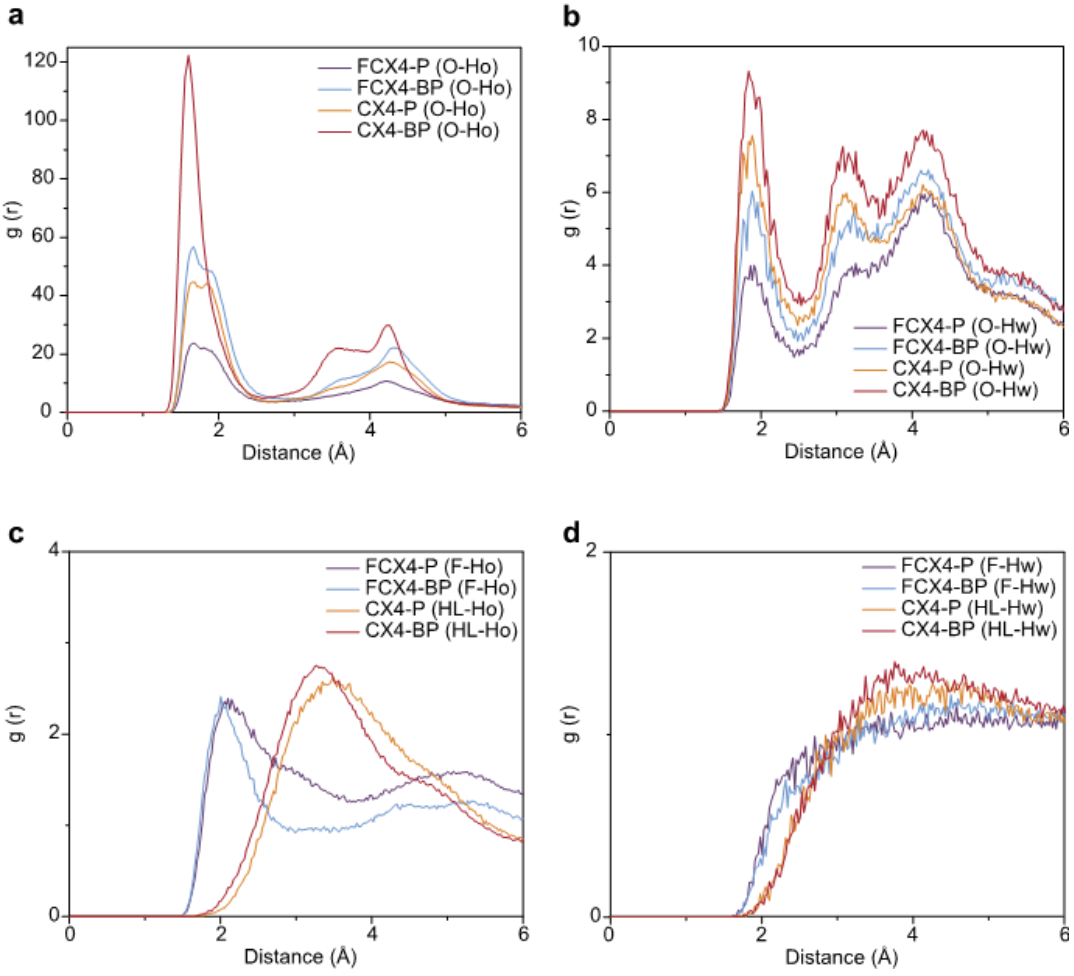

Figure 4-4. Radial distribution functions of specific interactions between the polymers and PFOA/water molecules. (a) O-Ho, (b) O-Hw, (c) HL-Ho and F-Ho, and (d) HL-Hw and F-Hw (O is oxygen of calixarene in all polymers, HL is hydrogen of linkers in **CX4-P** and **CX4-BP**, F is fluorine of linkers in **FCX4-P** and **FCX4-BP**, Ho is carboxyl hydrogen of PFOA, and Hw is hydrogen of water)

Substitution of linker hydrogens (HL) with fluorines (F) in the CX4-P polymer does not result in any change for the PFOA fluorine (Fc) and linker interaction (Figure 4-5). In the case of CX4-BP polymer, substitution of linker hydrogens (HL) with fluorines (F) results in an increase, albeit very small, for the PFOA fluorine (Fc) and linker interaction due to the fact that CX4-BP has a longer linker (Figure 4-5). Longer linker leads to providing more fluorine environment, hence probability of fluorine-fluorine interaction increases. However, still the effect of C-F···F-C interaction is much less significant compared to the change in the hydrogen bonding interaction observed up on fluorination of the linker.

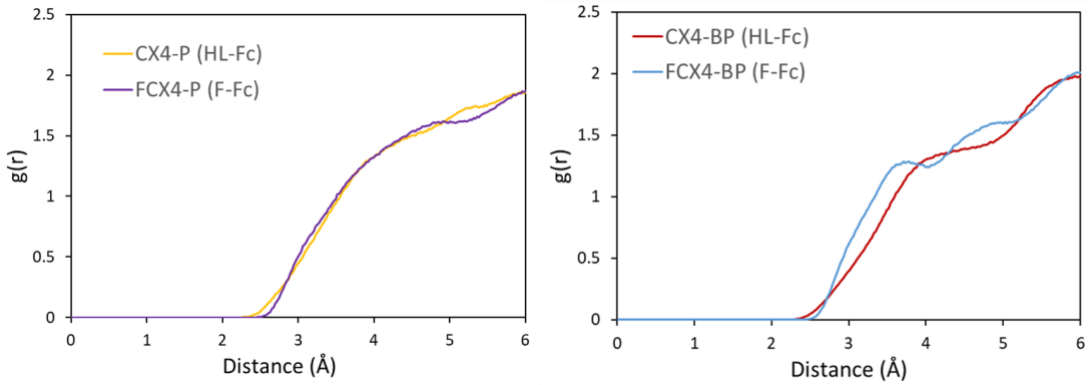

Figure 4-5. Radial distribution functions of interactions between linker hydrogen and fluorine of PFOA (HL-Fc), and between linker fluorine and fluorine of PFOA (F-Fc) in the polymers.

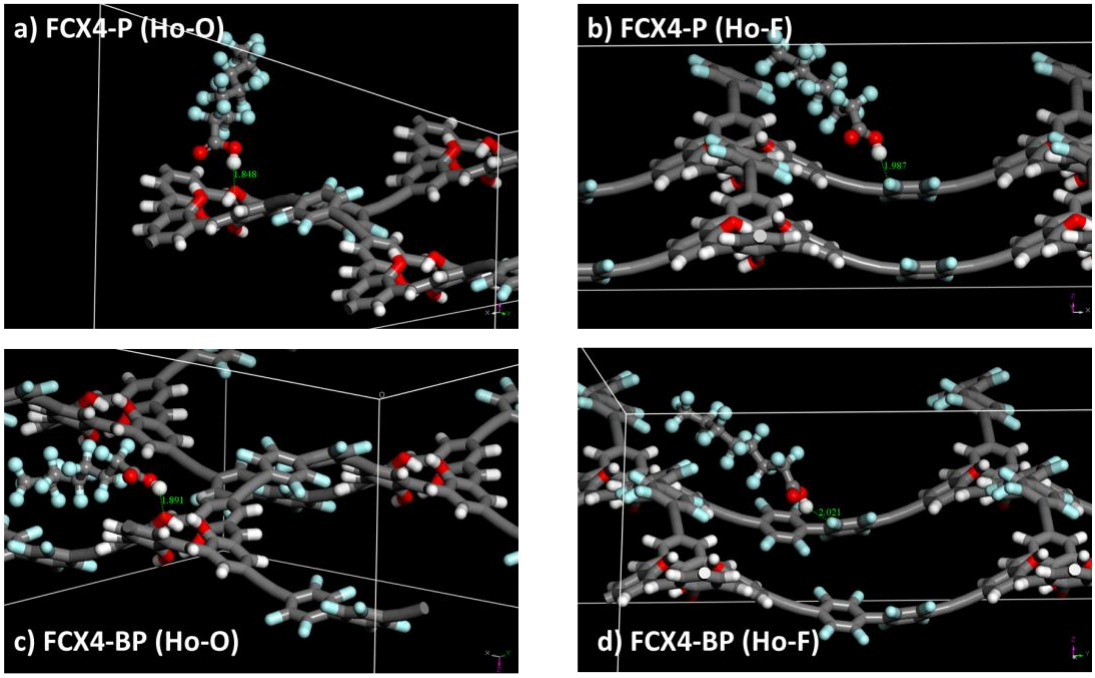

Figure 4-6. Simulation snapshots that illustrate PFOA-polymer interactions (distances are between 1.8-2.0 angstrom)

It was also found that fluorination leads to dramatic changes in the way the linkers interact with PFOA and water. In CX4-P and CX4-BP, the RDFs for the hydrogen atoms of the linkers and the carboxyl hydrogen atoms of the PFOA, denoted as HL-Ho, exhibited broad peaks around 3.4 Å (Figure 4-4c), which indicated that there were relatively weak interactions between PFOA and the linkers. For water, the interactions with the linkers are also limited; as such, the RDFs for the hydrogen atoms of the linkers and the hydrogen atoms of water, denoted as HL-Hw, showed only weak structuring around 3.8 Å (Figure 4-4d). In FCX4-P and FCX4-BP, however, substitution of the linker hydrogen atoms with fluorine atoms resulted in tighter PFOA binding to the linkers. This is demonstrated by the peaks observed at 2 Å in the RDFs for the fluorine atoms of the linkers and the carboxyl hydrogen atoms of the PFOA, denoted as F-Ho (Figure 4-4c and Figure 4-6). To understand the nature of this affinity, we computed the binding energy of PFOA to the polymers (Table 4.1).

Indeed, energy calculations revealed that fluorination increases the binding strength of PFOA to the linkers. The binding energy was reduced by 3.8 and 2.4 kJ/mol for FCX4-P and FCX4-BP, respectively, in accordance with the experimental observations [43] and RDF analysis. On the other hand, after fluorination, as shown above in Figure 4-3d water−linker interactions became weaker as the RDFs between the fluorine atoms of the linkers and the hydrogen atoms of water, denoted as F-Hw, did not show any structuring. This also suggests that fluorine-rich PFOA molecules, when adsorbed, can exclude water adsorption in the pores. All in all, our simulations provide strong evidence that fluorination creates new sites on the linkers for the adsorption of PFOA, which no longer needs to compete with water. In addition, fluorination stabilizes PFOA at the new binding site; resulting in enhanced PFOA binding to FCX4-P and FCX4-BP, as compared to the nonfluorinated polymers, CX4-P and CX4-BP.

4.3.2. Binding energy calculations

In order to quantify the change in the binding energy of PFOA with the polymers a result of fluorination, a PFOA molecule was placed near one of the linkers of CX4-P, CX4-BP, FCX4-P and FCX4-BP. The systems were then energy minimized using RASPA molecular simulation package and employing the Baker minimization method [97]. The binding energy is defined as:

$$\Delta U_{\mathrm{b}} = U_{\mathrm{PL}} - U_{\mathrm{P}} - U_{\mathrm{L}}$$

where, U_{PL}, U_{P}, U_{L} are total potential energies of polymer-ligand complex, polymer, and the ligand (PFOA) respectively. Then PFOA binding energy values for different polymers are shown in Table 4-1. The results presented that fluorination of linker

reduce the binding energy values which mean higher affinity between polymer and PFOA molecules.

Table 4-1. Binding Energy between PFAO and polymers

Calixarene Polymer	ΔU_b (kJ/mol)
CX4-P	-40.2
CX4-BP	-39.0
FCX4-P	-44.0
FCX4-BP	-41.4

4.4. Conclusion

In summary, we investigated the interaction mechanism between PFOA molecule and calixarene-based porous polymers. The effect of fluorination in this polymeric structure indicated the importance of hydrogen bond interaction between carboxylic group of PFOA and hydroxyl group of calixarenes. In addition to hydroxyl group of calixarene, hydrogen atom of PFOA indicate significant interaction with fluorinated polymer structures. Introducing extra binding site into polymers with fluorination improve the PFOA capturing ability of polymer that are strongly supported with experimental and simulation results.

Chapter 5. Computational Investigation of Structure-Function Relationship in Fluorine Functionalized MOFs for PFAO Capture from Water

5.1. Introduction

Previous studies showed that fluorine functionalization can improve the adsorptive removal of PFAS from water in porous materials, such as calixarenes [43], MOFs [50], polymers [98, 99] and graphene [100]. In this work, by employing molecular simulations, we investigate the fluorine functionalization of MOF materials for the removal of PFAS from water. MOFs are crystalline porous inorganic-organic hybrid materials that can be tuned to have desired pore size, shape and chemical functionality. As such, they are an ideal platform to investigate and compare different fluorine functionalization strategies for PFAS removal from water. We use perfluorooctanoic acid (PFOA), which is one of the most widely encountered PFAS in ground water, as the probe molecule in our molecular simulations. The PFOA molecule has a carboxyl group; i.e. hydrophilic head, and seven fluorinated carbons; i.e. hydrophobic tail. PFOA is in white powder form at room temperature, and it melts around 50 ºC.

5.2. Materials and Methods

Fluorinated MOFs considered in this study are shown in Table 5-1. We categorized these MOFs into different groups by following the convention given in Noro et. al [101].

Table 5-1. Fluroinated MOFs considered in this work

Functionalization method	MOF name	Formula	Ref.
Fluorinated anion, AF_6^{2-} (A=Si and Ti) bridging ligands	SIFSIX-1-Cu[a]	C_{20} H_{16} Cu N_4 Si F_6	[102]
	TIFSIX-1-Cu[b]	C_{20} H_{16} Cu N_4 Ti F_6	[103]
	Zn(4,4′-bpy) $_2$ (SiF_6)[c]	C_{20} H_{16} Zn N_4 Si F_6	[104]
	Cu(bpy-1)$_2$(SiF_6)[d]	C_{20} H_{16} Cu N_4 Si F_6	[105]
	SIFSIX-2-Cu[e]	C_{24} H_{16} Cu N_4 Si F_6	[106]
Trifluoromehtyl (-CF3) or fluorine substituted ligands	Zn(C_{17} H_8 F_6 O_4)[f]	C_{34} H_{16} F_{12} O_8 Zn_2	[107]
	FMOF-1[g]	C_{12} Ag_3 F_{18} N_9	[108]
	F-UiO-67[h]	C_{42} $H_{(26-n)}$ F_n O_{16} Zr_3	[109]
Perfluoraalkane grafting	NU-1000-PF[i]	(C_{44} H_{30} O_{16} Zr_3) + C_7 F_{15} COO	[110]

([a]Figure A-1; [b]Figure A-2; [c]Figure A-3; [d]Figure A-4; [e]Figure A-5; [f]Figure A-6; [g]Figure A-7; [h]Figure A-8; [i]Figure A-9)

The first category is fluorinated anion functionalized MOFs where AF_6^{2-} anions (A=Si and Ti) are used as bridging ligands [103-106, 111]. The second category is MOFs which have ligands that are substituted with trifluoromehtyl or fluorine [107, 108]. Two MOFs considered in this category, FMOF-1 [108] and Zn($C_{17}H_8F_6O_4$) [107] have trifluoromehtyl substituted ligands. For MOFs with ligands substituted with fluorine atoms, we considered fluorine functionalized UiO-67, denoted by F-UiO-67. Although a fluorine substituted UiO-67 has been reported experimentally in the literature [109, 112]; we would like to increase the amount fluorination of the UiO-67 gradually like fluorine functionalized UiO-66, which has shorter bridging ligands compared to UiO-67 but the same topology, was reported experimentally [113].

However, the pores of fluorinated UiO-66 are too small for PFOA molecules to enter. Therefore, we computationally constructed fluorine functionalized UiO-67 structures by substituting 25%, 50%, 75% and 100% of the hydrogens on the linkers with fluorine atoms, by following the same incremental fluorine substitution approach employed for UiO-66 experimentally [113]. Third and last category is MOFs that are fluorine functionalized by grafting perfluoraalkanes [110, 114]. In this category, we considered perfluoroalkane functionalized NU-1000, denoted as NU-1000-PF. NU-1000 is a Zr-based metal–organic framework and it was fluorine functionalized by inserting PFOA molecules as charge compensating moieties strongly bound to the Zr_6 nodes by employing solvent-assisted ligand incorporation (SALI) method [110]. Finally, all-silica zeolite Beta (Figure A-10), which is hydrophobic and was shown to be a highly selective adsorbent for PFAS, was included in this study for comparison with fluorinated MOFs [45, 115]. Pore size distribution of the structures were calculated with the Poreblazer v4.0 software [116].

5.2.1. DFT calculations

The crystal structures of MOFs and all-silica zeolite Beta were obtained from either Cambridge Crystallographic Data Centre (CCDC) [117] or from the references given in Table 1 and were geometry optimized with periodic density functional theory (DFT) calculation, which is performed by moving atoms of the structure to acquire the most stable structure with lowest ground state energy. The DFT calculations were carried out with the CASTEP 19.11 software [90]. The PBE functional and ultrasoft pseudopotentials were used with a 550 eV energy cut-off. Partial atomic charges of the geometrically optimized MOF structures were calculated using the REPEAT

method [118], which fits point charges to the DFT derived periodic electrostatic potential of the structures.

5.2.2. Force Field

The force field used in the molecular simulations included non-bonded and bonded interactions. Short-range van der Waals interactions and the long-range electrostatic interactions between non-bonded atoms were computed through the Lennard-Jones (LJ) and Coulomb potentials, respectively, with the following equation:

$$\mathrm{V}(r_{ij}) = 4\varepsilon_{ij}\left[\left(\frac{\sigma}{r_{ij}}\right)^{12} - \left(\frac{\sigma}{r_{ij}}\right)^{6}\right] + \frac{1}{4\pi\varepsilon_o}\frac{q_i q_j}{r_{ij}}$$

Where **V** is the total energy, **i** and **j** are interacting atoms, and r_{ij} is the distance between atoms **i** and **j**. ε_{ij} and σ_{ij} are the LJ well depth and diameter, respectively. q_i and q_j are the partial charges of the interacting atoms, and ε_o is the dielectric constant. LJ parameters between different types of atoms were calculated using Lorentz-Berthelot mixing rules (Eq. 12 and Eq. 13).

Partial atomic charges of MOF atoms were derived from DFT calculations as described in the previous section to have a consistent charge assignment in the whole MOF structure, and Lennard-Jones parameters for MOF atoms were taken from the UFF force field that is widely used force field for MOF simulations due to its adaptability to many chemical environment [86]. The water molecule was represented with the rigid TIP4P-Ew model because Ewald techniques is employed in simulations [92]. For the PFOA molecule, we developed a new model that treats CF3 and CF2

units as united-atom, whereas the atoms on the carboxyl group are treated explicitly to reduce computation time. Force field parameters for the new PFOA model were derived from previous force fields used for perfluoroalkanes [119, 120], ketone [121], alcohols [122] and carboxylic acid [123], and are given in Table 5-2.

Table 5-2. Force Field Parameters of PFOA

atom/group	ε/k_B (K)	σ (Å)	charge	**Ref.**
CF_3	87	4.36	0	93
CF_2	27.5	4.73	0	93
CF_2-(C)	27.5	4.73	0.12	93, 97
C	41	3.9	0.42	97
O=(C)	79	3.05	-0.45	97
O-(H)	93	3.02	-0.46	97
H-(O)	0	0	0.37	97

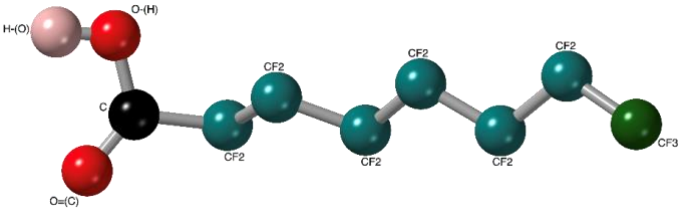

Bond (fixed length)	Length(Å)	Ref	Angle Bend†	θ(deg)	kθ/ k_B(K)	Ref.
CF_3-CF_2	1.54	93	CF_3-(CF_2)-CF_2	114	62500	93
CF_2-CF_2	1.54	93	CF_2-(CF_2)-CF_2	114	62500	93
C=O	1.214	97	H-O-C	107	17600	97
C-O	1.364	97	O-C=O	123	40300	97
O-H	0.97	97	O-C-CF_2	111	35300	97
			O=C-CF_2	126	40300	97

Torsion§	c0	c1	f_1	c2	c3	c4	Ref.
CF_2- CF_2- CF_2- CF_2	0	1666.25	0	247.6	-349.26	-532.94	94
CF_3- CF_2- CF_2- CF_2	0	1666.25	0	247.6	-349.26	-532.94	94
CF_2-CF_2-C=O	2035.58	−736.9	0	57.84	−293.23	0	95
CF_2-CF_2-C-O	0	176.6	0	-53.34	769.93	0	96
CF_2-C-O-H	0	630	0	1562.4	0	0	97
O=C-O-H	0	630	180	1562.4	0	0	97

† $V(\theta_{ij}) = \frac{(k_\theta)}{2}(\theta - \theta_0)^2$

§ $V(\emptyset) = c_0 + c_1(1 + \cos(\emptyset + f_1)) + c_2(1 - \cos(2\emptyset)) + c_3(1 + \cos(3\emptyset)) + c_4(1 - \cos(4\emptyset))$

§ 1-4 interactions are zero

To validate the PFOA model, we did a molecular dynamics (MD) simulation in the NPT ensemble and reproduced the experimental density of PFOA at 1atm and 298K, which is 1.8 g/cm^3.

5.2.3. Molecular Dynamic Simulations

Molecular Dynamics (MD) simulation is performed using RASPA software package to test the derived force field parameter of united-atom model perfluorooctanoic acid (PFOA) molecule. A simulation box with the size of 40x40x40 angstrom is filled with 100 PFOA molecules and molecular dynamics simulation is performed under constant temperature and pressure. The short-range van der Waals interactions were modelled with the Lennard-Jones (LJ) potential and the Lorentz−Berthelot combining rules were used to calculate the cross-interaction LJ parameters by applying shifted potential. The long-range coulomb interactions were calculated using Ewald summation method [124]. Both non-bonded and coulombic interactions were calculated with a 12 Å cutoff distance. NPT simulation is performed 500 000 cycles with Parrinello-Rahman barostat with a coupling time of 0.5 fs at 25^{o}C. As a result of 0.25 ns NPT simulation the density of PFOA molecules was the same as experimental value that validates our model.

5.2.4. Monte Carlo Simulations

Monte Carlo (MC) simulations were carried out i) to calculate Henry's law coefficients of PFOA and water, ii) to probe PFOA and water preferred adsorption sites and iii) to compute PFOA adsorption amount from water in MOFs and zeolite Beta. Henry's law coefficients of PFOA and water were calculated with the Widom's insertion method [125]. To probe preferred adsorption sites, MC simulations in the NVT ensemble at 298 K were carried out where translation, rotation and reinsertion of a single PFOA and water molecule were sampled separately in MOFs and zeolite Beta. For each structure, 10 independent simulations were carried out. From these

simulations, radial distribution functions (RDFs) between specific sites of the adsorbent materials and the PFOA and water were computed and averaged.

All MC simulations were performed using the RASPA molecular simulation software at 25^{o}C degree constant temperature where MOFs and water molecule (TIP4P-Ew) are rigid and PFOA molecule is flexible [91]. The cut-off distance for the LJ potential and the real part of the Ewald sum, which was used to compute electrostatic interactions, was set to 12 Å. The unit cells of the MOFs and zeolite Beta were replicated such that their shortest side was greater than twice the cut off distance.

5.3. Results and Discussion

In this section, we first discuss the results from the molecular simulations for each group of MOF based on the classification given in Table 1 separately and finish the section by comparing results from fluorinated MOF materials and zeolite Beta, which is our benchmark material.

5.3.1. Henry's Law Coefficients and Preferred Adsorption Sites of PFOA and Water in Fluorinated MOFs and Zeolite Beta

Henry's law coefficient provides information about the affinity between a sorbate molecule and an adsorbent material as it is related to enthalpy of adsorption at the infinite dilution; i.e. very low loadings. Its calculation is straightforward and computationally not expensive. Therefore, Henry's law coefficient can be a powerful tool to understand how pore size, geometry and chemical functionality affect the interaction of molecules with porous materials. On the other hand, preferred adsorption sites can be revealed by computing pair distribution functions; i.e. RDF, between specific atoms of the sorbate molecules and the adsorbent material. In PFOA adsorption, both electrostatic and hydrophobic interactions can play a role [43]. The

electrostatic interactions are due to the interaction of the carboxyl group of PFOA and the porous material; whereas, the hydrophobic interactions occur as a result of the interaction of the perfluoroalkyl chain of PFOA and the porous material. However, it is the stronger electrostatic interactions that is expected to give distinct peaks in RDF plots to indicate preferred adsorption sites of PFOA. Therefore; in our RDF analysis we focus on interactions between the atoms of the framework and the atoms of the carboxyl group of PFOA.

5.3.1.1. MOFs functionalized with fluorinated anions

Henry's law coefficients of PFOA and water are given in Table 5-3 for MOFs that are fluorine functionalized with fluorinated anions. For the same group of MOFs, PSD plots are given in Figure 1. Despite differences in the pore sizes, Henry's law coefficients of water molecules in the MOFs given in Table 5-3 are in the same order of magnitude, i.e. 10^{-3} mol/kgPa, and close to each other.

Table 5-3. Henry's law coefficients of PFOA and water in MOFs functionalized with fluorinated anion

MOF name	PFOA (mol/kgPa)	Water (mol/kgPa)
SIFSIX-1-Cu	4.91×10^{5}	2.82×10^{-3}
TIFSIX-1-Cu	2.34×10^{6}	3.14×10^{-3}
$Zn(4,4'\text{-bpy})_2(SiF_6)$	2.96×10^{6}	1.56×10^{-3}
$Cu(bpy\text{-}1)_2(SiF_6)$	5.11×10^{4}	4.07×10^{-3}
SIFSIX-2-Cu	2.0×10^{3}	1.17×10^{-3}

On the other hand, Henry's law coefficients of PFOA are much higher than those of for water, indicating a greater affinity that indicates strong interaction. Furthermore, Henry's law coefficient for PFOA shows a dependence on the pore size

(Figure 5-1) and varies between 10^3 to 10^6 mol/kgPa. With increasing pore diameter Henry's law coefficient for PFOA first increases but then decreases sharply when the pore diameter is larger than 10 Å, suggesting that too large and too narrow pores do not provide favourable interactions.

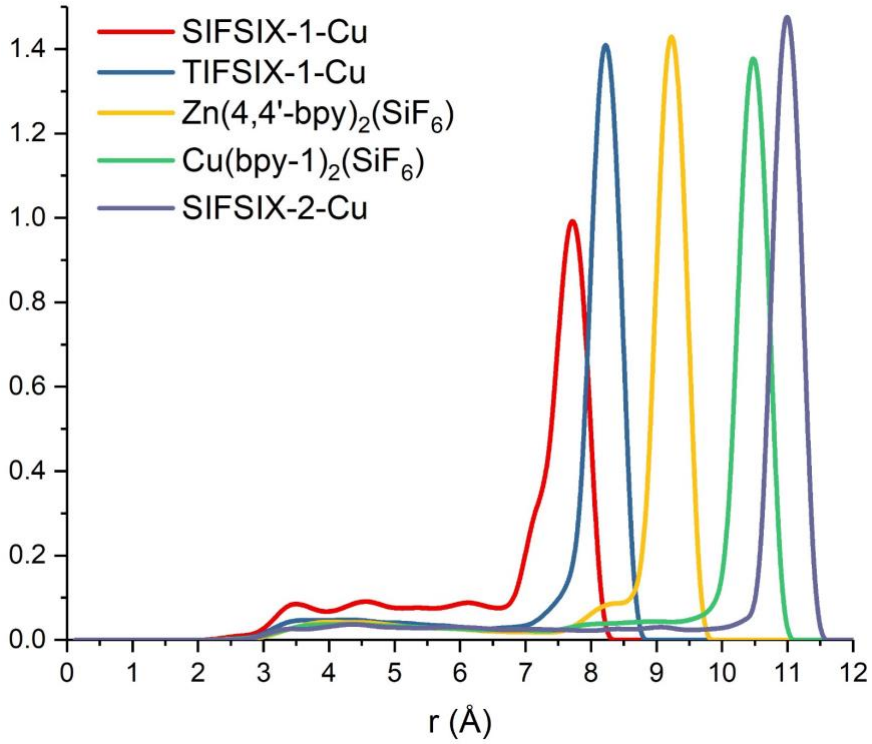

Figure 5-1. PSD plots of MOFs functionalized with fluorinated anions

To identify preferred adsorption sites we computed and compared RDFs between different pairs of atoms from NVT Monte Carlo simulations that we carried out with a single PFOA and single water probe molecule. The RDF plots between fluorine atoms of MOFs and the hydrogen of PFOA (F-H_O) and the hydrogens of water (F-H_W) both depict a large peak at around 1.7 Å (Figure 5-2), demonstrating that fluorine anions that are used as bridging ligands are preferred adsorption sites for both PFOA and water, thanks to the relatively large partial negative charge on the fluorine atoms. Analysis of other RDF plots did not show any distinct adsorption sites for either PFOA or water.

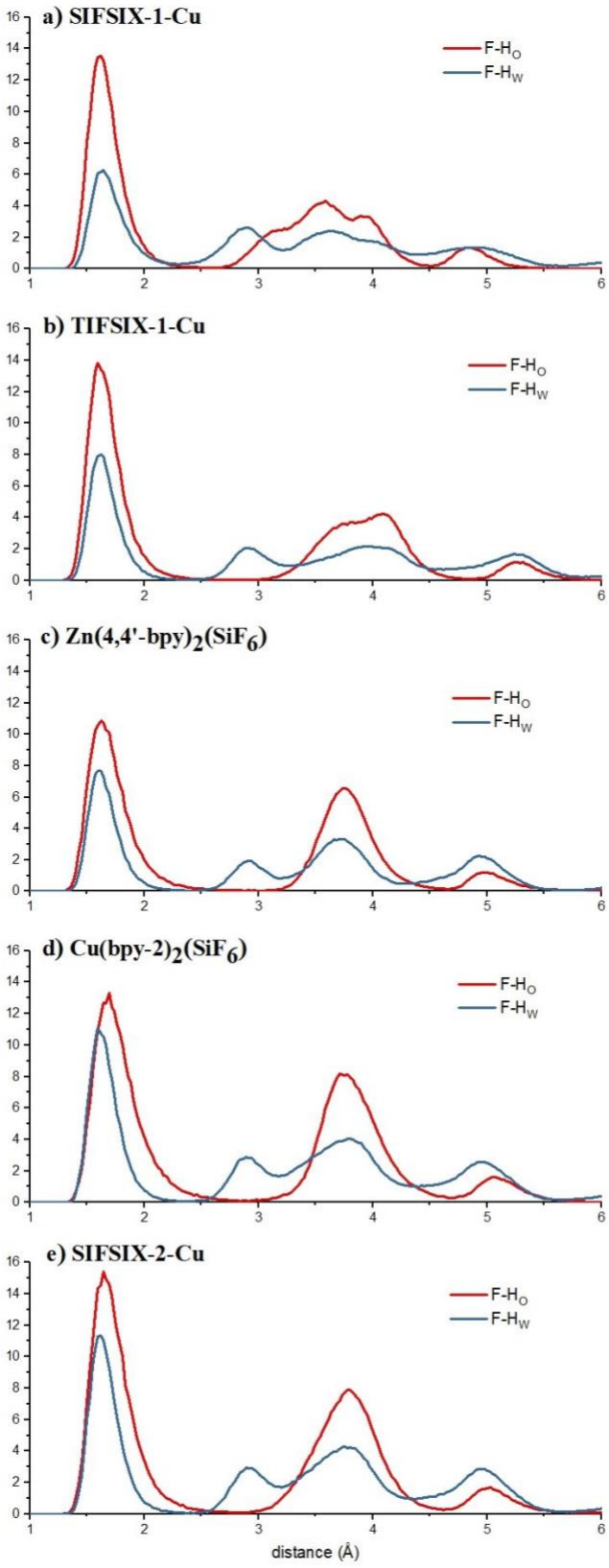

Figure 5-2. RDF plots in MOFs that are functionalized with fluorine anions. F, fluorine atoms of MOFs; H_o, hydrogen of PFOA; H_w, hydrogen of water

5.3.1.2. MOFs functionalized with trifluoromehtyl or fluorine substituted ligands

In Table 5-4, Henry's law coefficients of PFOA and water are given for MOFs that are fluorine functionalized with trifluoromehtyl substituted ligands.

Table 5-4. Henry's law coefficient of PFOA and water in MOFs functionalized with trifluoromethyl substituted ligands

MOF name	PFOA (mol/kgPa)	Water (mol/kgPa)
$Zn(C_{17}H_8F_6O_4)$	2.42×10^{-1}	1.67×10^{-6}
FMOF-1	1.11×10^{-3}	4.52×10^{-7}

For the same group of MOFs, PSD plots are shown in Figure 5-3. Henry's law coefficients of water in this group of MOFs are lower; i.e. more hydrophobic, compared to those of for MOFs functionalized with fluorinated anions. On the other hand, the low Henry's law coefficients of PFOA in $Zn(C_{17}H_8F_6O_4)$ and FMOF-1 may be attributed to their narrow pores.

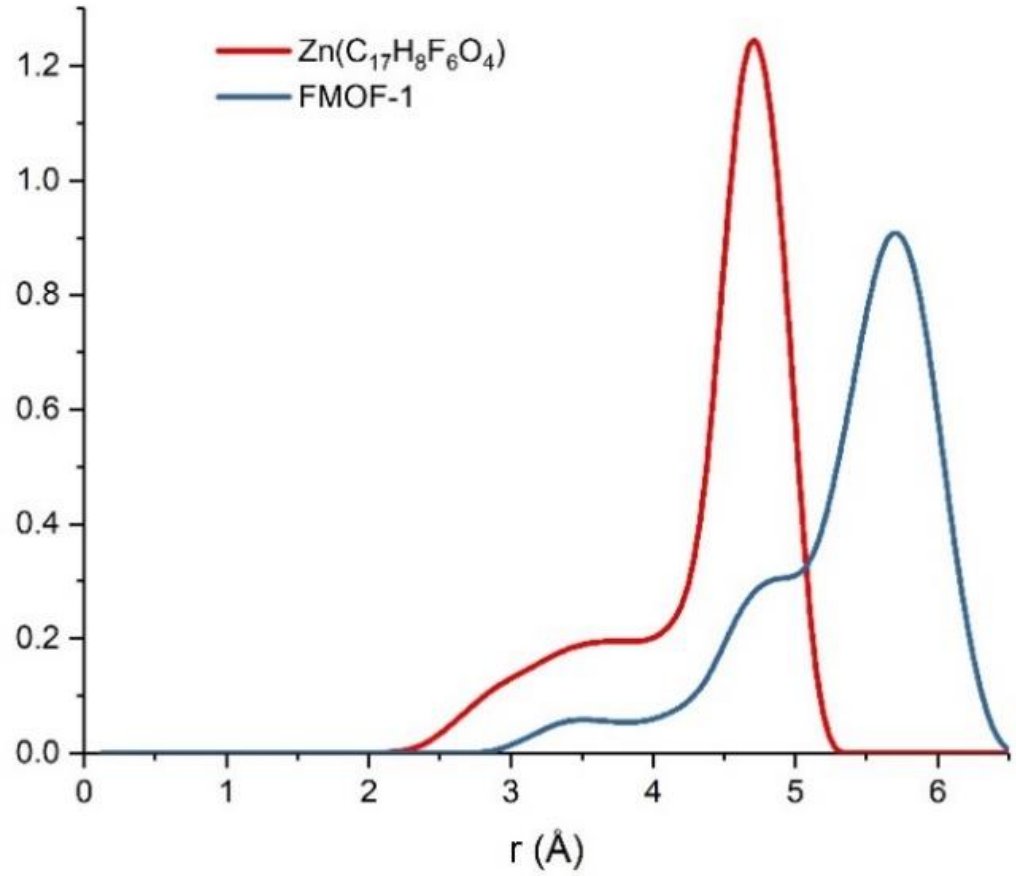

Figure 5-3. PSD plots of MOFs functionalized with trifluoromehtyl substituted ligands

RDF plots for MOFs functionalized with trifluoromehtyl substituted ligands are shown in Figure 5-4.

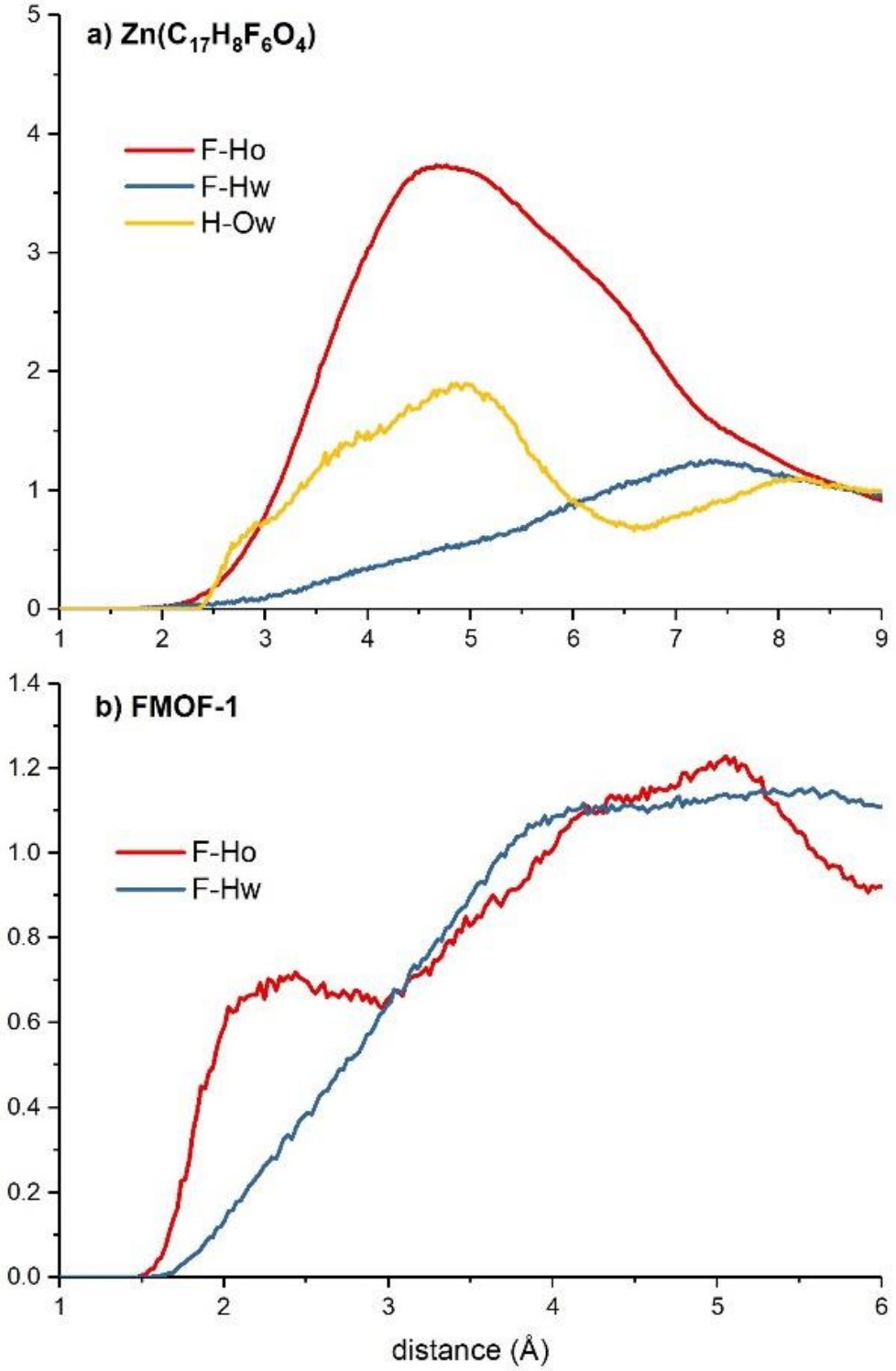

Figure 5-4. RDF plots of MOFs functionalized with trifluoromethyl substituted ligands

In $Zn(C_{17}H_8F_6O_4)$ there are two distinct pores, one fully fluorinated with trifluoromehtyl substituted ligands and the other one non-fluorinated. While PFOA prefers to be adsorbed in the fluorinated pores (Figure 5-4a, RDF plot for F-H_O), water prefers to be adsorbed in the non-fluorinated pores, where ligands have hydrogens (Figure 5-4a, RDF plot for H-O_W). This is further supported by the F-H_W RDF plot (Figure 5-4a) which shows that the water molecules remain far from the fluorine atoms of the $Zn(C_{17}H_8F_6O_4)$.

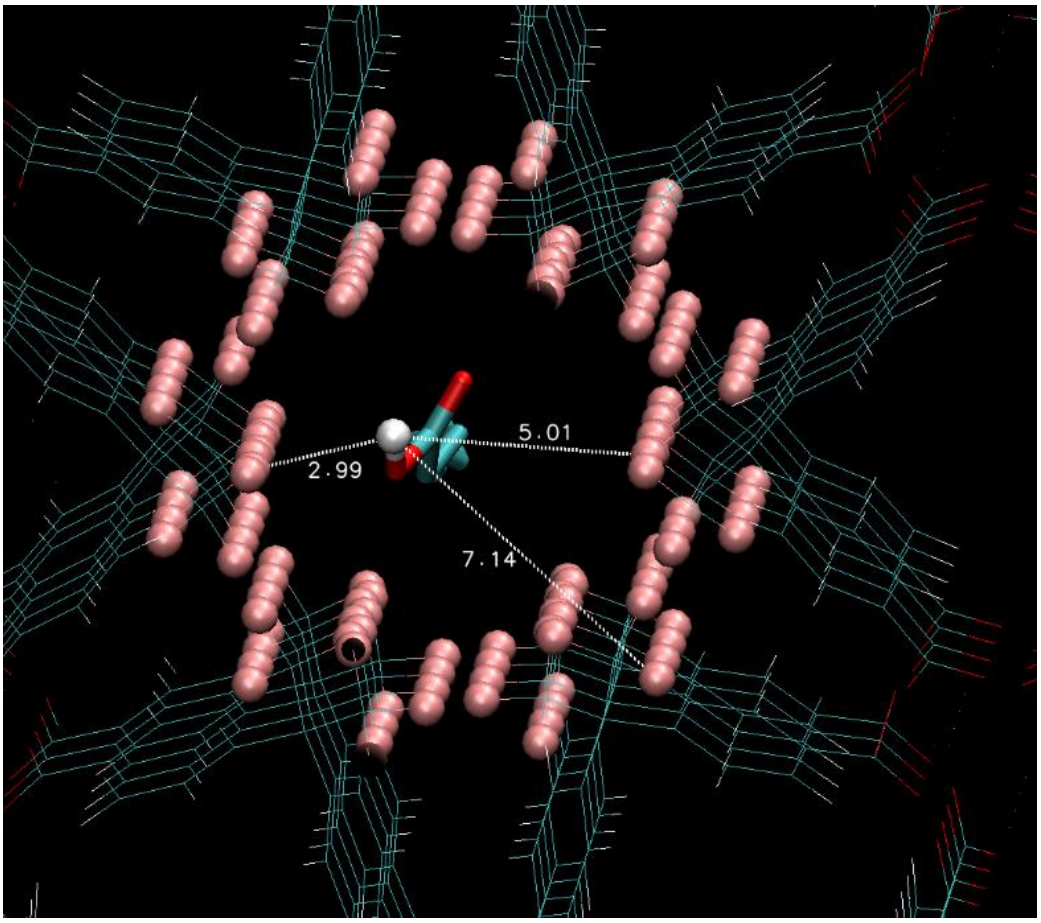

Figure 5-5. Snapshot that shows the distances between the hydrogen (white) atom of PFOA and the fluorine (pink) atoms of $Zn(C_{17}H_8F_6O_4)$; hence the broad F-H_O RDF peak in Figure 5-4

The broad nature of the peaks in the F-H_O and H-O_W RDF plots in $Zn(C_{17}H_8F_6O_4)$ is due to the homogenous nature of the pores; i.e. fully fluorinated or fully non-

fluorinated. For instance, while the distance between hydrogen of PFOA and the closest fluorine atom in the pore is around 3 Å, the distance with all other fluorine atoms in the same pores covers a range of approximately 3 to 7 Å (Figure 5-5), which results in a broader peak.

In FMOF-1, all pores are fluorinated; hence, this MOF has the lowest Henry's law coefficient for water. Therefore, RDF analysis did not reveal a preferred adsorption site for water (Figure 5-4b); whereas, the hydrogen of PFOA preferably interacts with fluorine of FMOF-1 as shown by the RDF plot of F-H_O in Figure 5-4b.

To study MOFs that are functionalized with fluorine substituted ligands, UiO-67 was fluorinated incrementally until all hydrogens on the linkers were substituted with fluorine atoms. Table 5-5 gives Henry's law coefficient of PFOA and water in UiO-67 and fluorine functionalized F-UiO-67-n% structures, where n is 25, 50, 75 and 100, indicating the percentage of fluorine functionalization.

Table 5-5. Henry's law coefficients of PFOA and water in UiO-67 and fluorine functionalized UiO-67s; i.e. F-UiO-67s, with different degrees of fluorine substitution

MOF name	PFOA (mol/kgPa)	Water (mol/kgPa)
UiO-67	0.97×10^{3}	3.94×10^{-6}
F-UiO-67-25%	1.6×10^{3}	4.32×10^{-6}
F-UiO-67-50%	2.23×10^{3}	4.61×10^{-6}
F-UiO-67-75%	3.11×10^{3}	4.89×10^{-6}
F-UiO-67-100%	4.31×10^{3}	5.3×10^{-6}

Their PSD plots are shown in Figure 5-6. Henry's law coefficients of water in all structures are all in the order of 10^{-6} mol/kgPa and it exhibits a gradual increase from the non-fluorinated UiO-67 until fully fluorinated F-UiO-67-100% resulting in 35%

increase between UiO-67 and F-UiO-67-100%. Although UiO-67 should become more and more hydrophobic due to increasing fluorine content, the small increase in Henry's law coefficient of water may be attributed to the pores becoming slightly narrower; hence, stronger framework-water interactions. On the other hand, Henry's law coefficients of PFOA are in the order of 10^3 mol/kgPa and the fluorine functionalization of ligands has a much more significant effect on PFOA Henry's law coefficients, as it increases about four times from non-fluorinated to fully fluorinated ligands.

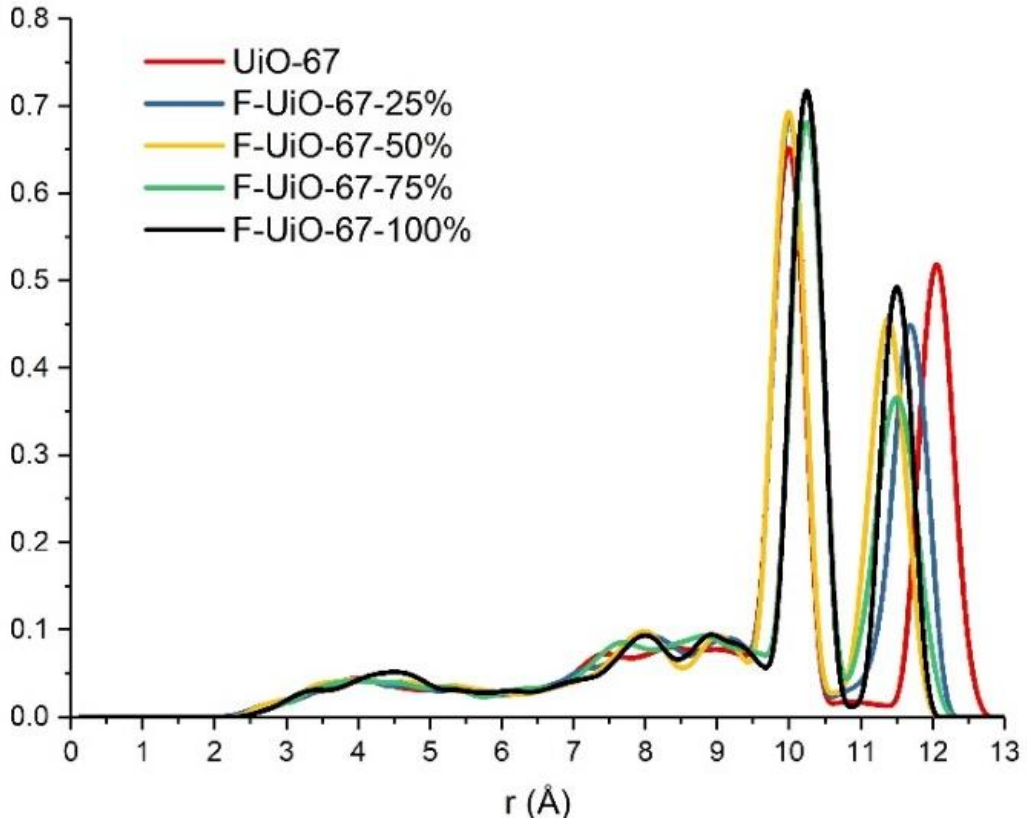

Figure 5-6. PSD plots of UiO-67 and fluorine functionalized F-UiO-67s with different degrees of fluorine substitution

RDF plots in UiO-67 and F-UiO-67s that have different degrees of fluorine functionalization provide insights about the preferred adsorption sites of PFOA and water molecules (Figure 5-7 and Figure 5-8).

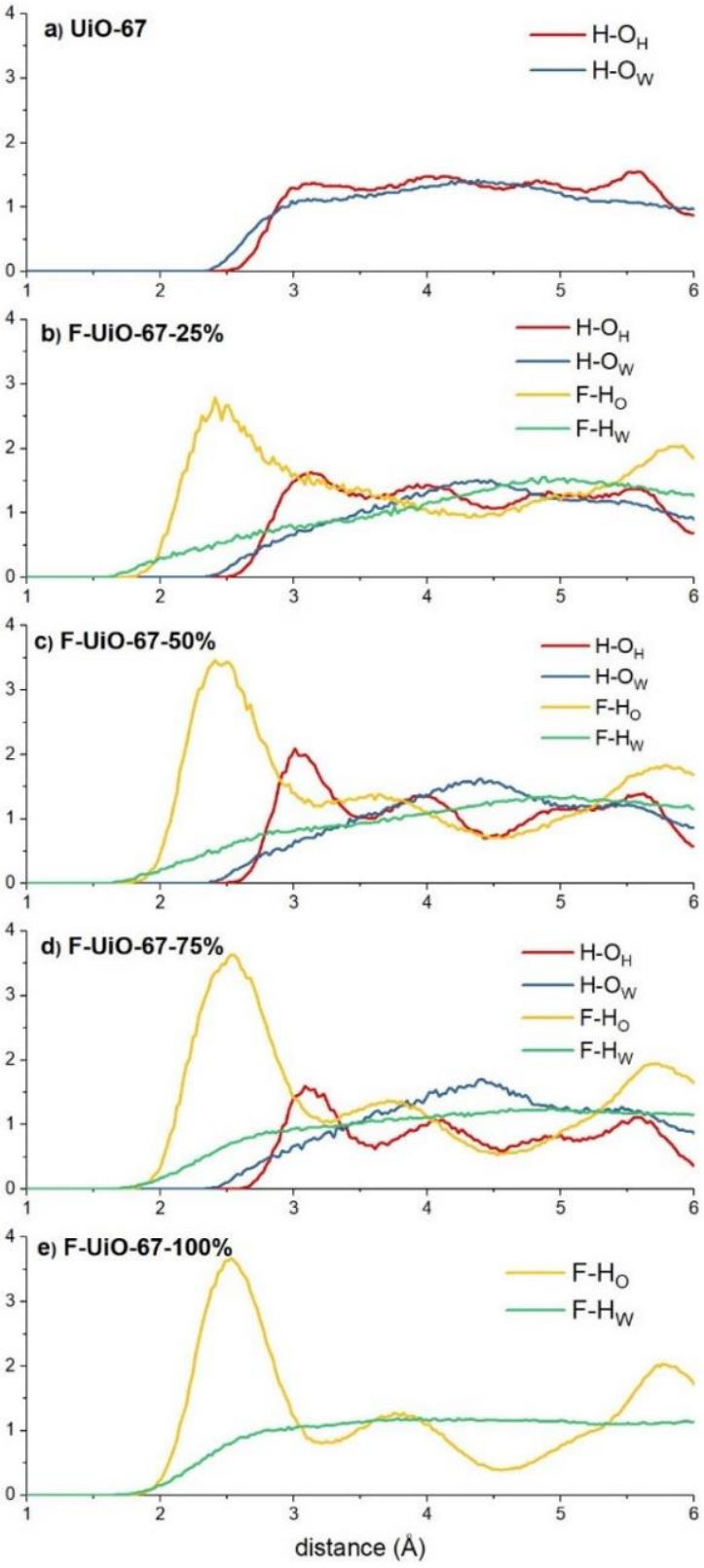

Figure 5-7. RDF plots in UiO-67 and F-UiO-67s. H, hydrogen atoms on the ligands of UiO-67 and F-UiO-67; F, fluorine atoms of F-UiO-67s; H_O, hydrogen atom of PFOA; H_W, hydrogen atoms of water

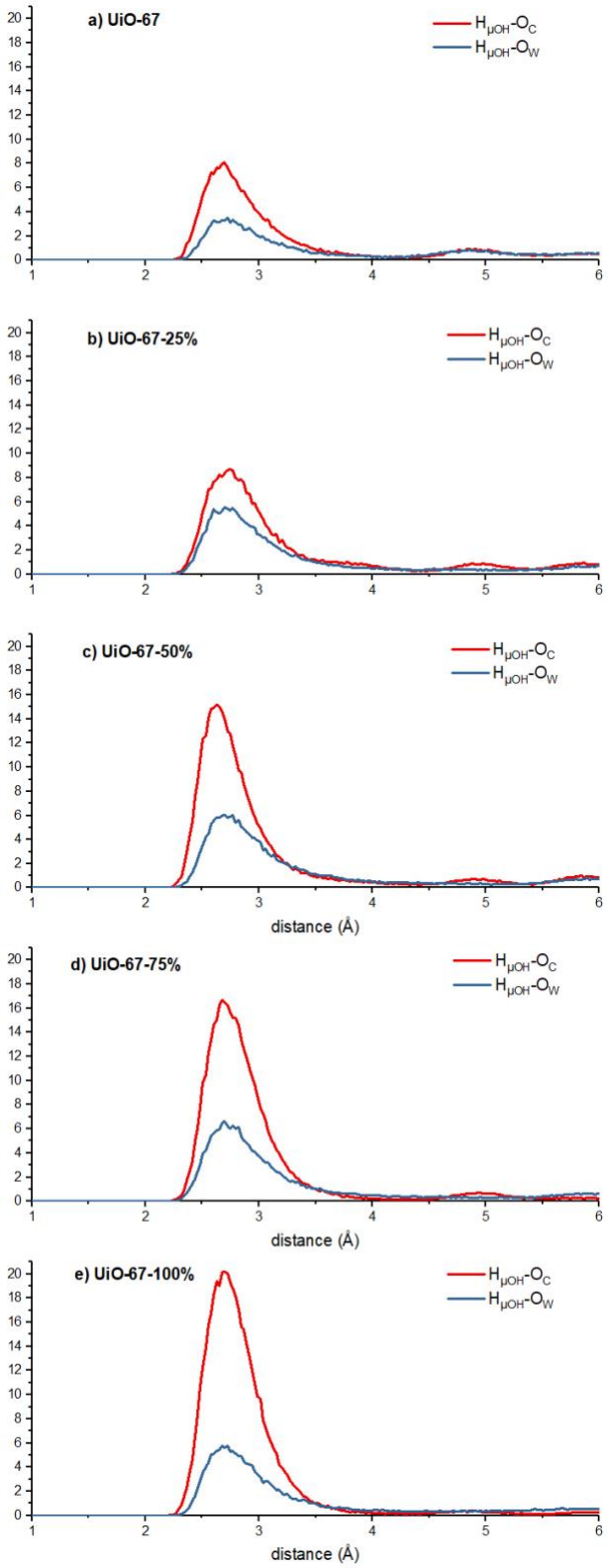

Figure 5-8. RDF plots in UiO-67 and fluorine functionalized UiO-67s; i.e. F-UiO-67s, with different degrees of fluorine substitution. H, hydrogen atoms on the ligands of UiO-67 and F-UiO-67-25%, 50%, 75%; O_C, oxygen atom of PFOA double bonded to carbon; and O_W, oxygen atom of water

Both PFOA and water molecule strongly interact with hydrogens of μOH sites in UiO-67 and F-UiO-67s (Figure 5-8, RDF plots for $H_{\mu OH}$-O_C and $H_{\mu OH}$-O_W), that is, PFOA and water compete for the same adsorption site.

Once fluorinated; however, a distinct adsorption site is created for the PFOA molecule. In Figure 5-7a, the RDF plots of the hydrogen atoms of the ligands and the hydroxyl oxygen of PFOA (H-O_H) and the oxygen atoms of water (H-O_W) show that the hydrogens on the MOF ligands are not preferred adsorption sites. However, the RDF plots between fluorine atoms of F-UiO-67s and hydrogen atom of PFOA (F-H_O) show sharp peaks around 2.5 Å (Figures 5-7b-e), indicating the creation of new binding sites on the ligand; whereas, it is clear that the hydrogens of water molecules do not bind to the fluorine atoms on the ligands (RDF plots for F-H_W in Figures 5-7b-e). As such, the increase in the PFOA affinity in UiO-67 with increasing fluorine substitution of UiO-67 ligands may be attributed to the introduction of distinct adsorption sites for PFOA.

5.3.1.3. MOFs functionalized with grafting of perfluorinated alkanes

For the experimentally reported MOFs considered before this section, fluorine functionalization of the framework was achieved during synthesis. However, MOFs can also be functionalized post-synthetically. One example of this is the perfluorinated alkane functionalization of NU-1000 through the SALI method [110]. Here, we consider the structure, denoted by NU-1000-PF, where the PFOA molecules were used as the source of the perfluoroalkyl chain that was covalently bonded to the terminal –OH group sites on the NU-1000 metal nodes as a result of the ligand

incorporation reaction (Figure 5-9). The incorporation is an acid-base reaction, which occurs between terminating hydroxyl groups on the Zr node of NU-1000 and carboxylic acid group of PFOA molecules that gives water molecules as side products. The water molecules are produced by combination of terminating –OH groups and hydrogens of PFOA's carboxylic acid or μOH sites of the nodes.

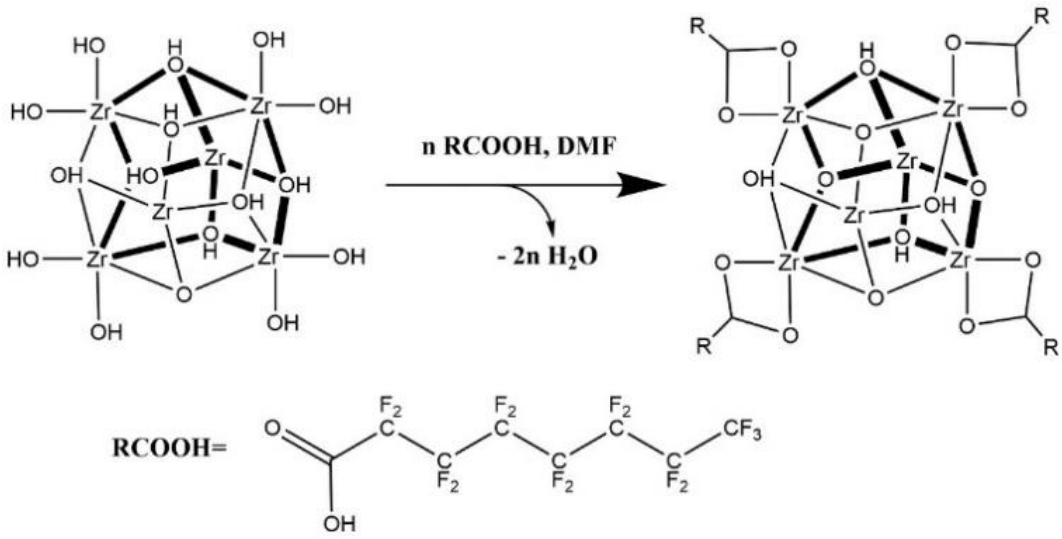

Figure 5-9. Schematic of ligand incorporation reaction of NU-1000

Table 5-6 gives Henry's law coefficient of PFOA and water in NU-1000 and NU-1000-PF. PSD plots of these two structures are given in Figure 5-10.

Table 5-6. Henry's law coefficient of PFOA and water in NU-1000

MOF name	PFOA (mol/kgPa)	Water (mol/kgPa)
NU-1000	3.00×10^{4}	4.01×10^{-6}
NU-1000-PF	1.82×10^{5}	3.82×10^{-6}

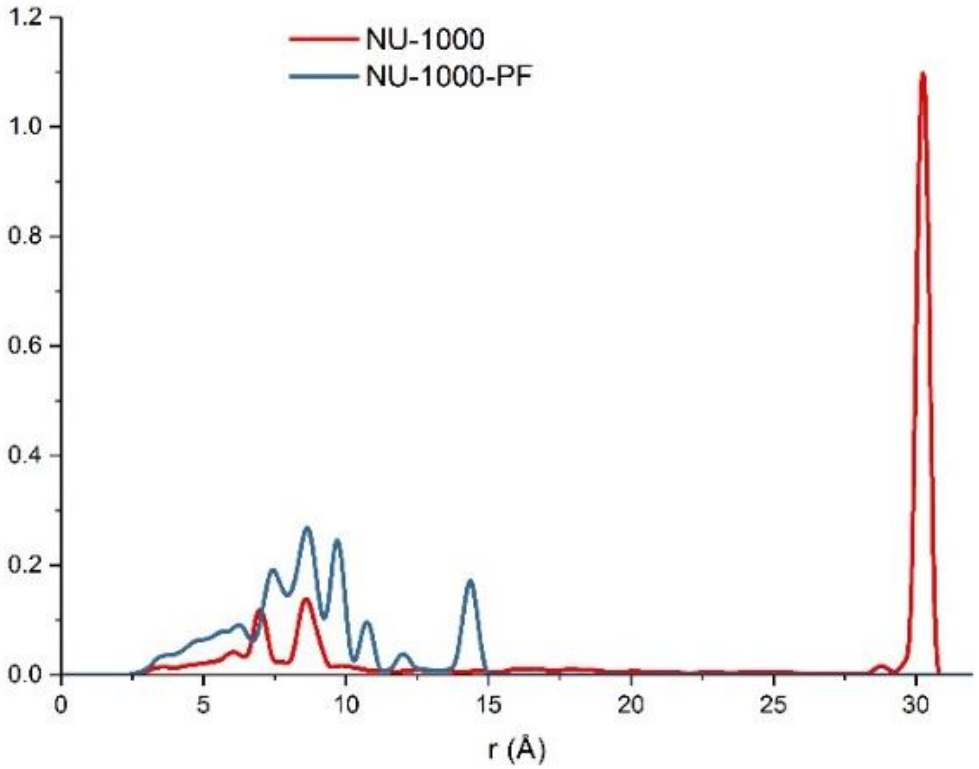

Figure 5-10. PSD plots of NU-1000 and NU-1000-PF

As a consequence of the incorporation of perfluoroalkyl chains, the size of the largest pore in NU-1000 reduces from ≈30 Å to ≈14 Å in NU-1000-PF, and both structures also have narrower pores ranging from 7 to 9 Å. Henry's law coefficient for water in both structures are almost the same and are in the order of 10^{-6} mol/kgPa, that is, their hydrophobicity is similar to those functionalized with trifluoromethyl and fluorine substituted ligands (Tables 5-4 and 5-6). For PFOA; however, the Henry's law coefficient is an order of magnitude higher in NU-1000-PF compared to NU-1000. This increase in the Henry's law coefficient may be attributed, at least partially, to stronger framework-PFOA interactions due to relatively narrow pores of NU-1000-PF. RDF analysis provide more insights about the increase in Henry's law coefficient of PFOA after NU-1000 is functionalized with perfluoroalkyl chains (Figure 5-11 and Figure 5-12).

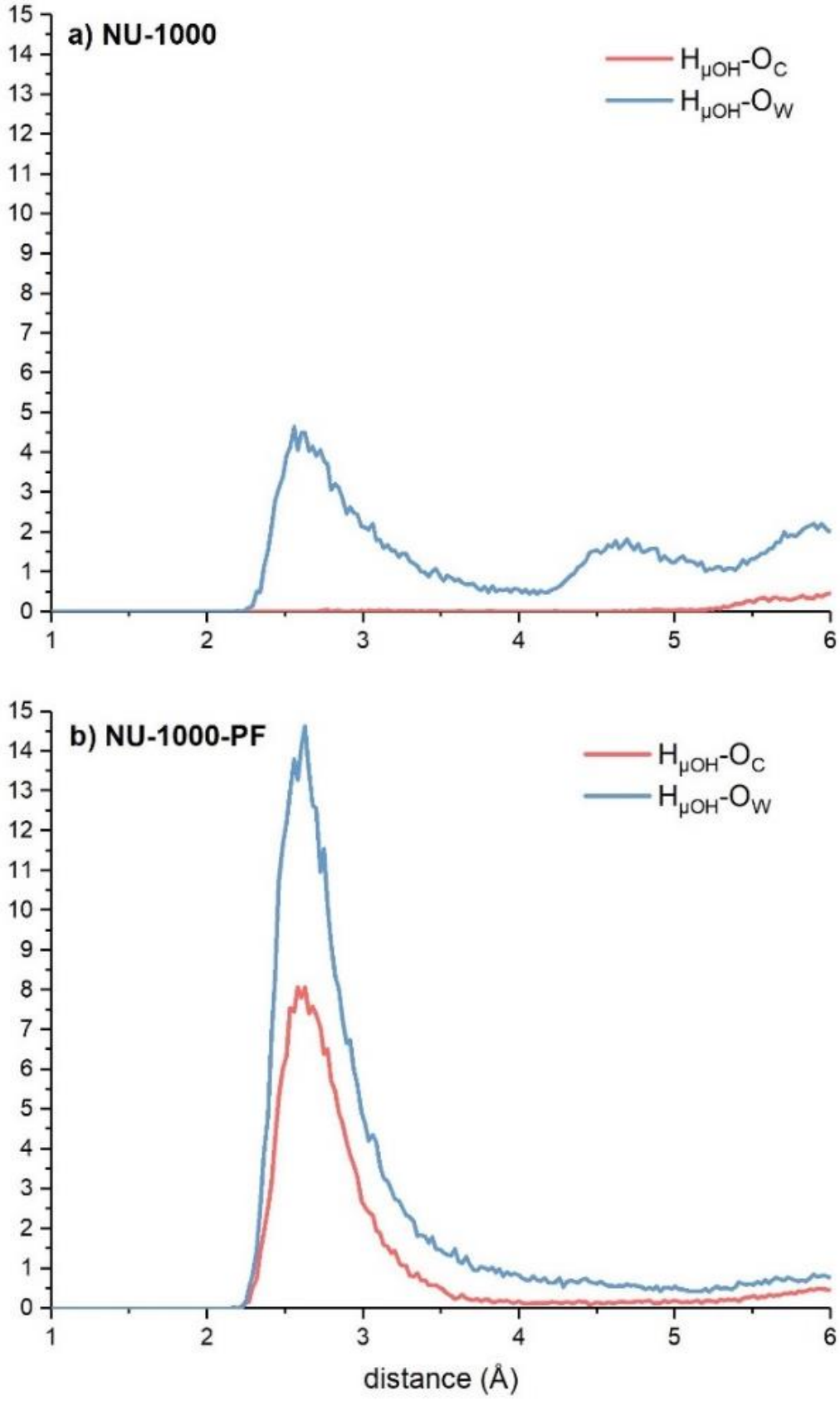

Figure 5-11. RDF plots of NU-1000 and NU-1000-PF

In NU-1000, PFOA molecule mainly prefers to be adsorbed in the triangular pores which are relatively narrow (Figure 5-12, RDF plots for C-H_O and C-CF_3).

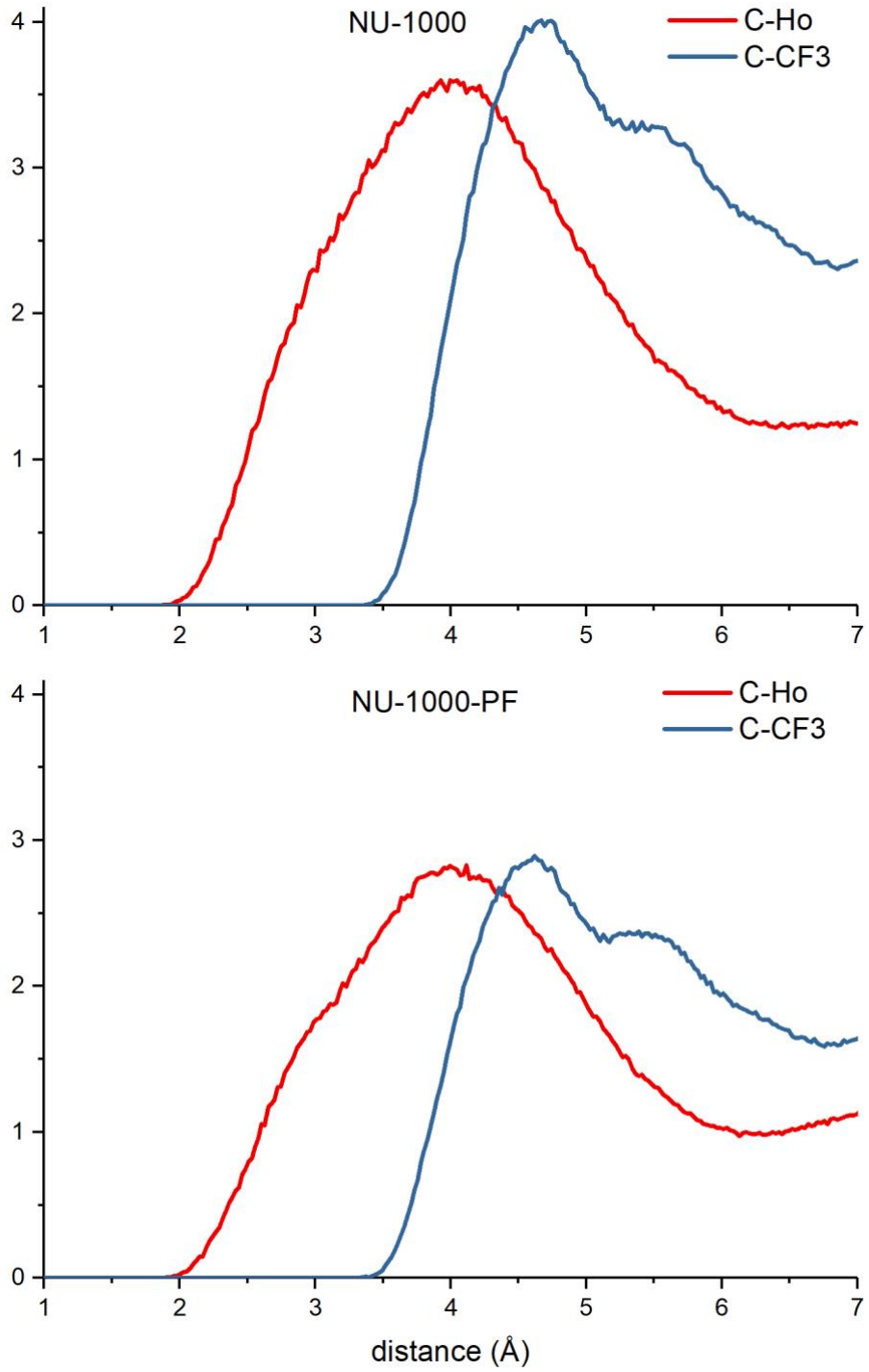

Figure 5-12. RDF plots in NU-1000 and NU-1000-PF. C, carbon atom of NU-1000 and NU-1000-PF; H_o, hydrogen atom of PFOA; and CF_3, trifluorocarbon united atom of PFOA

The hydrophilic head of PFOA, i.e. the carboxyl group, does not interact strongly with any particular site; whereas μOH is a preferred adsorption site for water molecules (Figure 5-11a, RDF plots for $H_{\mu OH}$-O_C and $H_{\mu OH}$-O_W). Interestingly, after perfluoroalkyl grafting, the μOH becomes a preferred adsorption site for the PFOA molecule as well, which is demonstrated by the peak observed in the RDF plot of $H_{\mu OH}$-O_C in NU-1000-PF (Figure 5-11b). The emergence of this new biding site for PFOA is also a factor in the increase of Henry's law coefficient of PFOA in NU-1000-PF compared to NU-1000. The intensity of the $H_{\mu OH}$-O_W peak in NU-1000-PF is higher compared to NU-1000, which is due to the decrease in the number of μOH sites as a result of the SALI reaction.

5.3.1.4. Zeolite Beta

Zeolites are crystalline porous materials that have been extensively used in adsorption processes. All-silica zeolite Beta, which has pores of ≈6 Å in diameter (Figure 5-13), has been shown to adsorb PFOA from water in experimental studies [45]. Henry's law coefficient of PFOA and water in zeolite Beta are given in Table 5-7. All-silica zeolite Beta is a hydrophobic material as the Henry's law coefficient of water is one of the lowest among all structures considered in this study. The Henry's law coefficient of PFOA is relatively high despite having no preferred adsorption sites in zeolite Beta (Figure 5-14), which suggest that the pore size of zeolite Beta provides a good fit for the PFOA molecule that results in relatively strong interactions with the framework.

Table 5-7. Henry's law coefficient of Zeolite Beta

Structure	PFOA (mol/kgPa)	Water (mol/kgPa)
Zeolite Beta	3.24×10^{4}	1.71×10^{-6}

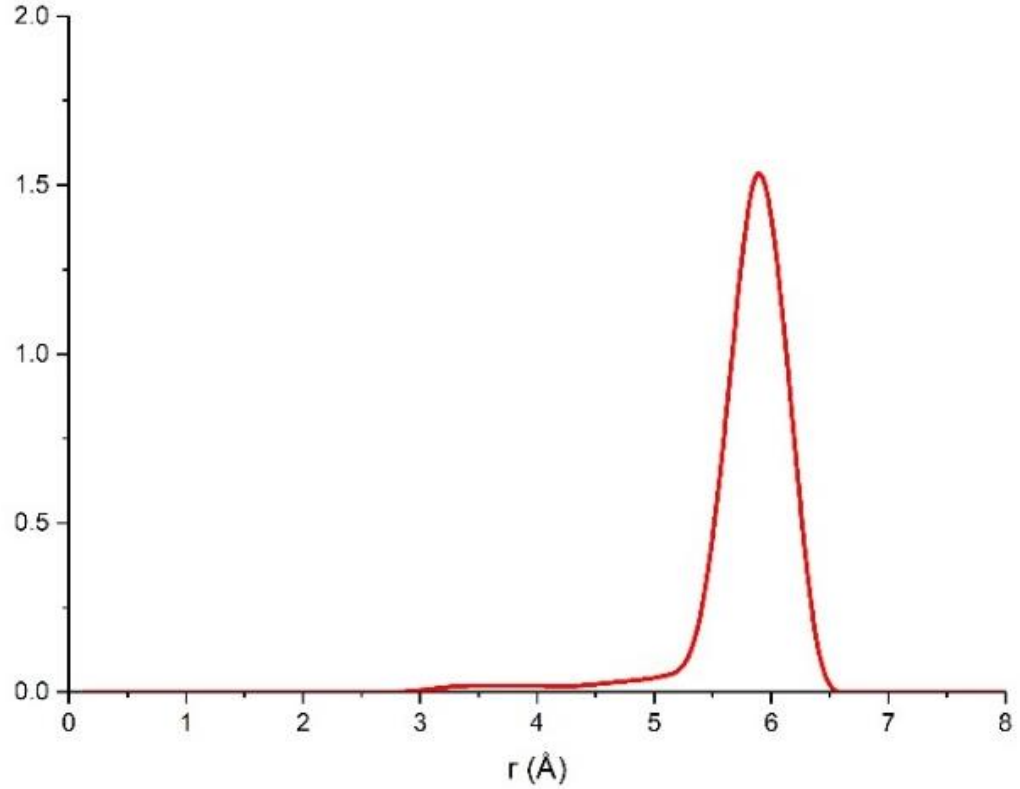

Figure 5-13. PSD plot of Zeolite Beta

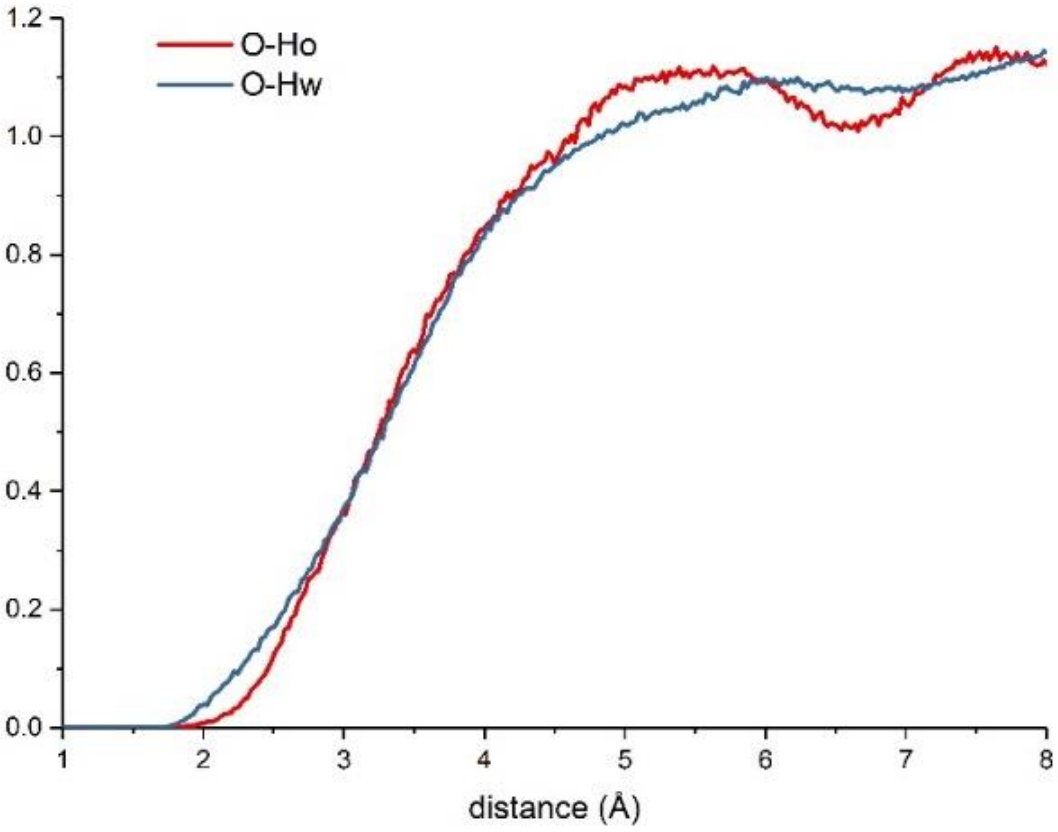

Figure 5-14. RDF plot of Zeolite Beta

5.4. Conclusions

In this study, we investigated the effect of different fluorine functionalization methods on the in MOFs that are functionalized by different strategies. We wanted to investigate their PFOA removal capability of these MOFs by exploiting their fluorine rich nature. Therefore, MOFs have been categorised and analysed based on their functionalization methods. The research started with deriving a reliable force field for PFOA model to probe MOFs efficiently and correctly. Hence, we accomplished deriving a united-atom PFAO model that can produce experimental density value of PFOA as a result of MD simulation in NPT ensemble. MOFs character analysis began with calculation of Henry's law coefficient values of PFOA and water molecules within each MOF. The results showed that all the fluorinated MOFs have higher affinity to PFOA molecule compared to water molecules. However, the amount of affinity is not the same. We observed that pore size distribution influences the PFOA affinity of MOFs that are functionalized with fluorine anions. In the case of introducing fluorine atoms by using fluorine substituted ligands or grafting perfluorinated alkanes also changes the affinity of PFOA to MOFs. NU-1000 and UiO-67 MOFs are functionalized with grafting perfluorinated alkanes and fluorine substituted ligands, respectively. As a result of chemical environment change within MOFs compared to non-fluorinated structures the PFOA affinity to MOFs increased. The adsorption behaviour of PFOA and water molecules are investigated by analysing the RDF plots. Although PFOA affinities of fluorine anion functionalized MOFs are different from each other, their preferred adsorption sites for PFOA and water molecules are same. The fluorine anion functionalized MOFs' fluorine atoms are strongly interacting with hydrogen atom of PFOA and water molecules. On the other

hand, introducing fluorine atoms into UiO-67 create a separate adsorption site for hydrogen of PFOA molecule that reduces the competition between PFOA and water molecule to be adsorbed by fluorinated UiO-67 structure. NU-1000 has preferred adsorption site only for water molecule and after fluorine functionalization of NU-1000 a preferred adsorption site for PFOA molecule is introduced however, the newly introduced adsorptio site is the same preferred adsorption site for water molecules.

Chapter 6. Adsorption Simulations of PFOA from Water

6.1. Introduction

In Chapter 5, we compared the Henry's law coefficients computed for PFOA and water in various MOFs that are fluorine functionalized by different approaches, non-fluorinated MOFs and zeolite Beta. Furthermore, preferred binding sites for PFOA and water molecules were identified through RDF plots which provided additional understanding of how fluorine functionalization affects MOF-PFOA and MOF-water interactions. To remove PFOA from water efficiently using a porous material its affinity for PFOA should be as large as possible and conversely its affinity for water should be as low as possible. This rationale can be used to identify porous materials that are promising for the removal of PFOA from water, and then the amount of PFOA removed from water in a porous material can be predicted by grand canonical monte carlo (GCMC) simulations.

6.2. Materials and Methods

When we look at the Henry's law coefficients of the MOFs that are fluorine functionalized with fluorinated anions (Table 6-1), two of them (TIFSIX-1-Cu and $Zn(4,4'\text{-bpy})_2(SiF_6)$) have the highest Henry's law coefficients for PFOA among all the materials considered in this study. However, despite showing strong affinity towards PFOA they also have very high Henry's law coefficient for water. That is, they are relatively hydrophilic and may not be efficient at removing PFOA. The two trifluoromethyl functionalized MOFs considered have the lowest Henry's law

coefficients for water (Table 6-1). On the other hand, they also have the lowest Henry's low coefficients for the PFOA due their pores being too narrow.

Table 6-1. Henry's law coefficient of PFOA and water in MOFs and zeolite

MOF name	PFOA (mol/kgPa)	Water (mol/kgPa)
Zeolite Beta	3.39×10^{4} +/- 2.74×10^{3}	1.71×10^{-6} +/- 7.13×10^{-9}
SIFSIX-1-Cu	5.5×10^{5} +/- 6.3×10^{5}	2.8×10^{-3}+/- 4.2×10^{-4}
TIFSIX-1-Cu	2.34×10^{6} +/- 2.94×10^{6}	3.14×10^{-3} +/- 7.3×10^{-4}
Zn(4,4′-bpy)$_2$(SiF$_6$)	2.96×10^{6} +/- 2.75×10^{6}	1.56×10^{-3} +/- 4.5×10^{-4}
Cu(bpy-2)$_2$(SiF$_6$)	5.11×10^{4} +/- 5.3×10^{4}	4.1×10^{-3} +/- 7.2×10^{-4}
SIFSIX-2-Cu	2.7×10^{3} +/- 1.3×10^{3}	1.2×10^{-3} +/- 3.1×10^{-4}
Zn(C$_{17}$H$_8$F$_6$O4)	2.6×10^{-1} +/- 3.1×10^{-2}	1.7×10^{-6} +/- 1.1×10^{-8}
FMOF-1	4.2 +/- 5.5×10^{-1}	4.5×10^{-7} +/- 2.6×10^{-9}
UiO-67	0.97×10^{3} +/- 0.42×10^{2}	3.94×10^{-6} +/- 1.48×10^{-7}
F-UiO-67-25%	1.6×10^{3} +/- 2.6×10^{2}	4.32×10^{-6} +/- 8.7×10^{-8}
F-UiO-67-50%	2.2×10^{3} +/- 6.6×10^{2}	4.6×10^{-6} +/- 9.8×10^{-8}
F-UiO-67-75%	3.11×10^{3} +/- 6.8×10^{2}	4.89×10^{-6} +/- 1.87×10^{-7}
F-UiO-67-100%	4.3×10^{3} +/- 7.4×10^{2}	5.3×10^{-6} +/- 1.34×10^{-7}
NU-1000	3.09×10^{4} +/- 6.7×10^{2}	4.18×10^{-6} +/- 8.66×10^{-8}
NU-1000-PF	1.7×10^{5} +/- 2.5×10^{4}	3.8×10^{-6} +/- 9.2×10^{-7}

MOFs functionalized with fluorine substituted ligands exhibit high levels of hydrophobicity (Table 6-1); however, the Henry's law coefficients for PFOA in these MOFs, even after complete fluorine substitution, are still not very high. The remaining three materials; NU-1000 and its perfluoralkane grafted version NU-1000-PF and zeolite Beta, do not have the highest Henry's law coefficients for the PFOA (Table 6-1); i.e. one to two orders of magnitude lower than those of for TIFSIX-1-Cu and

$Zn(4,4'\text{-bpy})_2(SiF_6)$; however, they have the highest PFOA/water Henry's law coefficient ratio among all materials considered (Figure 6-1).

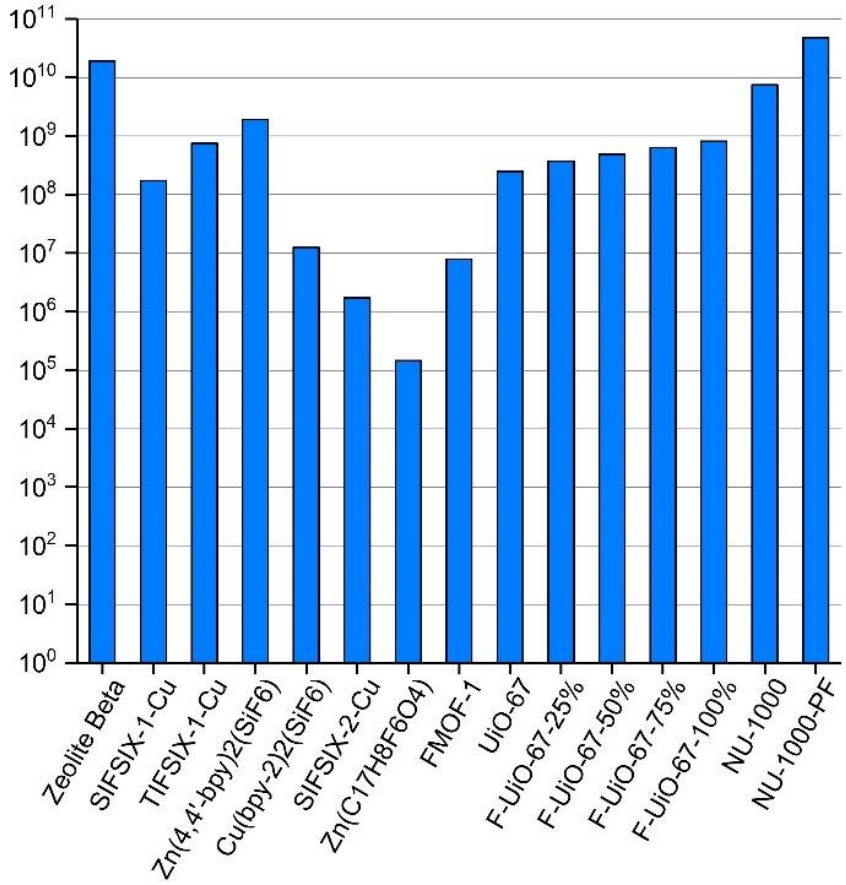

Figure 6-1. Ratio of PFOA to Water Henry's Law Coefficients

In NU-1000 and zeolite-Beta and in NU-1000 the PFOA/water Henry's law coefficient ratios are in the order of 10^{10} and 10^{11}, respectively. Whereas, in $Zn(4,4'\text{-bpy})_2(SiF_6)$, the same ratio is in the order of 10^{9}.

6.2.1. Grand Canonical Monte Carlo Simulations

Based on the above analysis, adsorption simulations were carried out in NU-1000, NU-1000-PF and all-silica zeolite Beta to predict their PFOA removal capacities. To calculate the adsorption amount of PFOA from water, we did Monte Carlo simulations in the grand canonical ensemble (GCMC). Translation, rotation, reinsertion and insertion/deletion of the PFOA and water molecules were sampled. In

GCMC simulations, insertion of large molecules in to narrow pores can be problematic. This is because there is a very high probability of the insertion being rejected due to the atoms of large molecule overlapping with framework atoms. To avoid such problems and increase the efficiency of the insertion/deletion of the PFOA molecule, we employed the continuous fractional component - Monte Carlo (CFC-MC) method [126, 127]. In the CFC-MC method, a fractional molecule coupled to the system with a λ parameter, which ranges between 0 and 1, is inserted to the system rather than insertion of a whole molecule. Changes in λ is randomly sampled besides the aforementioned MC moves. If λ reaches 1, a full molecule is inserted; whereas, if λ reaches to 0, a molecule is deleted. To ensure that the sampled probability of λ is flat, a weight function (W(λ))is used [126, 128]. A typical CFC-MC simulation we carried out started with 100,000 initialization cycles followed by 100,000 cycles of equilibration. During the latter W(λ) for the CFC-MC method is computed using the Wang-Landau algorithm [129, 130]. Finally, production runs that ranged between 1,000,000 to 10,000,000 cycles were performed and average PFOA and water uptakes were reported. Each MC cycle consists of N Monte Carlo trial moves, where N is equal to the number of molecules in the system. For the composition of the bulk mixture, mol fraction of PFOA in water was set to 10^{-9}. This PFOA mol fraction corresponds to 23 μg PFOA per litre of water which is representative of the concentration of PFOA detected in various water resources [16, 37, 131-134]. Higher equilibrium concentrations; i.e. up to 100 mg PFOA per litre of water, were also considered in the GCMC simulations. The acceptance/rejection rule for the insertion/deletion moves of the molecules requires the fugacity of water and PFOA in the mixture [135]. Given the very small concentrations of PFOA considered in this

study, it can be assumed that PFOA/water mixture is an ideal mixture, and that the fugacity of PFOA is equal to the mol fraction of PFOA in the mixture times the pure component fugacity of PFOA. Since the vapour pressure of PFOA at 298K is very low; i.e. 70 Pa, it can further be assumed that the fugacity of PFOA is equal to its vapour pressure. The fugacity of water on the other hand was calculated with the Peng Robinson equation of state [136].

All GCMC simulations were performed using the RASPA molecular simulation software [91]. The cut-off distance for the LJ potential and the real part of the Ewald sum, which was used to compute electrostatic interactions, was set to 12 Å. The force field parameters for all other criteria of simulation are the same as detailed description presented in Chapter 5. The unit cells of the NU-1000, NU-1000-PF and zeolite Beta were replicated such that their shortest side was greater than twice the cut off distance

6.3. Results and Discussion

Figure 6-2 shows the amount of PFOA and water adsorbed in NU-1000, NU-1000-PF and all-silica zeolite Beta as a function of PFOA equilibrium concentration in water. The loading amount of PFOA computed from GCMC simulations are in very good agreement with experimental data for all-silica zeolite Beta, which is only available at high equilibrium concentration[45]. The adsorption patterns of PFOA and water in zeolite Beta are similar at low PFOA concentration and at the same time different compared to those in NU-1000 and NU-1000-PF because after certain PFOA concentration there is sharp PFOA uptake in zeolite Beta. In zeolite Beta, the uptake of PFOA remains relatively constant at lower PFOA equilibrium concentrations. However, after passing certain PFOA equilibrium concentration PFOA loading increases sharply with increasing PFOA equilibrium concentration and plateaus

around 400 mg/g. Like zeolite Beta at lower PFOA equilibrium concentrations the PFOA uptake of both NU-1000 and NU-1000-PF is low like zeolite Beta. On the other hand, after certain PFOA equilibrium concentration the loading uptake of both NU-1000 and NU-1000-PF starts to increase but not in a same pattern as zeolite Beta.

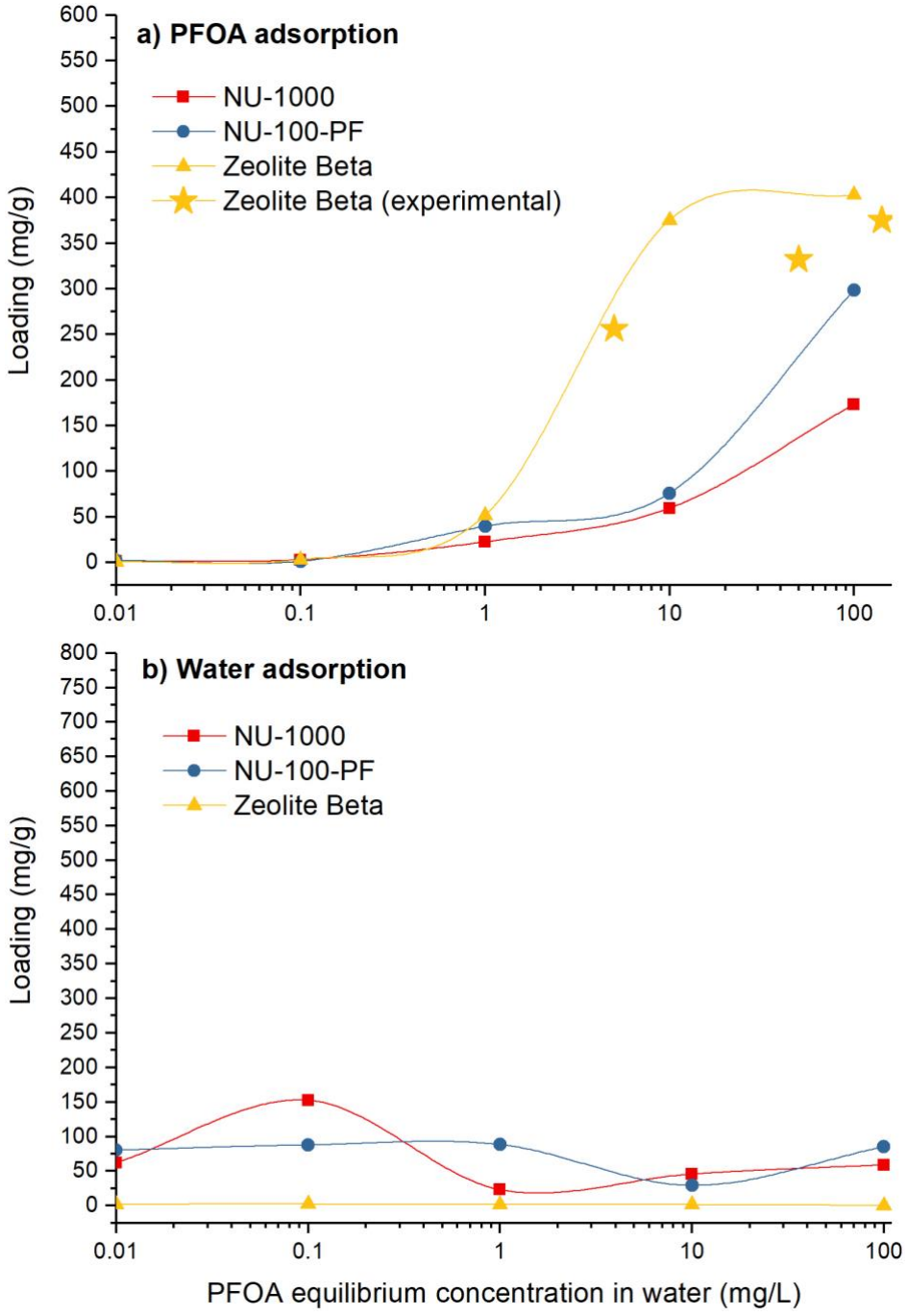

Figure 6-2. Adsorption isotherm of a) PFOA and b) water in NU-1000, NU-1000-PF and all-silica zeolite Beta

The loading uptake of NU-1000 and NU-1000-PF is increasing gradually up to around 173 and 298 mg/g, respectively, with increasing PFOA equilibrium concentration (Figure 6-2a).

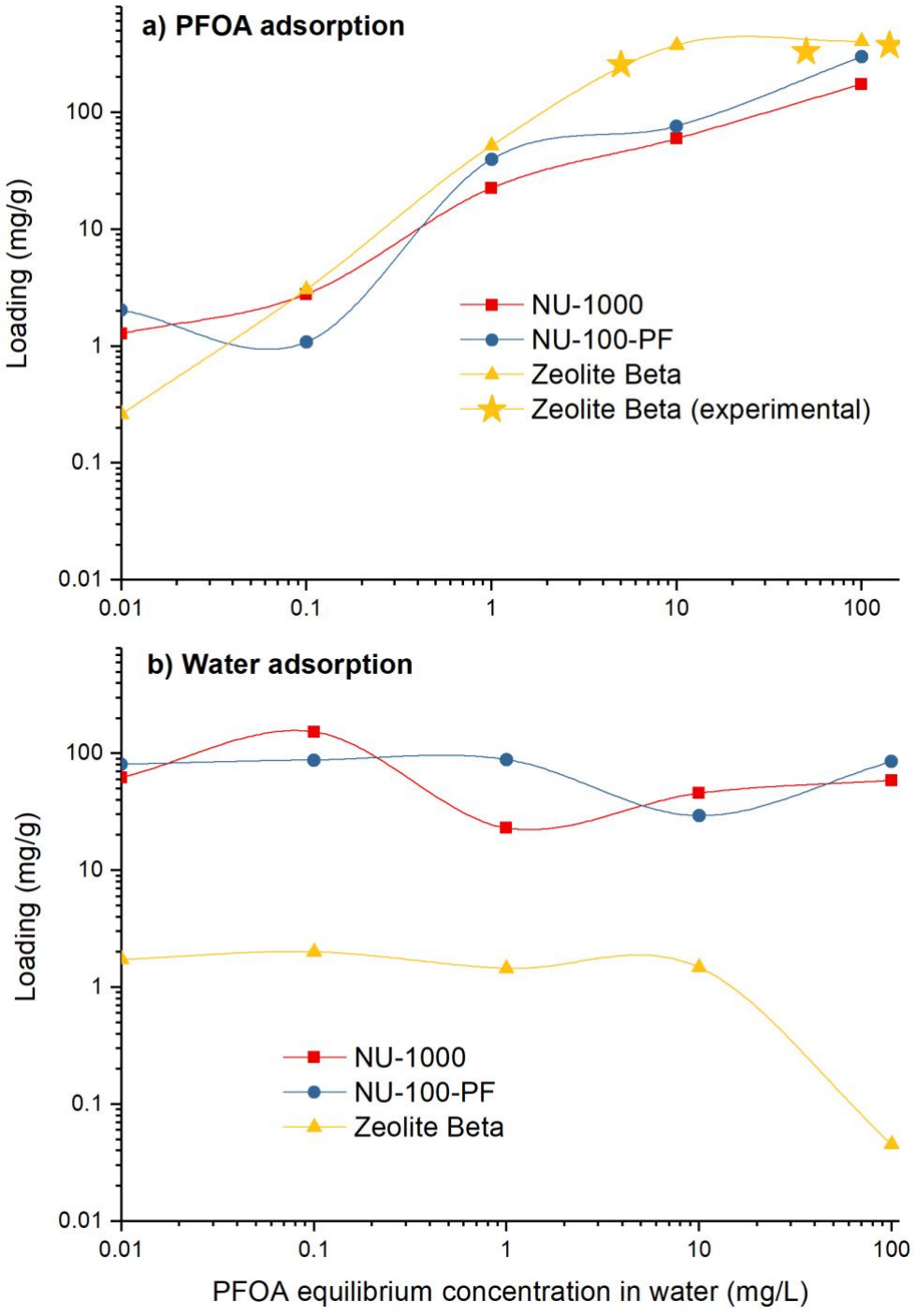

Figure 6-3. Logarithmic scale graph of Adsorption isotherm of a) PFOA and b) water in NU-1000, NU-1000-PF and all-silica zeolite Beta

To do further analysis of uptake behaviour of these structure loading uptake graph is plotted in logarithmic scale in the Figure 6-2. The initial relatively larger uptake of PFOA in zeolite-Beta compared to NU-1000 and NU-1000-PF may be attributed to their water adsorption characteristics. Among the three materials, zeolite Beta is the most hydrophobic and does not adsorb any appreciable amount of water; whereas, NU-1000 and NU-1000-PF initially adsorbs significant amounts of water due to different chemical composition. However, as the PFOA equilibrium concentration increases, the adsorbed PFOA molecules displace water molecules (Figure 6-2b and 6-3b). The initial large water uptake in NU-1000 and NU-1000-PF may be attributed to the presence of μOH sites. Water molecules bound to these sites (Figure 5-8) initiate water condensation leading to the filling of pores. In NU-1000, condensation does not take place in the large pores; i.e. 30Å, and only the small pores are filled (Figure 6-4).

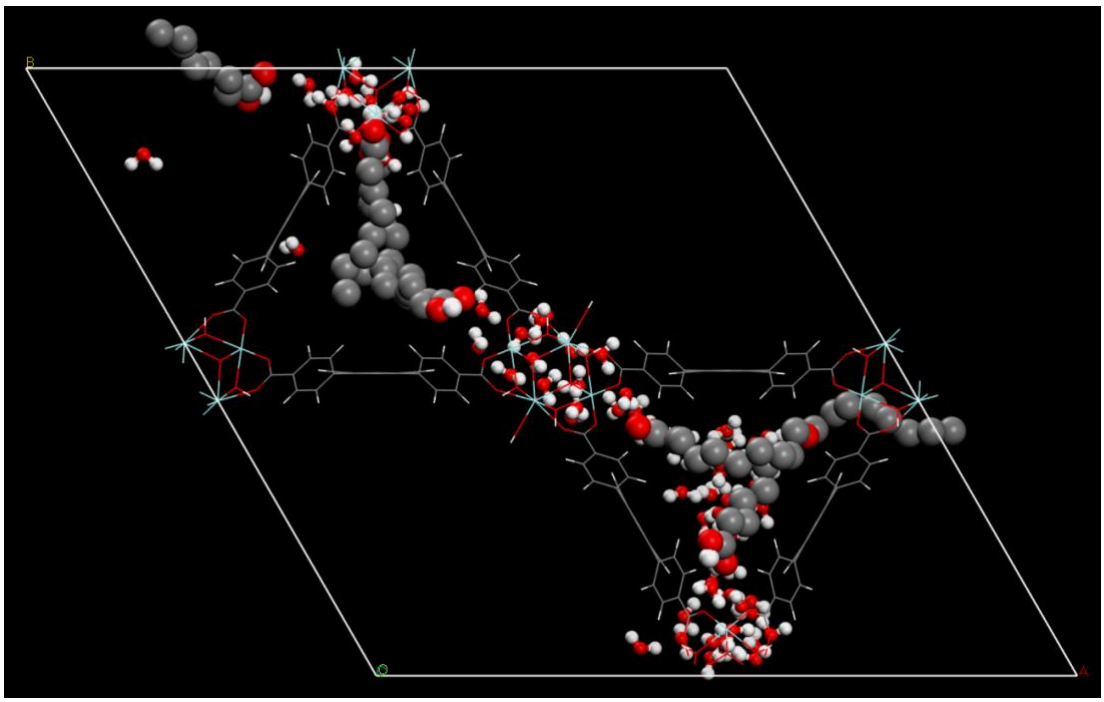

Figure 6-4. Snapshot from GCMC simulations of PFOA and water adsorption in NU-1000 (at 100mg/L concentration)

In NU-1000-PF; however, since all the pores are relatively small; i.e. 10-15Å, majority of the pore volume is filled water molecules (Figure 6-5).

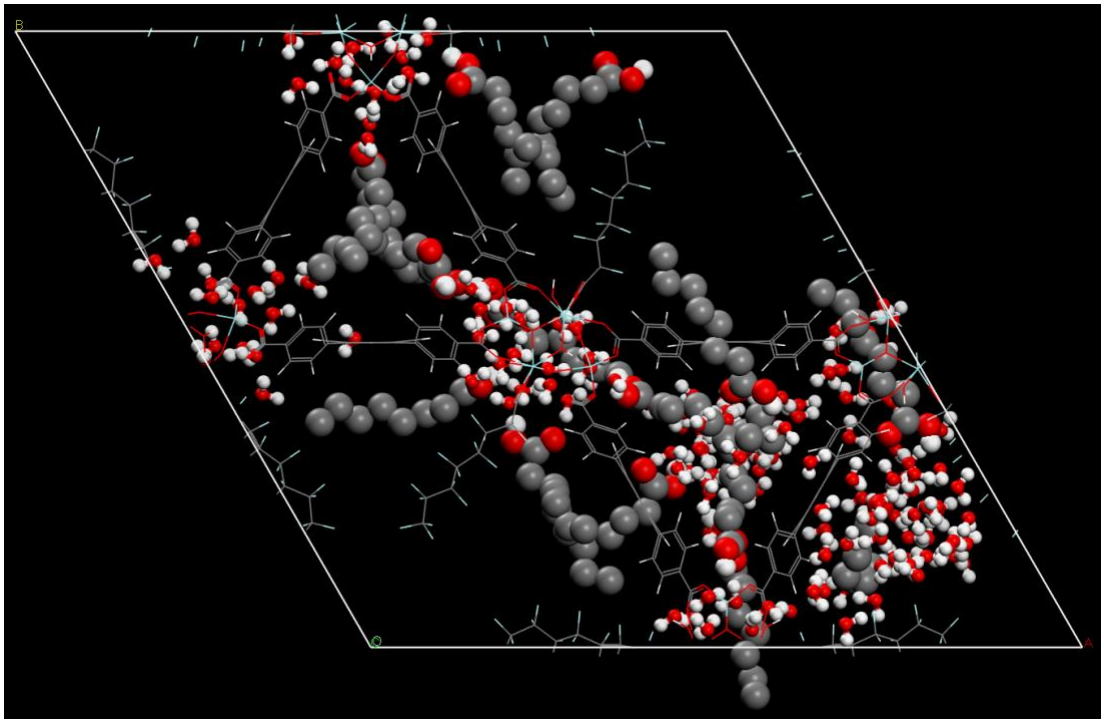

Figure 6-5. Snapshot from GCMC simulations of PFOA and water adsorption in NU-1000-PF

As the PFOA equilibrium concentration increases, water molecules in the centre of the pores are displaced by the adsorbed PFOA molecules. Although zeolite Beta has highest adsorption in the isotherm (Figure 6-2), the plateau at the end indicated that it is saturated unlike increasing trend of NU-1000 and NU-1000-PF. Since zeolite Beta reached its maximum capacity, we can surmise that at higher concentrations, NU-1000 and NU-1000-PF adsorb more PFOA compared to zeolite Beta which may be explained by their larger pore volumes. Finally, within the considered range of PFOA equilibrium concentration in water, NU-1000-PF adsorbs more PFOA compared to NU-1000 (Figure 6-2 and 6-3) thanks to functionalization by perfluoroalkyl grafting (Figure 5-6).

6.4. Conclusions

GCMC simulations are performed for three structures at different PFOA equilibrium concentration. These three structures were chosen because of their high affinity to PFOA molecule, however in addition to having high Henry's law coefficient of PFOA they should show enough low affinity to water molecules. At lowest PFOA concentration both NU-1000 and NU-1000-PF adsorbed significant amount of water molecules. Since PFOA and water molecules does not have different binding sites within MOFs the binding sites indicated in RDF plots are saturated with water molecules. However, with increasing PFOA concentration the adsorbed PFOA molecules are increasing considerably. Although the adsorbed amount of water is much higher than PFOA at low concentrations, at some point adsorbed amount of PFOA became much higher than adsorbed water molecules. The increasing trend on the graph implies that NU-1000 and NU-1000-PF can capture more PFOA molecules. Also the snapshots in Figure 6-4 and 6-5 are from the simulation with highest PFOA concentration solution and it has seen that more than half of the MOFs is empty. For zeolite Beta structure the adsorption isotherm trend is different than NU-1000 and NU-1000-PF. Due to high hydrophobicity and small pore size the adsorbed amount of water is never high for zeolite Beta structure. Besides, we reached the maximum PFOA adsorption capacity of zeolite Beta sooner than MOFs and computed maximum PFOA adsorption capacity of zeolite Beta is close to the experimental value. Observing good agreement with simulation and experimental data PFOA adsorption within zeolite Beta supports that new united-atom PFOA model developed in this study is a reliable molecule model to be employed in further studies.

Chapter 7. Conclusions and Future Studies

In this chapter will provide a summary of the general conclusion of this Thesis and how these results can lead to other works.

The removal of toxic substances especially something non-degradable is a significant topic for the whole world and many researchers are working on preventing environmental pollution. In this thesis we focused on one of the very resistant and very challenging classes of toxic substances that are contained per- and polyfluoroalkyl chains. These per- and polyfluoroalkyl substances (PFAS) are an emerging class of persistent polluters that do not break down in nature due to the presence of strong carbon-fluorine covalent bonds in their structures. PFAS are very small and mobile hence have been detected in surface and ground water sources. Due to significant increase of their concentration in water supplies and they are also found in human urine and serum samples that lead to serious effects on human health. The interaction characteristics of these toxic substances have been investigated in this thesis to understand the adsorption mechanism and find suitable adsorbent materials to clean water resources.

In Chapter 4 we started this quest with a polymeric material that contain calixarene molecule, which is known by its selective and effective adsorptive characteristics. Our collaborators worked on the experimental part of the research, and we worked on simulation part to understand the capturing mechanism of these molecules. Our molecule model was all-atom model and Monte Carlo simulations are performed to observe how the toxic molecule interact with calixarene contained polymeric materials. The simulations and experiments gave significant insight about toxic molecule and what kind of interaction mechanism it prefers to attach the adsorbent. In

this polymeric structure both PFOA molecule and water molecule interact with polymer by making hydrogen bonds between oxygen atom of calixarene and hydrogen atoms of PFOA and water molecules. Four different forms of calixarene polymer have been tested and two of them were fluorinated version of two compounds. Fluorinated polymers showed better adsorption performance, because fluorine atoms of the polymers indicated strong interaction with hydrogen atom of only PFOA molecules not water molecules in this case. The binding energy calculations performed and the simulations results are in agreement with experimental data. The radial distribution function plots showed interaction behavior of these molecules very clearly in simulations. In addition to simulation results, experimental adsorption studies support simulations results by adsorbing significantly more PFOA molecules than non-fluorinated polymeric materials.

In Chapter 5 we aim to investigate MOFs that can be employed in removal PFOA molecules from water and since previous study showed that fluorination improve the ability of capturing PFOA from water fluorinated MOFs have been researched. Besides investigating fluorinated MOFs to overcome long simulations times and also sample the effect of torsional moves of PFOA molecules a new PFAO model is needed to be developed. Hence, we introduced a united-atom model of PFOA. After extensive research we combined the relative force field parameters and accomplished to have proper force field for the united atom structure of PFOA. This model and force field indicated that we could simulate the experimental physical characteristics of the PFOA molecule. In addition to building more effective PFOA model we wanted to investigate metal organic frameworks (MOFs) and their adsorptive characteristics to remove these toxic substances from water. Since aforementioned results in the Chapter

4 indicated how fluorination increases the effectivity of PFOA adsorption, in this chapter fluorinated MOFs are investigated thoroughly. The fluorine functionalization of MOFs can be performed by employing different methods. Three different fluorine functionalization methods were considered in this study; incorporation of fluorinated anions as bridging ligands, trifluoromehtyl or fluorine substitution of the ligands, and grafting of perfluorinated alkanes. The MOF-PFOA and MOF-water affinities were quantified by calculating the Henry's law coefficients of PFOA and water within the structures. The affinity between MOFs and PFOA was higher than between MOFs and water for all structures. Also, the amount fluorine atoms within MOFs increase affinity between PFOA and MOFs. Besides Henry's law coefficient calculations PFOA and water molecules were simulated to probe structure to find preferred adsorption sites within the structures. The Monte Carlo simulations produced radial distribution functions plots that are indicated the interaction mechanism of water and PFOA molecules within structures and preferred binding sites of adsorbate molecules.

In Chapter 6 based on Henry's law coefficient values three promising structures, two MOFs and one zeolite Beta, were employed for adsorption study. GCMC simulations were performed on NU-1000, NU-100-PF and all-silica zeolite Beta structure to test the PFOA uptake of structures. PFOA and water loadings are computed at different PFOA equilibrium concentration to find out how the amount of PFOA loading changes with PFOA concentration in water solution. At very low concentration NU-1000 and NU-1000-PF indicate higher PFOA uptake compared to all-silica zeolite Beta due to their higher pore size than all-silica zeolite Beta and less hydrophobic characteristics of NU-1000 and NU-1000-PF facilitate adsorption of PFOA at very low concentrations. After a threshold PFOA equilibrium concentration PFOA uptake

of all-silica zeolite Beta increase very sharply and reach maximum PFOA loading capacity. Both NU-1000 and NU-1000-PF also indicate an increasing PFOA uptake trend after a threshold concentration, but it is not as sharp as all-silica zeolite Beta and they do not reach maximum PFOA uptake capacity even at the highest PFOA equilibrium concentration simulated in the study. Since the experimental PFOA uptake results are in good agreement with simulated values we can conclude that our PFOA model is good enough to simulate possible PFOA removal candidates.

7.1. Outlook

The results of these studies indicated that the PFOA simulation models are in good agreement with experimental values and showed the interaction behavior of PFOA with adsorbents. Similar to the revelation of how fluorine functionalization of materials contributes to improved PFOA molecule adsorption, various other types of functionalization can be applied to both similar and distinct porous structures. These investigations can help improving the PFOA capturing ability of materials and introduce more efficient water filtration systems. In all these structures there were specific binding sites that capture PFOA molecules and the non-binding sites were mostly linkers of the structures. Therefore, these fluorinated structures can be modified by changing their linker molecules. The linker change will influence chemical environment that can lead to enhance the effectivity of binding sites of adsorbent structures. This research is mostly focused on investigating the effect of surface chemistry of the porous material on adsorption behavior of PFOA molecule by introducing fluorine environment. Besides fluorine other chemical moieties can be tested on. Besides manipulating the surface chemistry, the effect of pore shape and size can also be studied to understand how spatial changes influence the interaction

between adsorbate and adsorbent. Further research can also be done for adsorption simulation studies. Since the adsorption simulations are performed with grand canonical Monte Carlo simulation that is a statistical approach and has provided limited information on adsorption simulations, deterministic approach can also be tested with Molecular Dynamics simulation to acquire more insight about how PFOA molecules behave within water solution in the adsorbent. One of the advantages of employing MD simulations is considering the flexibility of crystal structure. In this study, all crystal structures were rigid and flexibility of adsorbent materials can have significant effect on effectivity of capturing PFOA molecules.

Appendix A. Supporting information of Chapter 5 & Chapter 6

In the Appendix the schematics of MOFs and zeolite Beta that have been employed for the simulations are presented.

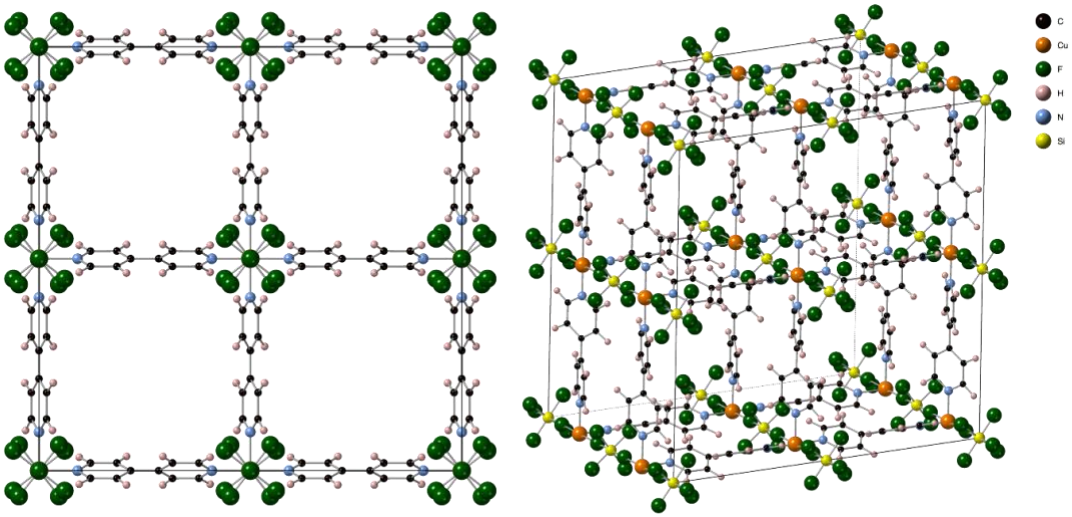

Figure A-1. SIFSIX-1-Cu

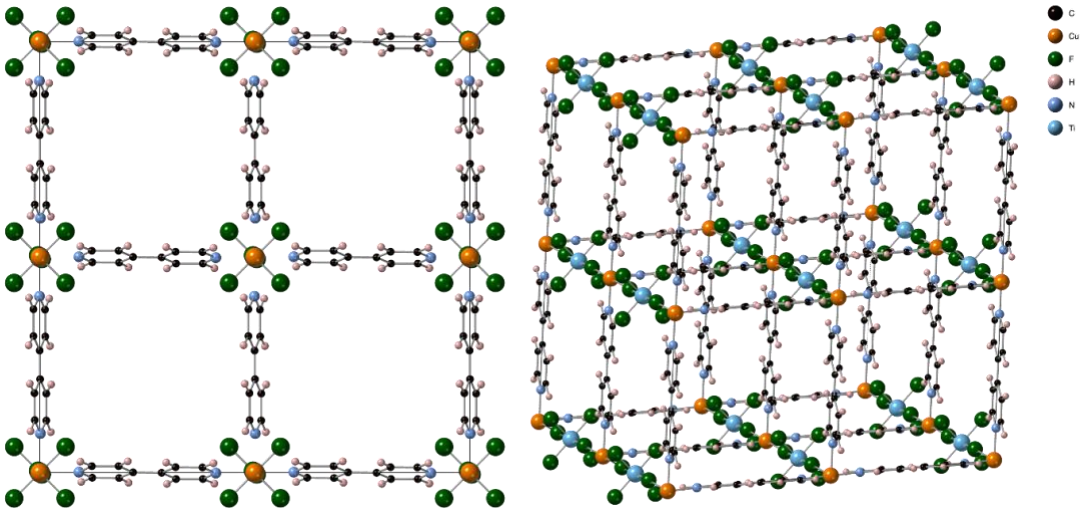

Figure A-2. TIFSIX-1-Cu

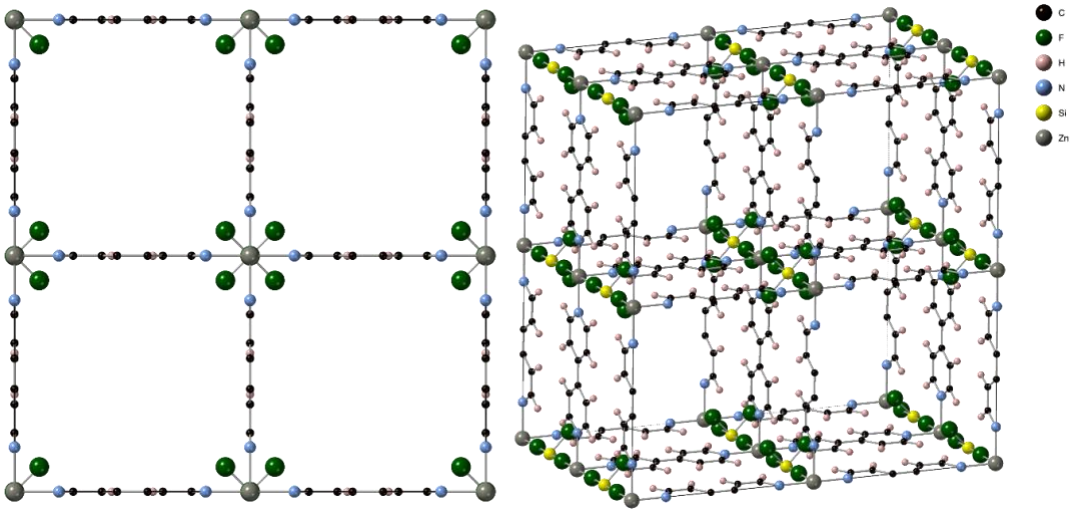

Figure A-3. $Zn(4,4'\text{-bpy})_2(SiF_6)$

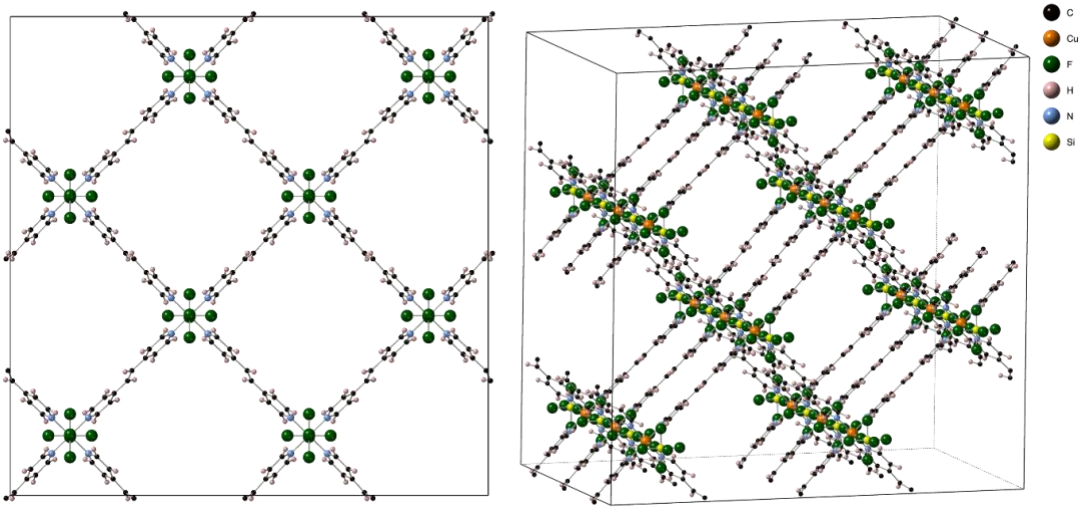

Figure A-4. $Cu(bpy\text{-}1)_2(SiF_6)$

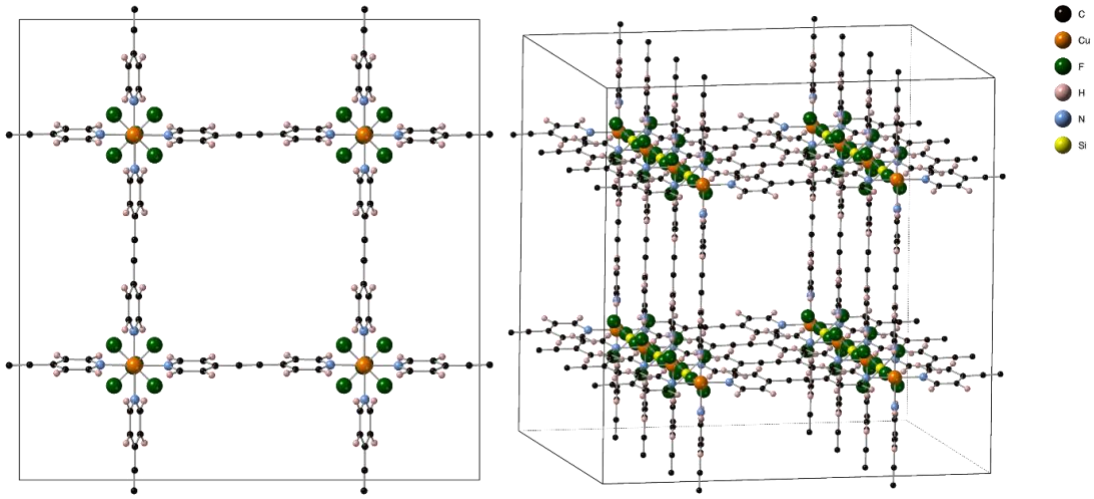

Figure A-5. SIFSIX-2-Cu

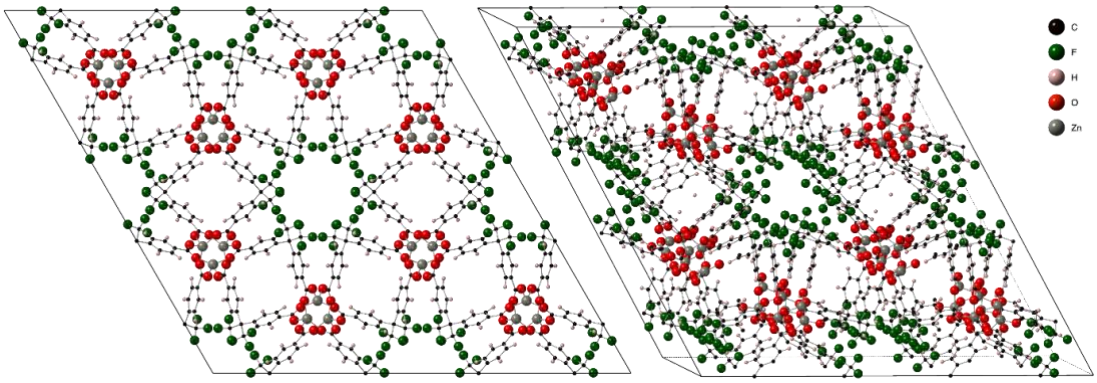

Figure A-6. $Zn(C_{17}H_8F_6O_4)$

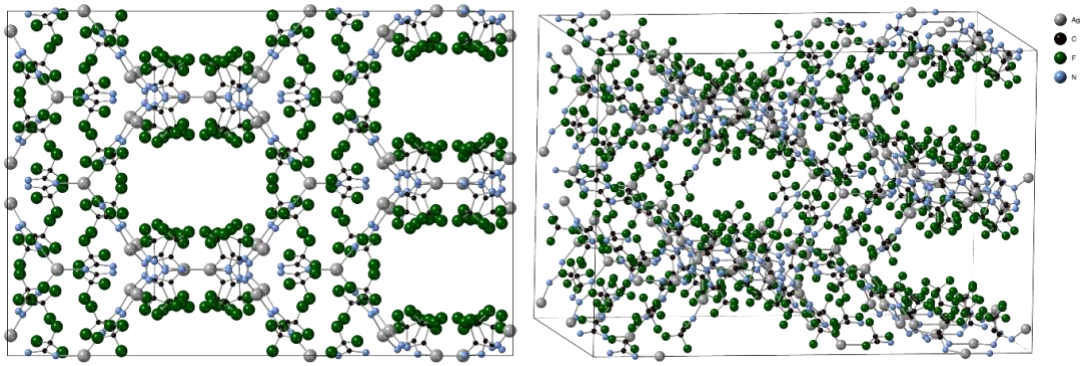

Figure A-7. FMOF-1

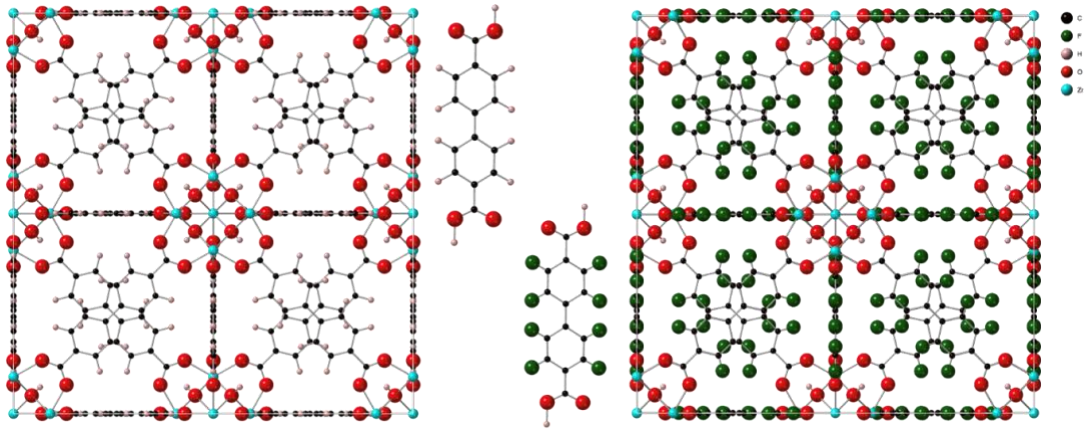

Figure A-8. UiO-67; H_2 biphenyl-4,4'-dicarboxylate (BPDC); H_2FBPDC linker and F-UiO-67-100%

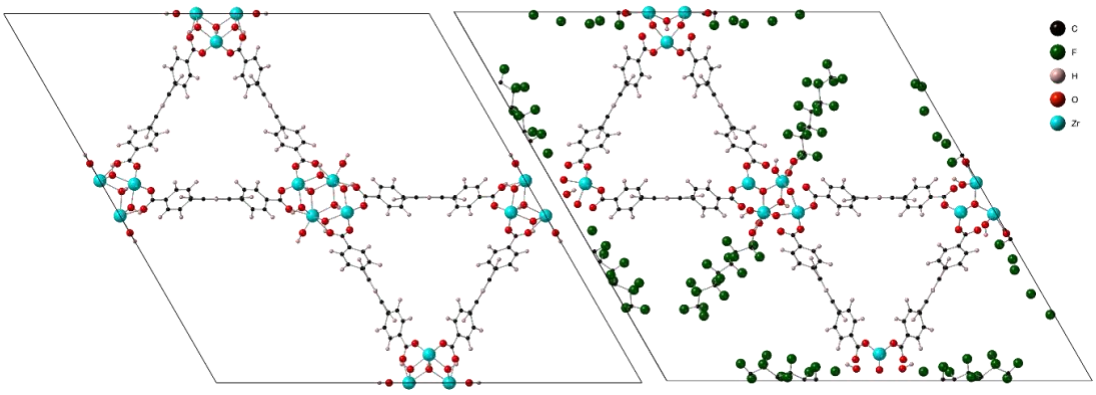

Figure A-9. NU-1000 & NU-1000-PF

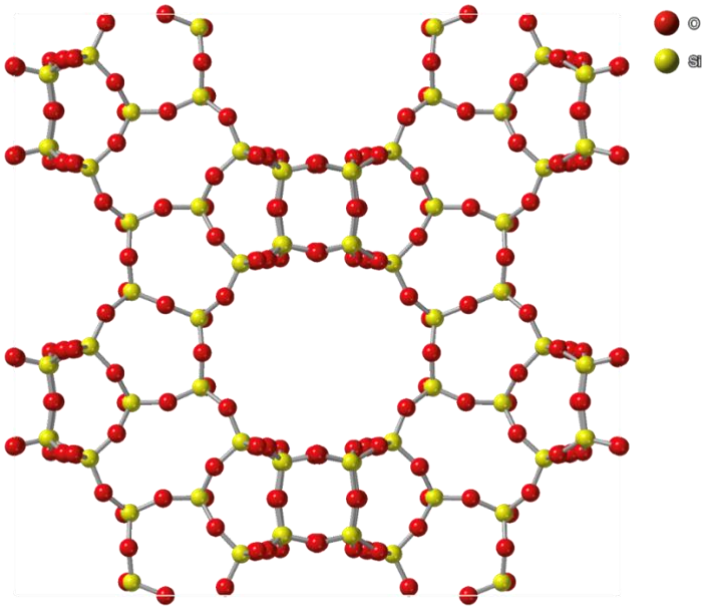

Figure A-10. All-silica zeolite Beta

Bibliography

1. Barry, V., A. Winquist, and K. Steenland, *Perfluorooctanoic Acid (PFOA) Exposures and Incident Cancers among Adults Living Near a Chemical Plant.* Environmental Health Perspectives, 2013. **121**(11-12): p. 1313-1318.
2. Lei, X., et al., *A review of PFAS adsorption from aqueous solutions: Current approaches, engineering applications, challenges, and opportunities.* Environmental Pollution, 2023. **321**: p. 121138.
3. Alengebawy, A., et al., *Heavy Metals and Pesticides Toxicity in Agricultural Soil and Plants: Ecological Risks and Human Health Implications.* Toxics, 2021. **9**(3).
4. Ukaogo, P.O., U. Ewuzie, and C.V. Onwuka, *21 - Environmental pollution: causes, effects, and the remedies*, in *Microorganisms for Sustainable Environment and Health*, P. Chowdhary, et al., Editors. 2020, Elsevier. p. 419-429.
5. Khan, M.A. and A.M. Ghouri, *Environmental pollution: its effects on life and its remedies.* Researcher World: Journal of Arts, Science & Commerce, 2011. **2**(2): p. 276-285.
6. Bell, M.L., D.L. Davis, and T. Fletcher, *A retrospective assessment of mortality from the London smog episode of 1952: the role of influenza and pollution.* Environmental health perspectives, 2004. **112**(1): p. 6-8.
7. Nemery, B., P.H.M. Hoet, and A. Nemmar, *The Meuse Valley fog of 1930: an air pollution disaster.* The Lancet, 2001. **357**(9257): p. 704-708.
8. Brunekreef, B. and S.T. Holgate, *Air pollution and health.* The Lancet, 2002. **360**(9341): p. 1233-1242.
9. Risom, L., P. Møller, and S. Loft, *Oxidative stress-induced DNA damage by particulate air pollution.* Mutation Research/Fundamental and Molecular Mechanisms of Mutagenesis, 2005. **592**(1): p. 119-137.
10. Kampa, M. and E. Castanas, *Human health effects of air pollution.* Environmental Pollution, 2008. **151**(2): p. 362-367.
11. Rodríguez-Eugenio, N., M. McLaughlin, and D. Pennock, *Soil pollution: a hidden reality*. 2018: FAO.

12. Ranieri, E., et al., *Soil Pollution Prevention and Remediation.* Applied and Environmental Soil Science, 2016. **2016**: p. 9415175.
13. Schwarzenbach, R.P., et al., *Global Water Pollution and Human Health.* Annual Review of Environment and Resources, 2010. **35**(1): p. 109-136.
14. Schwarzenbach, R.P., et al., *Global Water Pollution and Human Health.* Annual Review of Environment and Resources, 2010. **35**(1): p. 109-136.
15. Posthuma, L., et al., *Chemical pollution imposes limitations to the ecological status of European surface waters.* Scientific Reports, 2020. **10**(1): p. 14825.
16. Rahman, M.F., S. Peldszus, and W.B. Anderson, *Behaviour and fate of perfluoroalkyl and polyfluoroalkyl substances (PFASs) in drinking water treatment: A review.* Water Research, 2014. **50**: p. 318-340.
17. Moody, C.A. and J.A. Field, *Perfluorinated Surfactants and the Environmental Implications of Their Use in Fire-Fighting Foams.* Environmental Science & Technology, 2000. **34**(18): p. 3864-3870.
18. Dixit, F., et al., *PFOA and PFOS removal by ion exchange for water reuse and drinking applications: role of organic matter characteristics.* Environmental Science: Water Research & Technology, 2019. **5**(10): p. 1782-1795.
19. Trager, R., *A persistent perfluorinated Problem.* Chemistry World, 2019. **16**(9): p. 26-31.
20. Hale, S.E., et al., *What's in a Name: Persistent, Mobile, and Toxic (PMT) and Very Persistent and Very Mobile (vPvM) Substances.* Environmental Science & Technology, 2020. **54**(23): p. 14790-14792.
21. Brendel, S., et al., *Short-chain perfluoroalkyl acids: environmental concerns and a regulatory strategy under REACH.* Environmental Sciences Europe, 2018. **30**(1): p. 9.
22. Cousins, I.T., et al., *The high persistence of PFAS is sufficient for their management as a chemical class.* Environmental Science: Processes & Impacts, 2020. **22**(12): p. 2307-2312.
23. Brusseau, M.L., R.H. Anderson, and B. Guo, *PFAS concentrations in soils: Background levels versus contaminated sites.* Science of The Total Environment, 2020. **740**: p. 140017.

24. Chow, S.J., et al., *Detection of ultrashort-chain and other per- and polyfluoroalkyl substances (PFAS) in U.S. bottled water.* Water Research, 2021. **201**: p. 117292.

25. Calafat, A.M., et al., *Polyfluoroalkyl chemicals in the U.S. population: data from the National Health and Nutrition Examination Survey (NHANES) 2003-2004 and comparisons with NHANES 1999-2000.* Environmental health perspectives, 2007. **115**(11): p. 1596-1602.

26. Hekster, F.M., R.W.P.M. Laane, and P. de Voogt, *Environmental and Toxicity Effects of Perfluoroalkylated Substances*, in *Reviews of Environmental Contamination and Toxicology*. 2003, Springer New York: New York, NY. p. 99-121.

27. Wang, Z., et al., *Hazard assessment of fluorinated alternatives to long-chain perfluoroalkyl acids (PFAAs) and their precursors: Status quo, ongoing challenges and possible solutions.* Environment International, 2015. **75**: p. 172-179.

28. Gaballah, S., et al., *Evaluation of Developmental Toxicity, Developmental Neurotoxicity, and Tissue Dose in Zebrafish Exposed to GenX and Other PFAS.* Environmental Health Perspectives, 2020. **128**(4): p. 047005.

29. Sinclair, G.M., S.M. Long, and O.A.H. Jones, *What are the effects of PFAS exposure at environmentally relevant concentrations?* Chemosphere, 2020. **258**: p. 127340.

30. Lenka, S.P., M. Kah, and L.P. Padhye, *A review of the occurrence, transformation, and removal of poly- and perfluoroalkyl substances (PFAS) in wastewater treatment plants.* Water Research, 2021. **199**: p. 117187.

31. Scher, D.P., et al., *Occurrence of perfluoroalkyl substances (PFAS) in garden produce at homes with a history of PFAS-contaminated drinking water*. Chemosphere, 2018. **196**: p. 548-555.

32. Li, P., et al., *Research progress on the removal of hazardous perfluorochemicals: A review.* Journal of Environmental Management, 2019. **250**: p. 109488.

33. Trojanowicz, M., et al., *Advanced Oxidation/Reduction Processes treatment for aqueous perfluorooctanoate (PFOA) and perfluorooctanesulfonate (PFOS) – A review of recent advances.* Chemical Engineering Journal, 2018. **336**: p. 170-199.

34. Yang, L., et al., *Persulfate-based degradation of perfluorooctanoic acid (PFOA) and perfluorooctane sulfonate (PFOS) in aqueous solution: Review on influences, mechanisms and prospective.* Journal of Hazardous Materials, 2020. **393**: p. 122405.

35. Bao, Y., et al., *Removal of perfluorooctane sulfonate (PFOS) and perfluorooctanoate (PFOA) from water by coagulation: Mechanisms and influencing factors.* Journal of Colloid and Interface Science, 2014. **434**: p. 59-64.

36. Yuan, J., et al., *Evaluating perfluorooctanoic acid (PFOA) and perfluorooctanesulfonic acid (PFOS) removal across granular activated carbon (GAC) filter-adsorbers in drinking water treatment plants.* Science of The Total Environment, 2022. **838**: p. 156406.

37. Liu, L., et al., *Removal of perfluorooctanoic acid (PFOA) and perfluorooctane sulfonate (PFOS) from water by carbonaceous nanomaterials: A review.* Critical Reviews in Environmental Science and Technology, 2020. **50**(22): p. 2379-2414.

38. Wang, R., et al., *Evaluating the Removal of Per- and Polyfluoroalkyl Substances from Contaminated Groundwater with Different Adsorbents Using a Suspect Screening Approach.* Environmental Science & Technology Letters, 2020. **7**(12): p. 954-960.

39. Ateia, M., et al., *Efficient PFAS Removal by Amine-Functionalized Sorbents: Critical Review of the Current Literature.* Environmental Science & Technology Letters, 2019. **6**(12): p. 688-695.

40. Xu, C., H. Chen, and F. Jiang, *Adsorption of perflourooctane sulfonate (PFOS) and perfluorooctanoate (PFOA) on polyaniline nanotubes.* Colloids and Surfaces A: Physicochemical and Engineering Aspects, 2015. **479**: p. 60-67.

41. Skorjanc, T., D. Shetty, and A. Trabolsi, *Pollutant removal with organic macrocycle-based covalent organic polymers and frameworks.* Chem, 2021. **7**(4): p. 882-918.

42. Olshansky, Y., et al., *Synthesis and Characterization of Customizable Polyaniline-Derived Polymers and Their Application for Perfluorooctanoic Acid Removal from Aqueous Solution.* ACS ES&T Water, 2021. **1**(6): p. 1438-1446.

43. Shetty, D., et al., *Rapid and Efficient Removal of Perfluorooctanoic Acid from Water with Fluorine-Rich Calixarene-Based Porous Polymers.* ACS Applied Materials & Interfaces, 2020. **12**(38): p. 43160-43166.

44. Xiao, L., et al., *β-Cyclodextrin Polymer Network Sequesters Perfluorooctanoic Acid at Environmentally Relevant Concentrations.* Journal of the American Chemical Society, 2017. **139**(23): p. 7689-7692.

45. Van den Bergh, M., et al., *Highly Selective Removal of Perfluorinated Contaminants by Adsorption on All-Silica Zeolite Beta.* Angewandte Chemie International Edition, 2020. **59**(33): p. 14086-14090.

46. Ochoa-Herrera, V. and R. Sierra-Alvarez, *Removal of perfluorinated surfactants by sorption onto granular activated carbon, zeolite and sludge.* Chemosphere, 2008. **72**(10): p. 1588-1593.

47. Wang, W., et al., *Cationic covalent organic framework for efficient removal of PFOA substitutes from aqueous solution.* Chemical Engineering Journal, 2021. **412**: p. 127509.

48. Ji, W., et al., *Removal of GenX and Perfluorinated Alkyl Substances from Water by Amine-Functionalized Covalent Organic Frameworks.* Journal of the American Chemical Society, 2018. **140**(40): p. 12677-12681.

49. Wang, B., et al., *Covalent triazine-based framework: A promising adsorbent for removal of perfluoroalkyl acids from aqueous solution.* Environmental Pollution, 2016. **216**: p. 884-892.

50. Sini, K., et al., *Metal–organic framework sorbents for the removal of perfluorinated compounds in an aqueous environment.* New Journal of Chemistry, 2018. **42**(22): p. 17889-17894.

51. Chen, M.-J., et al., *Influence of crystal topology and interior surface functionality of metal-organic frameworks on PFOA sorption performance.* Microporous and Mesoporous Materials, 2016. **236**: p. 202-210.

52. Li, R., et al., *Efficient Removal of Per- and Polyfluoroalkyl Substances from Water with Zirconium-Based Metal–Organic Frameworks.* Chemistry of Materials, 2021. **33**(9): p. 3276-3285.

53. Liu, K., et al., *Understanding the Adsorption of PFOA on MIL-101(Cr)-Based Anionic-Exchange Metal–Organic Frameworks: Comparing DFT Calculations with*

Aqueous Sorption Experiments. Environmental Science & Technology, 2015. **49**(14): p. 8657-8665.

54. Asfari, M.-Z., et al., *Calixarenes 2001*. 2007: Springer Science & Business Media.

55. Gutsche, C.D. and R. Muthukrishnan, *Calixarenes. 1. Analysis of the product mixtures produced by the base-catalyzed condensation of formaldehyde with para-substituted phenols.* The Journal of Organic Chemistry, 1978. **43**(25): p. 4905-4906.

56. Gutsche, C.D., *Calixarenes.* Accounts of Chemical Research, 1983. **16**(5): p. 161-170.

57. Mandolini, L. and R. Ungaro, *Calixarenes in action*. 2000: world scientific.

58. Abubakar, S., et al., *Porous Polycalix[n]arenes as Environmental Pollutant Removers.* ACS Applied Materials & Interfaces, 2021. **13**(13): p. 14802-14815.

59. Gutsche, C.D. and L.J. Bauer, *Calixarenes. 13. The conformational properties of calix[4]arenes, calix[6]arenes, calix[8]arenes, and oxacalixarenes.* Journal of the American Chemical Society, 1985. **107**(21): p. 6052-6059.

60. Vicens, J., J. Harrowfield, and L. Baklouti, *Calixarenes in the Nanoworld*. 2007: Springer.

61. Mokhtari, B. and K. Pourabdollah, *Applications of calixarene nano-baskets in pharmacology.* Journal of Inclusion Phenomena and Macrocyclic Chemistry, 2012. **73**(1): p. 1-15.

62. Deska, M., B. Dondela, and W. Sliwa, *Selected applications of calixarene derivatives.* ARKIVOC, 2015. **2015**(6): p. 393-416.

63. Redshaw, C., *Coordination chemistry of the larger calixarenes.* Coordination Chemistry Reviews, 2003. **244**(1): p. 45-70.

64. Ludwig, R., *Calixarenes in analytical and separation chemistry.* Fresenius' Journal of Analytical Chemistry, 2000. **367**(2): p. 103-128.

65. Shinkai, S., *Calixarenes - the third generation of supramolecules.* Tetrahedron, 1993. **49**(40): p. 8933-8968.

66. Shinkai, S., et al., *Chiral calixarene.* Journal of the Chemical Society, Chemical Communications, 1987(19): p. 1495-1496.

67. Li, S.-Y., et al., *Inherently Chiral Calixarenes: Synthesis, Optical Resolution, Chiral Recognition and Asymmetric Catalysis.* International Journal of Molecular Sciences, 2011. **12**(1): p. 429-455.

68. Sánchez Peña, M., Y. Zhang, and I.M. Warner, *Enantiomeric Separations by Use of Calixarene Electrokinetic Chromatography.* Analytical Chemistry, 1997. **69**(16): p. 3239-3242.

69. James, S.L., *Metal-organic frameworks.* Chemical Society Reviews, 2003. **32**(5): p. 276-288.

70. Marakulin, A.V., et al., *New one-, two-, and three-dimensional metal-organic frameworks based on magnesium(II): synthesis and structure.* Russian Chemical Bulletin, 2020. **69**(2): p. 360-368.

71. Mueller, U., et al., *Metal–organic frameworks—prospective industrial applications.* Journal of Materials Chemistry, 2006. **16**(7): p. 626-636.

72. Zhou, H.-C.J. and S. Kitagawa, *Metal–Organic Frameworks (MOFs).* Chemical Society Reviews, 2014. **43**(16): p. 5415-5418.

73. Moosavi, S.M., et al., *Understanding the diversity of the metal-organic framework ecosystem.* Nature Communications, 2020. **11**(1): p. 4068.

74. *Introduction to Metal–Organic Frameworks.* Chemical Reviews, 2012. **112**(2): p. 673-674.

75. Wang, Z. and S.M. Cohen, *Postsynthetic modification of metal–organic frameworks.* Chemical Society Reviews, 2009. **38**(5): p. 1315-1329.

76. Boone, P., et al., *Designing optimal core–shell MOFs for direct air capture.* Nanoscale, 2022.

77. Brandt, P., et al., *Comparative Evaluation of Different MOF and Non-MOF Porous Materials for SO2 Adsorption and Separation Showing the Importance of Small Pore Diameters for Low-Pressure Uptake.* Advanced Sustainable Systems, 2021. **5**(4): p. 2000285.

78. Sabouni, R., H. Kazemian, and S. Rohani, *Carbon dioxide capturing technologies: a review focusing on metal organic framework materials (MOFs).* Environmental Science and Pollution Research, 2014. **21**(8): p. 5427-5449.

79. Kazemi, S. and V. Safarifard, *Carbon dioxide capture in MOFs: The effect of ligand functionalization.* Polyhedron, 2018. **154**: p. 236-251.

80. Gadipelli, S. and Z. Guo, *Postsynthesis Annealing of MOF-5 Remarkably Enhances the Framework Structural Stability and CO2 Uptake.* Chemistry of Materials, 2014. **26**(22): p. 6333-6338.

81. Theodorou, D.N., *Progress and Outlook in Monte Carlo Simulations.* Industrial & Engineering Chemistry Research, 2010. **49**(7): p. 3047-3058.

82. Duan, Y., et al., *A point-charge force field for molecular mechanics simulations of proteins based on condensed-phase quantum mechanical calculations.* Journal of Computational Chemistry, 2003. **24**(16): p. 1999-2012.

83. Jorgensen, W.L., *OPLS Force Fields*, in *Encyclopedia of Computational Chemistry*. 1998.

84. Vanommeslaeghe, K., et al., *CHARMM general force field: A force field for drug-like molecules compatible with the CHARMM all-atom additive biological force fields.* Journal of Computational Chemistry, 2010. **31**(4): p. 671-690.

85. Mayo, S.L., B.D. Olafson, and W.A. Goddard, *DREIDING: a generic force field for molecular simulations.* The Journal of Physical Chemistry, 1990. **94**(26): p. 8897-8909.

86. Rappe, A.K., et al., *UFF, a full periodic table force field for molecular mechanics and molecular dynamics simulations.* Journal of the American Chemical Society, 1992. **114**(25): p. 10024-10035.

87. Frenkel, D. and B. Smit, *Understanding molecular simulation: from algorithms to applications*. 2023: Elsevier.

88. Kaxiras, E., *Atomic and electronic structure of solids*. 2003.

89. Bartell, S.M. and V.M. Vieira, *Critical review on PFOA, kidney cancer, and testicular cancer.* Journal of the Air & Waste Management Association, 2021. **71**(6): p. 663-679.

90. Segall, M.D., et al., *First-principles simulation: ideas, illustrations and the CASTEP code.* Journal of Physics: Condensed Matter, 2002. **14**(11): p. 2717-2744.

91. Dubbeldam, D., et al., *RASPA: molecular simulation software for adsorption and diffusion in flexible nanoporous materials.* Molecular Simulation, 2016. **42**(2): p. 81-101.

92. Horn, H.W., et al., *Development of an improved four-site water model for biomolecular simulations: TIP4P-Ew*. The Journal of Chemical Physics, 2004. **120**(20): p. 9665-9678.

93. Dauber-Osguthorpe, P., et al., *Structure and energetics of ligand binding to proteins: Escherichia coli dihydrofolate reductase-trimethoprim, a drug-receptor system.* Proteins: Structure, Function, and Bioinformatics, 1988. **4**(1): p. 31-47.

94. Frisch, M.J., et al., *Gaussian 16 Rev. C.01*. 2016: Wallingford, CT.

95. Campañá, C., B. Mussard, and T.K. Woo, *Electrostatic Potential Derived Atomic Charges for Periodic Systems Using a Modified Error Functional.* J Chem Theory Comput, 2009. **5**(10): p. 2866-78.

96. Talapaneni, S.N., et al., *Pillar[5]arene Based Conjugated Microporous Polymers for Propane/Methane Separation through Host–Guest Complexation.* Chemistry of Materials, 2016. **28**(12): p. 4460-4466.

97. Baker, J., *Geometry optimization in Cartesian coordinates: Constrained optimization.* Journal of Computational Chemistry, 1992. **13**(2): p. 240-253.

98. Tan, X., et al., *Amphiphilic Perfluoropolyether Copolymers for the Effective Removal of Polyfluoroalkyl Substances from Aqueous Environments.* Macromolecules, 2021. **54**(7): p. 3447-3457.

99. Chen, P.-Y., et al., *Polyacrylonitrile fiber functionalized with fluorous hyperbranched polyethylenimine for selective removal of perfluorooctane sulfonate (PFOS) in firefighting wastewaters.* Colloids and Surfaces A: Physicochemical and Engineering Aspects, 2021. **619**: p. 126539.

100. Wang, W., et al., *Rapid and efficient removal of organic micropollutants from environmental water using a magnetic nanoparticles-attached fluorographene-based sorbent.* Chemical Engineering Journal, 2018. **343**: p. 61-68.

101. Noro, S.-i. and T. Nakamura, *Fluorine-functionalized metal–organic frameworks and porous coordination polymers.* NPG Asia Materials, 2017. **9**(9): p. e433-e433.

102. Noro, S.-i., et al., *A New, Methane Adsorbent, Porous Coordination Polymer [{CuSiF6(4,4'-bipyridine)2}n].* Angewandte Chemie International Edition, 2000. **39**(12): p. 2081-2084.

103. Nugent, P., et al., *Enhancement of CO2 selectivity in a pillared pcu MOM platform through pillar substitution.* Chemical Communications, 2013. **49**(16): p. 1606-1608.

104. Subramanian, S. and M.J. Zaworotko, *Porous Solids by Design: [Zn(4,4'-bpy)2(SiF6)]n·xDMF, a Single Framework Octahedral Coordination Polymer with Large Square Channels.* Angewandte Chemie International Edition in English, 1995. **34**(19): p. 2127-2129.

105. Burd, S.D., et al., *Highly Selective Carbon Dioxide Uptake by [Cu(bpy-n)2(SiF6)] (bpy-1 = 4,4'-Bipyridine; bpy-2 = 1,2-Bis(4-pyridyl)ethene).* Journal of the American Chemical Society, 2012. **134**(8): p. 3663-3666.

106. Nugent, P., et al., *Porous materials with optimal adsorption thermodynamics and kinetics for CO2 separation.* Nature, 2013. **495**(7439): p. 80-84.

107. Monge, A., et al., *One teflon®-like channelled nanoporous polymer with a chiral and new uninodal 4-connected net: sorption and catalytic properties.* Chemical Communications, 2005(10): p. 1291-1293.

108. Yang, C., et al., *Fluorous Metal–Organic Frameworks with Superior Adsorption and Hydrophobic Properties toward Oil Spill Cleanup and Hydrocarbon Storage.* Journal of the American Chemical Society, 2011. **133**(45): p. 18094-18097.

109. Ji, P., et al., *Tuning Lewis Acidity of Metal–Organic Frameworks via Perfluorination of Bridging Ligands: Spectroscopic, Theoretical, and Catalytic Studies.* Journal of the American Chemical Society, 2018. **140**(33): p. 10553-10561.

110. Deria, P., et al., *Perfluoroalkane Functionalization of NU-1000 via Solvent-Assisted Ligand Incorporation: Synthesis and CO2 Adsorption Studies.* Journal of the American Chemical Society, 2013. **135**(45): p. 16801-16804.

111. Cui, X., et al., *Pore chemistry and size control in hybrid porous materials for acetylene capture from ethylene.* Science, 2016. **353**(6295): p. 141-144.

112. Cheplakova, A.M., et al., *A comparative study of perfluorinated and non-fluorinated UiO-67 in gas adsorption.* Journal of Porous Materials, 2020. **27**(6): p. 1773-1782.

113. Piscopo, C.G., et al., *Positive effect of the fluorine moiety on the oxygen storage capacity of UiO-66 metal–organic frameworks.* New Journal of Chemistry, 2016. **40**(10): p. 8220-8224.

114. DeChellis, D.M., C.M. Ngule, and D.T. Genna, *Removal of hydrocarbon contaminants from water with perfluorocarboxylated UiO-6X derivatives.* Journal of Materials Chemistry A, 2020. **8**(12): p. 5848-5852.

115. Stelzer, J., et al., *Hydrophobic properties of all-silica zeolite beta1Dedicated to Professor Lovat V.C. Rees in recognition and appreciation of his lifelong devotion to zeolite science and his outstanding achievements in this field.1.* Microporous and Mesoporous Materials, 1998. **22**(1): p. 1-8.

116. Sarkisov, L. and A. Harrison, *Computational structure characterisation tools in application to ordered and disordered porous materials.* Molecular Simulation, 2011. **37**(15): p. 1248-1257.

117. Groom, C.R., et al., *The Cambridge Structural Database.* Acta Crystallographica Section B, 2016. **72**(2): p. 171-179.

118. Campañá, C., B. Mussard, and T.K. Woo, *Electrostatic Potential Derived Atomic Charges for Periodic Systems Using a Modified Error Functional.* Journal of Chemical Theory and Computation, 2009. **5**(10): p. 2866-2878.

119. Zhang, L. and J.I. Siepmann, *Pressure Dependence of the Vapor−Liquid−Liquid Phase Behavior in Ternary Mixtures Consisting of n-Alkanes, n-Perfluoroalkanes, and Carbon Dioxide.* The Journal of Physical Chemistry B, 2005. **109**(7): p. 2911-2919.

120. Potoff, J.J. and D.A. Bernard-Brunel, *Mie Potentials for Phase Equilibria Calculations: Application to Alkanes and Perfluoroalkanes.* The Journal of Physical Chemistry B, 2009. **113**(44): p. 14725-14731.

121. Stubbs, J.M., J.J. Potoff, and J.I. Siepmann, *Transferable Potentials for Phase Equilibria. 6. United-Atom Description for Ethers, Glycols, Ketones, and Aldehydes.* The Journal of Physical Chemistry B, 2004. **108**(45): p. 17596-17605.

122. Chen, B., J.J. Potoff, and J.I. Siepmann, *Monte Carlo Calculations for Alcohols and Their Mixtures with Alkanes. Transferable Potentials for Phase Equilibria. 5. United-Atom Description of Primary, Secondary, and Tertiary Alcohols.* The Journal of Physical Chemistry B, 2001. **105**(15): p. 3093-3104.

123. Kamath, G., F. Cao, and J.J. Potoff, *An Improved Force Field for the Prediction of the Vapor−Liquid Equilibria for Carboxylic Acids.* The Journal of Physical Chemistry B, 2004. **108**(37): p. 14130-14136.

124. Ewald, P.P., *Die Berechnung optischer und elektrostatischer Gitterpotentiale.* Annalen der Physik, 1921. **369**(3): p. 253-287.

125. Widom, B., *Some Topics in the Theory of Fluids.* The Journal of Chemical Physics, 1963. **39**(11): p. 2808-2812.

126. Shi, W. and E.J. Maginn, *Continuous Fractional Component Monte Carlo: An Adaptive Biasing Method for Open System Atomistic Simulations.* Journal of Chemical Theory and Computation, 2007. **3**(4): p. 1451-1463.

127. Rahbari, A., et al., *Recent advances in the continuous fractional component Monte Carlo methodology.* Molecular Simulation, 2021. **47**(10-11): p. 804-823.

128. Shi, W. and E.J. Maginn, *Improvement in molecule exchange efficiency in Gibbs ensemble Monte Carlo: Development and implementation of the continuous fractional component move.* Journal of Computational Chemistry, 2008. **29**(15): p. 2520-2530.

129. Torres-Knoop, A., et al., *A Comparison of Advanced Monte Carlo Methods for Open Systems: CFCMC vs CBMC.* Journal of Chemical Theory and Computation, 2014. **10**(3): p. 942-952.

130. Wang, F. and D.P. Landau, *Determining the density of states for classical statistical models: A random walk algorithm to produce a flat histogram.* Physical Review E, 2001. **64**(5): p. 056101.

131. Emmett, E.A., et al., *Community Exposure to Perfluorooctanoate: Relationships Between Serum Concentrations and Exposure Sources.* Journal of Occupational and Environmental Medicine, 2006. **48**(8): p. 759-770.

132. Bonato, M., et al., *PFAS Environmental Pollution and Antioxidant Responses: An Overview of the Impact on Human Field.* International Journal of Environmental Research and Public Health, 2020. **17**(21): p. 8020.

133. Post, G.B., et al., *Occurrence and Potential Significance of Perfluorooctanoic Acid (PFOA) Detected in New Jersey Public Drinking Water Systems.* Environmental Science & Technology, 2009. **43**(12): p. 4547-4554.

134. Post, G.B., P.D. Cohn, and K.R. Cooper, *Perfluorooctanoic acid (PFOA), an emerging drinking water contaminant: A critical review of recent literature.* Environmental Research, 2012. **116**: p. 93-117.

135. Dubbeldam, D., A. Torres-Knoop, and K.S. Walton, *On the inner workings of Monte Carlo codes.* Molecular Simulation, 2013. **39**(14-15): p. 1253-1292.
136. Peng, D.-Y. and D.B. Robinson, *A New Two-Constant Equation of State.* Industrial & Engineering Chemistry Fundamentals, 1976. **15**(1): p. 59-64.